Mémoire

Auteur : Batlle Mari, Lucas
Promoteur(s) : Van Grootel, Valérie
Faculté : Faculté des Sciences
Diplôme : Master en sciences spatiales, à finalité approfondie
Année académique : 2024-2025
URI/URL : http://hdl.handle.net/2268.2/22970

University of Liège - Faculty of Sciences

Mode identification in pulsating subdwarf B stars observed by Kepler and TESS

Master thesis completed in order to obtain the degree of Master in Space Sciences, Research focus

Author:
Lucas Batlle Mari

Supervisor:
Valérie Van Grootel

Committee members:
Manu Stalport
Gaël Buldgen
Dominique Sluse
Emmanuel Jehin

Academic Year 2024-2025

Acknowledgements

First and foremost, I would like to express my sincere gratitude to Pr. Valérie Van Grootel, the supervisor of this master thesis. Her continuous availability and support through the year greatly contributed to its final outcome.

Besides my supervisor, I am grateful to the reading committee members Pr. Dominique Sluse, Pr. Emmanuel Jehin, Dr. Manu Stalport and Dr. Gaël Buldgen for their investment. Special thanks also go to Nathan for his guidance all over the master thesis. His comments guided my steps towards the completion of this work.

I would also like to thank my partner Claire for giving me motivation and her beautiful smile throughout the year. Finally, my greatest gratitude goes to my parents, who supported my choice to go back to the university for one year more and who always believed in me.

Abstract

The study of hot subdwarf B (sdB) stars gives valuable insights for understanding the internal physics of core He-burning (CHeB) stars. This master thesis first presents a review of the pulsating sdB stars observed by the *Kepler* space telescope to classify their pulsation types. One of these pulsators, KIC5807616 (Kepler-70 or KPD 1943+4058), is then selected as the focus of this work, with the primary goal of identifying its gravity (g-) mode pulsations. Mode identification consists in determining the geometrical properties of pulsation modes, a key asset for the future asteroseismic modeling of such stars. This thesis presents a methodology based on quantitative quality criteria, using period-spacing diagrams and rotational multiplets analysis, in order to reduce the part of arbitrary commonly faced in mode identification procedures. This methodology is preliminarily tested and validated on the sdB star TIC441725813 (TYC 4427-1021-1), observed by *TESS*, for which a recent and complete mode identification is available in the literature.

Among the 18 sdB stars observed by *Kepler*, 14 are dominated by g-modes (7 pure and 7 hybrid pulsators), 2 are dominated by pressure (p-) modes (1 pure and 1 hybrid pulsators), and 2 could not be categorized. Concerning KIC5807616, the methodology developed in this thesis leads to the identification of 79 pulsation modes. Three possible identification configurations are discussed, including two configurations showing strong evidences of mode trapping. The rotation period of the envelope is also inferred from rotational splitting observed on p-modes: 40.0 ± 4.7 days.

Keywords : Stellar pulsations, Hot subdwarf B, Asteroseismology, *Kepler*, *TESS*.

Contents

Acronyms

AGB Asymptotic Giant Branch
CCD Charge-Coupled Device
CHeB core helium-burning
EHB Extreme Horizontal Branch
FAP False Alarm Probability
FFI Full-Frame Images
FFT Fast Fourier Transform
HB Horizontal Branch
HR Hertzsprung-Russell
KS Kolmogorov-Smirnov
LC Long Cadence
LEO Low Earth Orbit
LSP Lomb-Scargle Periodogram
MAST Barbara A. Mikulski Archive for Space Telescopes
NASA National Aeronautics and Space Administration
MESA Modules for Experiments in Stellar Astrophysics
NLLS Non-Linear Least Square
RGB Red Giant Branch
SC Short Cadence
sdB subdwarf B
SED Spectral Energy Distributions
S/N Signal-to-Noise Ratio
STELUM STELlar modeling from the Université de Montréal

Introduction

For centuries, astronomers tried to observe farther and farther, convinced that stars would never reveal their deepest secrets, carefully hidden behind a sealed surface. This idea resonated through generations until this book, *The Internal Constitution of the Stars*, written by Eddington in 1926, uncovered a breach. Yes, it is possible to know what is happening inside, beyond the surface, thanks to the analysis of stellar pulsations, introducing what is called now asteroseismology.

More recently, in the past 15 years, our understanding of pulsating stars advanced significantly, largely due to space telescopes, such as *CoRoT* (2006-2014), *Kepler* (2009-2018) and *TESS* (2018-ongoing). The continuous and precise monitoring of stellar light curves by these telescopes has guided asteroseismology forward, enabling the development of techniques to probe with improved precision stellar interiors.

The main goal of this work is to identify the pulsation gravity (g-) modes of hot subdwarf B (sdB) stars observed by space telescopes. A review of pulsating sdB stars observed in the original *Kepler* field is first presented, in order to select one star to focus on in this work. In this context, KIC5807616 (also known as Kepler-70 or KPD 1943+4058) is studied using a specific methodology based on clear quality criteria, aiming to reduce as much as possible the arbitrary nature of mode identification. The sdB star TIC441725813 (TYC 4427-1021-1), observed by *TESS* and recently studied by Su et al. (2024), who proposed a complete mode identification using their own approach, is also studied to test and develop the methodology used in this work. The mode identification aims to be integrated in seismic modeling of sdB stars, contributing to research in the field.

First, chapter 1 introduces the key theoretical concepts of this master thesis. It begins with an overview of sdB stars in the context of stellar evolution. The chapter then dives into the physics of stellar light curves. Then, the current sdB stellar models and the method for carrying out asteroseismic modeling are explained. Finally, the main goals of this work are presented.

Then, chapter 2 presents the methodology developed in this work. It covers the whole process starting by the observational data from *Kepler* and *TESS*, continuing with the frequency extraction process with the dedicated code FELIX and ending by the main techniques to identify pulsation modes from rotationally-splitted components and asymptotic period spacing.

After that, chapter 3 provides an overview of the 18 pulsating sdB stars observed in the original *Kepler* field, including a literature review and analysis of the Lomb-Scargle periodograms associated to their light curves. The selection of KIC5807616 as the main target of this work is then presented.

Chapter 4 presents the results of the identification of pulsation modes. First, the identification of TIC441725813 is performed and compared to the literature, validating the methodology of chapter 2. Then, the main identification of KIC5807616 is presented. The details of the implementation of the methodology are also discussed in this chapter.

Finally, a general conclusion and perspectives of this work are presented.

Chapter 1

Theoretical Background

Mode identification consists in determining the geometrical properties of pulsation modes, such as their angular degree ℓ, azimuthal order m and radial order k. Mode identification makes the bridge between observations and their exploitation to constrain stellar models. The properties of stellar pulsations being a direct consequence of the stellar internal structure, they can be used to constrain stellar models, through a technique called asteroseismology.

This chapter is dedicated to the description of the important theoretical concepts used in this work. First, an overview of subdwarf B (sdB) stars and their place in stellar evolution is presented. Then, several concepts from asteroseismology, the theory behind pulsations in stars, are explained. After that, the current sdB models and method for asteroseismic modeling are described. Finally, the chapter ends by explaining the main goals of this master thesis.

1.1 Hot subdwarf B stars

Before diving in stellar pulsations, it is important to have an idea of the typical structure of sdB stars and their location in stellar evolution. Explanations given in this section are based on the lectures from Dupret (2025) [1] and the PhD thesis from Van Grootel (2008) [2].

During their evolution on the so-called main sequence, stars begin their life by burning hydrogen into helium in their core. As the main sequence ends, the core becomes increasingly rich in He and poor in H, leading the contraction of the core while H fusion continues in a surrounding shell. In this phase, the star slowly climbs the Red Giant Branch (RGB) of the Hertzsprung-Russell (HR) diagram, and the core is increasingly growing in mass due to the H-burning shell. This phase is characterized by a very dense He core and a very diluted envelope, with a thin H-burning shell in between.

For low-mass stars ($M < 2.2 M_\odot$), the degeneracy is attained before reaching the temperature required to enable He fusion by the triple-α process, which fuses three He nuclei into C. The fusion starts in the degenerate core, where pressure does not depend on temperature, but the triple-alpha reaction rate is highly sensitive to temperature (scaling as $\approx T^{40}$). Thus, an increase of temperature leads to an even more efficient production of energy. However, due to the degeneracy, the core cannot expand in response to this heating, which would normally act as a cooling mechanism. Consequently, there is a thermal

runaway until the lifting of this degeneracy. This event is called the helium flash and results in a core helium-burning (CHeB) star.

In the HR diagram, CHeB stars are located in the Horizontal Branch (HB) and have the particularity to nearly all have the same He core mass, around 0.470 $M_\odot$[1]. Thus, CHeB stars are classified depending on the mass of their envelope M_{env}. As the mass of the core does not change, their effective temperature is higher when the mass of their envelope is smaller.

Stars on the HB burn He in their core, and also H in a shell above it. When He is exhausted in the core, the HB stars generally climb the Asymptotic Giant Branch (AGB) in the HR diagram. During the second part of their life on the HB, when enough C is available, the fusion of He and C into O is also happening in addition to the triple-alpha process. After that, their mass is not high enough to trigger C or O burning, so there will no be another burning phase in the core. During the AGB phase, the star has a core constituted of carbon and oxygen (C-O) and simultaneously have a He-burning shell and a H-burning shell. Finally, the external envelope is expelled and the star ends its evolution as a white dwarf.

This master thesis focuses hot subdwarf B (sdB) stars, which are CHeB stars having the particularity to have lost nearly all their hydrogen envelope during the RGB, and that are therefore in the blue (hot) end of the HB, the so-called Extreme Horizontal Branch (EHB), of the HR diagram. EHB stars corresponds to CHeB stars with envelope mass $M_{\text{env}} < 0.01 M_\odot$ [3]. As a consequence, such stars do not have H-shell burning above the He-burning core. As another consequence, such stars, contrarily to stars located in the HB, are not ascending the AGB at the end of the He-burning phase. They follow alternative and more direct ways to end up as white dwarfs. To summarize, a schematic representation of the evolution of low-mass star is shown on Fig. 1.1.

As indicated in their name, sdB stars have the spectral type B, with similar effective temperatures of main sequence OB stars but with a much lower luminosity of 10-100 $L_\odot$ (hence the sub-dwarf term) [5]. Their effective temperature ranges between 20,000 K and 40,000 K, while their surface gravities $\log g$, defined as

$$\log g = \log\left(\frac{GM}{R^2}\right), \tag{1.1}$$

are between 5.0 and 6.2 [5]. These stars being characterized by their He-burning core covered by a $M_{\text{env}} < 0.01 M_\odot$ envelope, their typical mass is around $0.47 M_\odot$. Their mass distribution is indeed peaked around this value, as shown by Fontaine et al. (2012) [6] from asteroseismology and eclipsing binaries, and by Schaffenroth et al. (2022) [7] from masses computed from the spectroscopic $\log g$ and the radius derived by Spectral Energy Distributions (SED) fitting. The internal structure and chemical stratification of sdB stars is illustrated on Fig. 1.2. On the left, the star is represented as a function of its radius and on the right, as a function of its mass fraction $\log q$, defined as

$$\log q = \log\left(\frac{1 - M(r)}{M_*}\right), \tag{1.2}$$

[1] CHeB stars from stars having $> 2.2\ M_\odot$ ignite He core fusion under non-degenerate conditions, and show a wider range of core masses. Such more massive progenitors are much more rare, though.

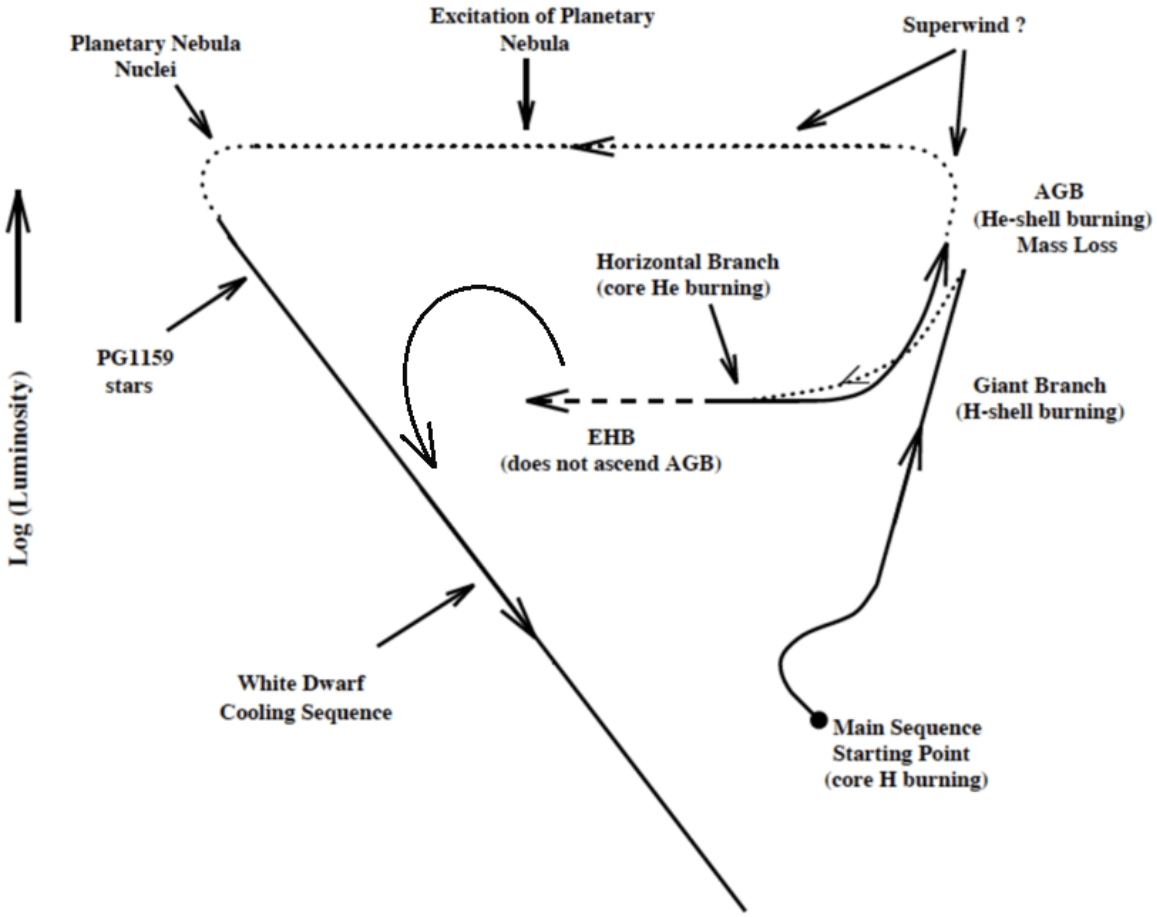

Figure 1.1: Representation of the evolution of a low-mass star in the HR diagram [4].

where $M(r)$ is the mass contained from the center to the radius r and M_* the total mass of the star. As the envelope is very thin, the representation of the different chemical layers with respect to $\log q$ is useful to have a better visualization of envelope and superficial layers.

The core of sdB stars is divided in two parts: the convective core (I), where He is burnt and the radiative core (II), mostly composed of He. In the convective core, He is burnt through the triple-α process, and is transformed in C. At some point of the evolution, enough C is available to fuse He and C into O. Hence, the convective core is composed of He, C and O. As the temperature decreases with the distance to the center of the star, the He burning becomes rapidly difficult to be triggered for higher radii and stops at some point, constituting the border between the convective and radiative zones (between I and II). This transition between the convective and the radiative parts of the core is the main uncertainty in stellar sdB models [8]. In the radiative core (II), the temperature is too low to trigger nuclear burning and thus it is mostly composed of He (in sdB literature, this radiative part of the core is often referred to as "the mantle"). The presence of He in this zone results from the main sequence phase described before. Continuing towards the surface, the envelope (III and IV) is a radiative region in sdB stars. For the cooler sdB stars having the most "massive" envelope, $M_{\rm env} \sim 0.01 M_\odot$, there is a small H-burning shell at the base of the envelope, of negligible power. Because the envelope is radiative, He sinks during the evolution on the EHB, so there is a He+H envelope of approximately solar

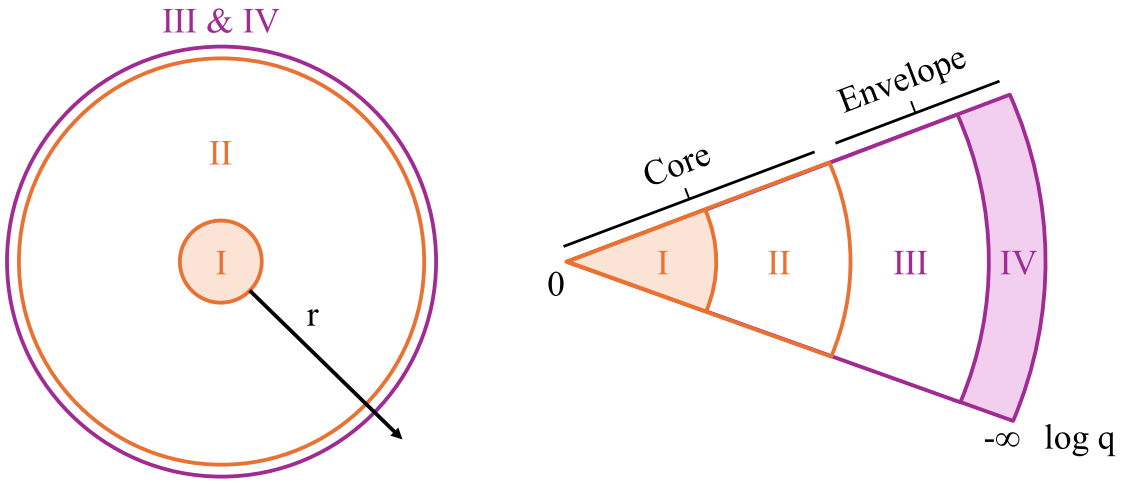

Figure 1.2: Illustration of the typical chemical structure of a sdB star [2]. Details about the different parts are available in the text. Note that this illustration is not scaled and aims to give orders of magnitude.

composition (III), surrounded by an almost pure H envelope (IV). Some heavier elements, like iron, can levitate in the radiative envelope, leading to local overabundances.

The modeling of sdB stars is still challenging, and very recently, Guyot et al. (2025) [8] proposed several possible structures for sdB stars. For the moment, the transition zone between the convective core and the radiative core is the main uncertainty in stellar models. Current models are discussed later in Sec. 1.3.

1.2 Asteroseismology

The main purpose of this work is to to identify the geometrical properties ℓ, m and k of the gravity modes observed in sdB stars. Stellar pulsations are the topic of asteroseismology, and it is thus important to have a sufficient background in order to properly understand the main outcomes of this master thesis. The description provided here is inspired by the work of Aerts et al. (2010) [9] and the lecture slides from Dupret (2024) [10], where most of the mathematical derivations are provided.

1.2.1 Starting equations

The theory of stellar pulsations is governed by the equations of hydrodynamics. Neglecting the rotation of the star, and assuming adiabatic pulsations (no heat exchange with the medium), the equations of hydrodynamics are given by the conservation of mass, also known as the continuity equation,

$$\frac{\partial \rho}{\partial t} + \nabla \cdot (\rho \mathbf{v}) = 0 \ , \tag{1.3}$$

the conservation of momentum, where the viscosity is neglected,

$$\frac{\partial \mathbf{v}}{\partial t} + \mathbf{v} \cdot \nabla \mathbf{v} = -\nabla \Phi - \frac{\nabla P}{\rho} \ , \tag{1.4}$$

and the Poisson equation

$$\nabla^2\Phi = 4\pi G\rho \ . \tag{1.5}$$

In this system, ρ represents the density, $\mathbf{v}$ is the velocity vector and P the pressure. The gravitational field Φ is also linked to ρ by the Poisson equation. The adiabatic relation is finally used to link ρ and P, completing the system of equations. It is given by

$$\frac{d\ln P}{d\ln\rho} = \left.\frac{\partial\ln\rho}{\partial\ln\rho}\right|_s \equiv \Gamma_1 \ , \tag{1.6}$$

where s is the entropy (constant in this case) and Γ_1 the adiabatic index. Usually, stellar models are not assuming adiabaticity and instead include the conservation and transport of energy equations, as this effect becomes non-negligible for some parts of the star. In our introductive case, we are nevertheless sticking to the adiabatic stellar pulsations.

The stellar pulsations theory assumes that quantities in stars, such as ρ or P, are pulsating around an equilibrium value obtained by cancelling all time derivatives. Then, if the amplitudes of pulsations are small, the system can be linearized owing to the small perturbations theory. In this theory, two formalisms are used: Eulerian and Lagrangian. The Eulerian formalism studies the variation of a quantity at a fixed point of the space and is not following the motion. An Eulerian perturbation is expressed as

$$X(\mathbf{r},t) = X_0(\mathbf{r}) + X'(\mathbf{r},t) \ , \tag{1.7}$$

where $X(\mathbf{r},t)$ is the value of the quantity at a time t, $X_0(\mathbf{r})$ the equilibrium value and $X'(\mathbf{r},t)$ the perturbed quantity in the Eulerian formalism. The Lagragian formalism follows the motion of an element of mass m, and a perturbed quantity is given by

$$X(\mathbf{r},t) = X_0(\mathbf{r_0},t) + \delta X(\mathbf{r},t) \ , \tag{1.8}$$

where $\delta(\mathbf{r},t)$ is the perturbed quantity in the Lagragian formalism. Using Taylor series, the link between both descriptions can be obtained, and is given by

$$\delta X(\mathbf{r},t) \simeq X'(\mathbf{r},t) + \delta\mathbf{r}\cdot\nabla X_0(\mathbf{r},t) \ , \tag{1.9}$$

where $\delta\mathbf{r}$ is the displacement, for which the time derivatives gives the velocity $\mathbf{v}$. After linearization and the substraction of equilibrium values, the initial system constituted of Eqs. (1.3), (1.4) and (1.5) for small perturbations is given by

$$\rho' + \nabla(\rho_0\delta\mathbf{r}) = 0 \ , \tag{1.10}$$

$$\frac{\partial^2\delta\mathbf{r}}{\partial^2 t} = -\frac{\nabla P'}{\rho_0} - \nabla\Phi' + \frac{\rho'}{\rho_0^2}\nabla P \text{ and} \tag{1.11}$$

$$\nabla^2\Phi' = 4\pi G\rho' \ , \tag{1.12}$$

where the subscript 0 is used for equilibrium quantities. The adiabatic relation finally links ρ' and P'.

1.2.2 Geometrical properties of pulsation modes

As no rotation is assumed, the spherical symmetry is maintained and the problem can be expressed in spherical coordinates (r, θ, ϕ). The linearized system of partial derivatives is solved by using the separation of variables given by

$$X'(r,\theta,\phi,t) = X'(r)Y_\ell^m(\theta,\phi)e^{i\sigma_{kl}t} \ , \tag{1.13}$$

and following the development of Unno et al. (1989) [11]. $Y_\ell^m(\theta,\phi)$ are the normalized spherical harmonics, expressed as

$$Y_\ell^m(\theta,\phi) = (-1)^m \frac{(2\ell+1)(\ell-m)!}{4\pi(\ell+m)!} P_\ell^m(\cos\theta)e^{im\phi} \ . \tag{1.14}$$

In this expression, a Legendre polynomial P_ℓ^m and the geometrical properties of pulsation modes ℓ and m appear. The numbers ℓ and m are thus defined as the indices of the spherical harmonic function specifying the mode's angular geometry [12]. The ℓ number takes integer values higher or equal to 0, and the m number can take (2 ℓ + 1) integer values between ℓ and -ℓ. In stars, purely radial pulsations are characterized by ℓ = 0, meaning that quantities only have a radial motion. Modes corresponding to $\ell > 0$ are denoted non-radial modes, and are the result of a combined radial and horizontal pulsations. Finally, as the system is linear, the solution is given by the following sum:

$$X'(r,\theta,\phi,t) = \sum_{k,\ell,m} \alpha_{k\ell m} X'_{k\ell m}(r,\theta,\phi,t) \ , \tag{1.15}$$

where the coefficients $\alpha_{k\ell m}$ are the amplitudes of modes having the components k, ℓ and m. In stars, modes are fully defined by their k, ℓ and m "quantum" numbers. The number k represents the number of radial nodes the pulsation mode has from the center to the surface of a star. Concerning ℓ, introduced in Eq. (1.13), it represent the number of nodes appearing at the surface and is also known as the angular degree. The number m, also known as the azimuthal order, represents the number of nodes, among the ℓ surface nodes, that are appearing as longitudes of the star, i.e. surface lines that are perpendicular to the equator of the star. A representation of the spherical harmonics for several (ℓ, m) configurations is shown on Fig. 1.3.

The spherical harmonics described here have a direct consequence on the possible observations. Increasing the degree ℓ leads to more pulsating regions with opposite velocity. Consequently, since the observed luminosity is integrated over the entire visible hemisphere for a distant observer, the spatial features become harder to resolve [13]. For stars as observed from the Earth (including sdB stars), observed pulsation modes are mostly ℓ = 0, 1 and 2 modes. Higher degrees (ℓ = 4, 6) are possible only in the best observations. This effect represents what is called partial cancelling, and the higher the effect, the closer the cancelling will be to 0, no matter the sign. To estimate it for non-radial modes, Aerts et al. (2010) [9] integrated the $m = 0$ spherical harmonics $Y_\ell^0(\theta,0)$ (see Eq. (1.13)) over the disk for θ between 0 and 90°, shown on Fig. 1.4.

In sdB stars, p-modes can correspond to radial modes, but not g-modes, which are always non-radial pulsations, i.e. $\ell > 0$. In this work, the mode identification focuses g-modes, thus $\ell = 1$, $\ell = 2$ and possibly $\ell = 4$ pulsation modes. It is also expected to observe more $\ell = 1$ than $\ell = 2$ (and a fortiori $\ell = 4$) modes.

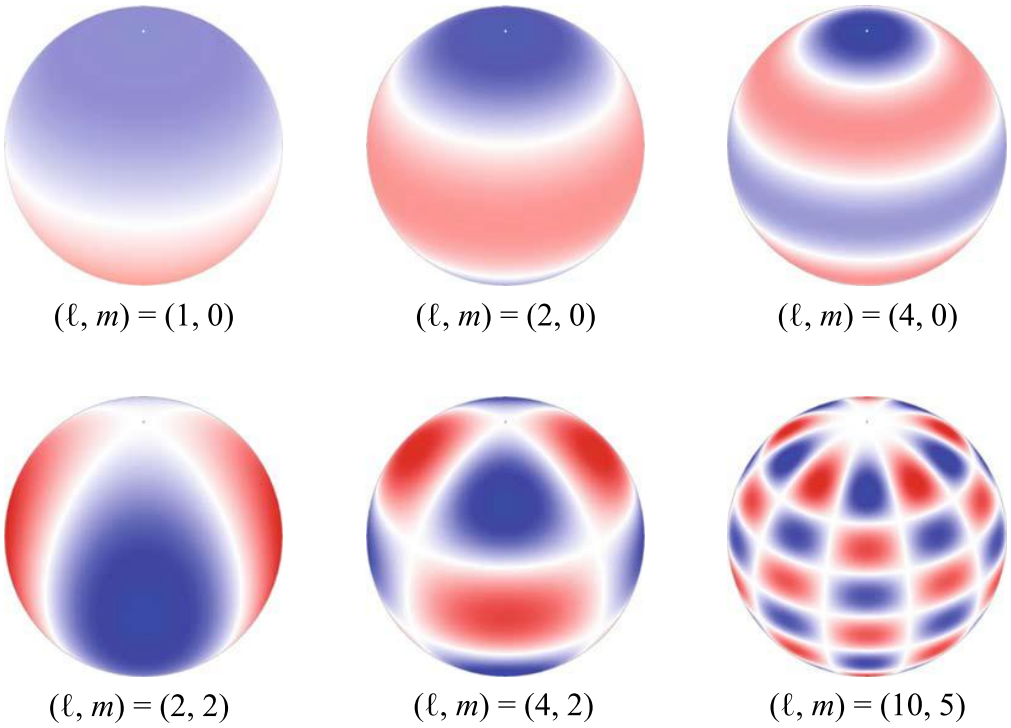

Figure 1.3: Representation of the radial components of some specific modes defined by their ℓ and m components, for an observer placed at an inclination angle of 55° [9]. The blue and red colors stand for a radial component towards the center and away from it, respectively. The white color represents nodes occurring at the surface.

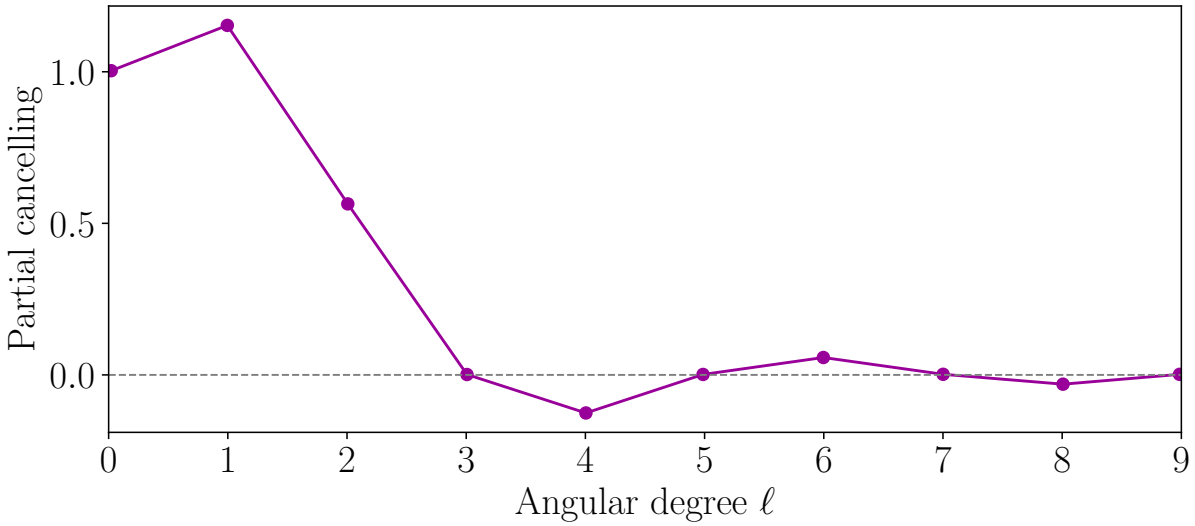

Figure 1.4: Representation of the partial cancelling of modes as a function of the angular degree ℓ between 0 and 9, normalized to the $\ell = 0$ radial mode [9]. Note that the limb darkening effects on the stellar surface are neglected.

When there is no rotation, there is not privileged axis in the star. This means that the frequencies corresponding to pulsation modes having the same (k, ℓ) but different m numbers are the same. In this case, modes are said to be degenerated [12]. However, for slow rotation, this is no longer the case and such modes are rotationally splitted, having nearly the same frequency spacing between components. This will have an impact on the mode identification, and a more detailed description will be provided in Sec. 2.3.3.

1.2.3 Pressure and gravity modes

Coming back to the adiabatic system of equations in spherical coordinates, the displacement vector $\boldsymbol{\xi}$ can be defined as [11]:

$$\boldsymbol{\xi} = \left[\xi_r(r), \xi_h(r)\frac{1}{\partial\theta}, \xi_h(r)\frac{1}{\sin\theta}\frac{1}{\partial\theta} \right] Y_l^m(\theta,\phi)e^{i\sigma t}, \tag{1.16}$$

where ξ_r and ξ_h are its radial and horizontal components, respectively. Expressing the system as a function of $\boldsymbol{\xi}$ components, solutions are assumed to be bounded at the surface of the star. Then, under the Cowling approximation (1941) [14], the system of adiabatic pulsations reduces to the equation

$$\frac{d^2\xi_r}{dr^2} + k^2(r)\xi_r \simeq 0, \tag{1.17}$$

where k^2 is the wave number (not to be confused with the number of radial nodes defined before). Note that the simplifications made here essentially aim to have a better understanding of what are called g- and p-modes, and are not done in stellar models and pulsation codes. The wave number is given by

$$k^2 = \frac{\sigma^2}{c^2}\left(\frac{N^2}{\sigma^2} - 1\right)\left(\frac{L_\ell^2}{\sigma^2} - 1\right) \ , \tag{1.18}$$

where c is the sound speed of the mode and σ its frequency. It this expression, two important frequencies are introduced: the Brunt-Väisälä frequency N^2, also known as buoyancy frequency, and the Lamb frequency L_ℓ^2, varying as a function of the radius. The expression of N^2 is given by [8]

$$N^2 = \frac{g^2\rho}{P}\frac{\chi_T}{\chi_\rho}(\nabla_{\rm ad} - \nabla_T + B) \ , \tag{1.19}$$

where ∇_T and $\nabla_{\rm ad}$ are the actual and adiabatic temperature gradients, respectively, given by [8]

$$\chi_T = \left.\frac{\partial \ln P}{\partial \ln T}\right|_\rho \ , \ \chi_\rho = \left.\frac{\partial \ln P}{\partial \ln \rho}\right|_T \text{ and } B = \frac{-1}{\chi_T}\left.\frac{\partial \ln P}{\partial \ln \mu}\right|_{\rho,T}\frac{d\ln\mu}{d\ln P} \ , \tag{1.20}$$

where B is the Ledoux term. On the other hand the Lamb frequency is given by

$$L_\ell^2 = \frac{\ell(\ell+1)c^2}{r^2} \ . \tag{1.21}$$

It can be seen from Eq. (1.17) that N^2 and L_ℓ^2 define propagations cavities ($\sigma^2 > N^2, L_\ell^2$ or $\sigma^2 > N^2, L_\ell^2$), where modes are propagating, and evanescent zones ($L_\ell^2 < \sigma^2 < N^2$ or $L_\ell^2 > \sigma^2 > N^2$), where the amplitude of modes is decreasing exponentially (same mechanism as quantum tunnelling). In stars, two distinct propagation cavities exist, each associated with different types of pulsation mode: pressure modes ($\sigma^2 > L_\ell^2$ and N^2), denoted p-modes, and gravity modes ($\sigma^2 < L_\ell^2$ and N^2), denoted g-modes. These cavities are sources of information about the stellar interior, as the pulsation modes mainly propagate within them.

The p-modes are comparable to acoustic waves propagating in the envelope of the star, governed by the pressure as the restoring force of the perturbation. As the cavity is wider for greater values of σ^2, the number of radial nodes k increases with respect to σ^2. They are primarily associated to the profile of the sound speed $c(r)$ and by extension bring important information about the physical conditions in the envelope.

Concerning g-modes, they are the result of the buoyancy restoring force, and are located in the radiative parts, generally in deeper layers than p-modes. The smaller the pulsation frequency σ^2, the higher the number of radial nodes k in this case. In the asymptotic regime, characterized by $k \gg \ell$, the g-mode pulsation periods of consecutive k tend to be equally spaced [15, 16]:

$$\Delta P = P_{\ell,k+1} - P_{\ell,k} \approx \frac{2\pi^2}{\sqrt{\ell(\ell+1)}} \left(\int_{r_b}^{r_t} \frac{|N|}{r} \mathrm{d}r \right)^{-1} = \frac{\Pi_0}{\sqrt{\ell(\ell+1)}} \,, \tag{1.22}$$

where Π_0 is the reduced period spacing in the asymptotic limit. The radii r_t and r_b are the radius of the upper and lower boundary of the g-mode cavity, respectively. This property is the starting point of the mode identification from period spacing used in this work.

The mentioned p- and g-mode cavities can be highlighted in a propagation diagram, showing the location in the star on the x-axis and the frequency σ^2 on the y-axis. Such diagrams were made very recently by Guyot et al. (2025) [8] for several sdB models. One of them is presented on Fig. 1.5, on the left (Fig. 1.5a) as a function of the mass $m(r)$ inside a radius r, and on the right (Fig. 1.5b) as a function of $\log g$, highlighting the envelope of the star. In this diagram are represented the theoretical $\ell = 1$ g-modes of the sdB (horizontal red lines) for each radial order k. N^2 and L_1^2 (L_ℓ^2 for $\ell = 1$) are also represented in blue and in green, respectively. One clearly sees the g-mode propagation cavity for σ^2, smaller than both Brunt-Väisälä and Lamb frequencies, and where all radial nodes are located. The p-modes are not shown in this diagram but their cavity can be guessed in Fig. 1.5b, corresponding the zone in between $\log q = -2$ and nearly the surface of the star, for $\log \sigma^2$ higher than N^2.

In some stars like red giants, there can be frequencies for which modes propagate in both g- and p-mode cavities. Such modes are called mixed modes and are difficult to characterize. The fact that sdB stars have extremely thin envelope make them very interesting to study in practice, as pure g-modes and p-modes can be directly observed. Observations of pulsating sdB stars have shown that these objects typically have either only g-modes, only p-modes, or both. The latter are therefore classified as hybrid pulsators. An overview of observations made with the *Kepler* space telescope for sdB pulsators of interest is conducted in Chap. 3.

The last key concept of this section is the mode trapping. Some modes, said to be trapped, propagate preferentially (have more important amplitudes) in certain sub-cavities of the

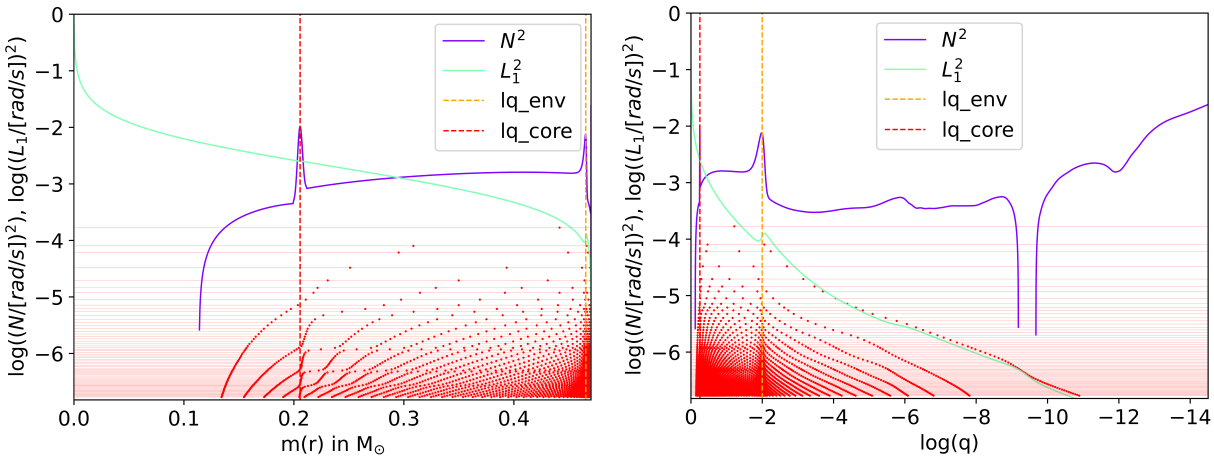

(a) Focus on the core.

(b) Focus on the envelope.

Figure 1.5: Propagation diagram of a sdB star model for $\ell = 1$ g-modes, from $k = 1$ to $k = 70$ g-modes [8]. Horizontal lines are the frequencies of different radial orders k and the red dots indicate the location of the radial nodes. The "lq_env" line marks the boundary between the core and the envelope and the "lq_core" line marks the boundary between the convective and the radiative parts of the core.

star, called the trapping regions. Mode trapping witnesses the presence of sharp chemical composition changes or convective-radiative transitions [8], sometimes referred to as "structural glitches" in asteroseismology literature. Mode trapping occurs when the structural changes take place on scales comparable to (or smaller than) the local wavelength of the mode, which provokes partial reflection of the mode on this structural change. Trapped modes are especially interesting for the study of sdB stars and He-burning cores in general as they are trapped in the region just above the convective core (bottom of the region II in Fig. 1.2), as recently shown by Guyot et al. (2025) [8]. This region is also clearly visible in Fig. 1.5a, where an important N^2 change occurs around the "lq_core" vertical line. The identification of trapped modes in the observed frequency spectrum thus carries precise information about this transition zone, which is the main uncertainty in stellar models [8].

In a sequence of observed g-modes of same degree ℓ, such trapped modes typically show a much smaller period difference with their neighbors of adjacent radial orders, leaving a minimum in the period spacing sequence. Indeed, Eq. (1.22) shows that the period spacing is affected by changes of N. At the time of writing, observations of 4 sdB pulsators revealed the potential presence of mode trapping [17, 18, 19, 20]. Their identification is thus possible, provided a high amount of detected modes.

It is finally worth mentioning that pulsations in sdB stars are excited due to a non-adiabatic process called the κ-mechanism. In sdB stars, pulsations are driven by an opacity bump caused by the local overabundances of heavy elements (like Fe) in the envelope [21, 22].

1.3 Stellar models and seismic modeling

Structure models of sdB stars are of several nature, static and evolutionary [8]. Static models are mainly developed for seismic modeling (see next paragraph) and are defined from a series of input parameters, independently from stellar evolution. The main philosophy behind this strategy lies in the greater flexibility that static models offer for seismic modeling, in contrast to evolutionary models. Also, when using static models, stellar structures are much less dependent on uncertainties accumulating over time through stellar evolution, instead acquiring an "instantaneous" structure corresponding directly to the pulsation modes propagating in the star. This aspect is often ignored despite being very sensitive for evolved stars [8].

Several generations of sdB static models exist, with the third (3G) one presented in Van Grootel et al. (2013) [23] and the 4G ones presented in Guyot et al. (2025) [8] (see these papers for a full description of these models). Evolutionary models for sdB stars also exist, as computed by stellar evolution codes such as Modules for Experiments in Stellar Astrophysics (MESA) [24] or STELlar modeling from the Université de Montréal (STELUM) [25].

Each type of static or evolutionary model has its own prescription for the transition between the convective He/C/O core and the radiative He mantle, leading to different thermal and chemical stratifications. Through seismic modeling, it is hoped to disentangle the various models and select which He-burning core description best reproduces the observed pulsation spectra and best describes the actual stars [8].

The main goal of seismic modeling by using the direct (or forward) modeling approach is to match as best as possible the theoretical frequencies as computed from stellar models with observed frequencies, also reproducing other observational non-seismic constraints. The non-seismic constraints are related to stellar properties that can be inferred without asteroseismology. Examples of non-seismic parameters are the luminosity $L/L_\odot$, the effective temperature $T_{\rm eff}$ or the surface gravity $\log g$ from spectroscopy, the radius R from interferometry or as derived from SED fitting. First, a set of N free parameters, denoted $\mathbf{a}$ is guessed, depending on the model. For static sdB models, it could be [8]:

- the total mass M_*;
- the masses contained in different zones of the star, such as $M_{\rm core}/M_*$ (mass contained from the center to "lq_core", in Fig. 1.5) and $M_{\rm env}/M_*$ (from "lq_env" to the surface);
- the mass of the pure H envelope (region IV in Fig. 1.2);
- the abundances of He, C, O, and Z (metallicity) in the core, as well as the abundance of H in the He+H envelope (region III).

Then, an iterative process is done to minimize a merit function χ^2, given by

$$\chi^2 = \sum_{i=1}^{N} \frac{(x_{\rm th,\,i}(\mathbf{a}) - x_{\rm obs,\,i})^2}{\omega_i} \,, \tag{1.23}$$

where $x_{\rm th,\,i}(\mathbf{a})$ is the theoretical value obtained from a guess on $\mathbf{a}$, $x_{\rm obs,\,i}$ the observed value and ω_i a chosen weight factor. Then, the set of free parameters is changed until having a satisfactory model, minimizing χ^2.

In practice, this technique gives most of the time a high amount of different solutions when observed frequencies are directly compared the to the model frequencies, even in the presence of tight non-seismic constraints. Identifying the geometrical properties of observed pulsation modes greatly eases the optimization process and reduced the number of possible seismic solutions. However, even if mode identification is based on known period spacing features, the part of arbitrary remains large. In the literature, the identification with period spacing typically involves trial-and-error processes to attribute the values of k and ℓ, guided by the observed rotationally-splitted modes frequency spacings, until a satisfactory model is achieved.

1.4 Aim and Scope of the work

The primary goal of this work is to identify the g-mode pulsations in sdB stars, in order to make the bridge between observations and their integration in seismic modeling of sdB stars. To support this, a review of pulsating sdB stars from the original *Kepler* field is first provided, serving as a basis for the selection of KIC5807616 as the main studied star. This review, presented in Chap. 3 depicts for all sdB stars observed by *Kepler* their Lomb-Scargle periodograms, in order to determine their p-mode, g-mode, or hybrid behavior.

In this context, the study is performed by using a dedicated methodology built on a few clear quality criteria, presented in Sec. 2.4, with the aim of minimizing the part of arbitrary typically involved in mode identification. To verify and further confirm the used methodology, a preliminary study in performed on TIC441725813, observed by *TESS* and on which a mode identification has already been made by Su et al. (2024) using their own methodology. Finally, the main identification of KIC5807616 is performed. The derived possible configurations are intended to be incorporated into future seismic modeling of this star.

Chapter 2

General methodology

This section aims to describe in detail the instruments, numerical tools, and methods used for the identification of the pulsation modes. This description is divided in three main parts. First, the observations by *Kepler* and *TESS* space telescopes are downloaded from the *Barbara A. Mikulski Archive for Space Telescopes (MAST)* [26] observational data. Then, the extraction of the frequencies of the pulsation modes is performed with the code FELIX [27, 28]. Finally, the main process to identify extracted pulsation modes by using different techniques is described.

2.1 Telescope data

KIC5807616 and TIC441725813 have been observed by the *Kepler* and *TESS* space telescopes, respectively. These telescopes were primarily dedicated to the detection of exoplanets by using the transit method. Briefly, the detection of a potential exoplanet can be done by monitoring the flux coming from a star as a function of time, to obtain what is called a light curve. When a potential planet passes in front of the observed star, there is a drop in the incoming flux coming to the observer. The properties of the transit drop can be used to infer some exoplanet's properties.

In addition to transit, the mostly uninterrupted, long duration and high precision photometry offered by space telescopes allow us to accurately observe stellar pulsations. Until that time, observations were made from the ground. Pulsation gravity modes of sdB stars, given their long periods (1-3 hours) and low amplitudes ($<$0.1% of the star's mean flux), are very difficult to observe from the ground, but the principle of the method is the same. A general description of *TESS* and *Kepler* space telescopes is presented in the next paragraphs.

2.1.1 *Kepler* space telescope

The *Kepler* mission was the first mission searching for exoplanets of the National Aeronautics and Space Administration (NASA). The *Kepler* space telescope was in a Earth-trailing heliocentric orbit, offering thermally stable environment and allowing the telescope to point the same area for the duration of the primary mission. The telescope was pointing towards a 105x105 degrees field located in the Cygnus-Lyrae region [17]. This field is often referenced as the original *Kepler* field and is denoted this way in this work. The satellite was equipped with a 0.95m aperture Schmidt telescope and the imager with 21

Charge-Coupled Device (CCD) modules (2 CCDs per module), reaching a resolution of 4 arcseconds per pixel. Concerning the wavelength range, *Kepler* observed in one broad bandpass between 420 and 900 nm, centered on the R_C band.

Observations of the original *Kepler* field were divided in quarters representing a duration of 3 month (90 days) each and denoted QX.Y (X for the quarter number and Y for the monthly sub-quarter), except for Q1, which had a duration of 33.5 days [29]. Observations started the 2nd of May 2009 (Q0) and stopped the 11st of May 2013 (Q17.2), due to the failure of the second reaction wheel. A survey for pulsating stars was conducted the first year (Q0-Q4) and observed for at least one quarter of a total of 72 sdB stars at a Short Cadence (SC) of 1 min. The survey revealed 18 pulsating sdB stars [29], for which more SC quarters were attributed to have a nearly continuous dataset for the rest of the mission. In parallel, Long Cadence (LC) observations of 30 min were made on them, as well as for most of remaining sdB stars of the field. Pulsating sdB stars of the original *Kepler* field are still actively studied, and KIC5807616 is one of them.

It is worth mentioning that, after the second reaction wheel failure, the satellite was still able to point fields around the ecliptic. The mission was rebranded *K2*, redesigned to observe these new fields for a duration of about 80 days each, denoted campaigns. The mission started in March 2014 until July 2019 for a total of 19 campaigns (0 to 18) [29]. The mission ended because no more propellant was available. More sdB stars were observed with the *K2* mission, but most of them were observed for only one or two campaigns either in SC, LC or both [29].

2.1.2 *TESS* space telescope

TESS, for Transiting Exoplanet Survey Satellite, was launched by NASA and its operations started in July 2018 for an initial mission duration of 2 years, aiming to cover ∼90% of the whole sky, divided in 13 sectors per hemisphere (S1 to S26). These sectors are nearly continuous strips of the sky of 24x96 degrees observed about 27 days each. To cover the entire field of view (FOV), *TESS* is equipped with 4 identical refractive telescopes having a FOV of 24x24 degrees. Each of them is composed of 4 CCDs, a lens assembly and a lens hood. The lens assembly has a an entrance diameter of 10.5 cm, allowing to have a resolution of 21 arcseconds/pixel. Unlike the *Kepler* space telescope, *TESS* observes in wavelengths between 600 and 1000 nm, centered on the I_C filter [30]. Concerning its orbit, it uses a high-Earth elliptical orbit, having the advantage to be more stable to do precise photometry, compared to Low Earth Orbit (LEO) options [31].

Sectors are overlapping especially for high ecliptic latitudes and allow some stars to be observed for long durations [32]. The primary mission ended in July 2020, but it was extended with the goal to revisit all already observed sectors. To refer to those new sectors, the count is simply increased from S26. At the time of writing (June 2025), after 8 years of operations, the mission is still ongoing and overview again nearly the whole sky, including some ecliptic, northern and southern surveys [33].

The primary mission was conducted with SC observations of 2 min sampling for selected stars and a sampling of 30 min for Full-Frame Images (FFI), containing all stars in the FOV for the corresponding sector [29]. The extended mission proposed an ultrashort cadence of 20s for a limited number of targets, the 2-min SC observations, and FFIs now with a cadence of 10 min.

2.2 Frequency extraction with FELIX

The code FELIX, for Frequency Extraction for LIght curve eXploitation [27, 28] has been developed by S. Charpinet, and aims to extract the properties of pulsation modes in time-series data, in particular for pulsating sdB data analysis. The extraction process with FELIX is summarized in Fig. 2.1.

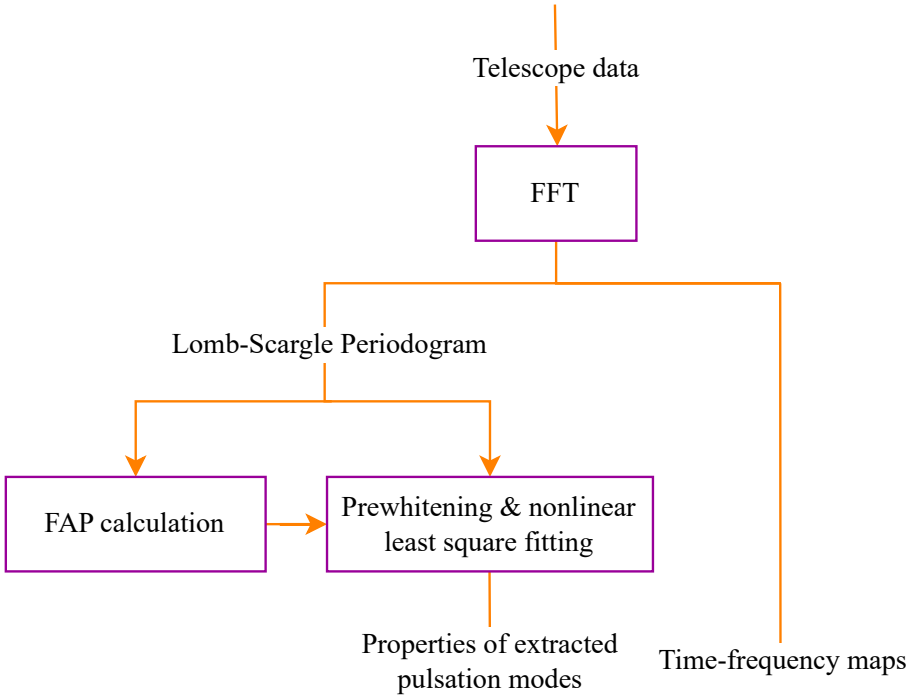

Figure 2.1: Summary of the extraction process by FELIX. The purple boxes represent the different steps of the process and the orange lines their inputs and outputs.

Starting with light curves downloaded from telescope data, a Fast Fourier Transform (FFT) is computed on the temporal data to highlight the periodicities and the result is displayed as a Lomb-Scargle Periodogram (LSP) [34]. FELIX uses prewhitening and Non-Linear Least Square (NLLS) fitting techniques to extract the properties of the pulsation modes [35]. The prewhitening technique aims to sequentially subtract in the time domain all periodic variations detected above a predefined threshold in the LSP. The code detects first the highest peak in the LSP and determines its amplitude A_0, frequency f_0 and phase ϕ_0. Taking these values as initial guesses, FELIX uses the Levenberg-Marquardt algorithm to perform the NLLS fit of a cosine wave, defined as [36]

$$y(t) = A\cos\left(2\pi f t + \phi\right) . \tag{2.1}$$

After the fit, the resulting cosine of amplitude A, frequency f and phase ϕ is subtracted from the light curve. The process is then iterated until no more peak is above a defined threshold in the LSP. At each step, except for the first peak extraction, the code reevaluates the model: a new NLLS fit of all extracted frequencies is performed, resulting in updated values for A, f and ϕ [36]. The prewhitening technique is commonly used for heat-driven pulsators, such as sdB stars, as pulsations are perfectly periodic. Indeed, the long lifetimes of heat-driven pulsations, driven by the stellar evolution, is much higher than the duration of typical observations [36].

The predefined threshold is expressed as a Signal-to-Noise Ratio (S/N) level. A S/N = x represents a signal x times stronger than the local noise, estimated within a sliding window of 300 resolution elements, centered at each point of the LSP [36]. Setting the threshold too low will be likely to cause the detection of false peaks, due to the noise of the data. Inversely, having a too large threshold will be more likely to let some low amplitude real physical frequencies undetected. To determine this important threshold, FELIX calculates the False Alarm Probability (FAP) associated to the data. By using the same time sampling and the same window, FELIX artificially builds the LSP of 10,000 light curves only composed of pure gaussian white noise. Then, by iterating over a given range of potential S/N thresholds, it counts the number of times a peak, only due to noise, is above the S/N threshold. Finally, it divides this count by 10,000 to obtain the FAP. In other words, the FAP represents the probability $P_n(x)$ that the number of peaks produced by the noise itself detected above a given S/N threshold ($= x$) is higher than n [27, 28]. Usually, the minimum significance used for frequency extractions is 4σ [36], representing a FAP of 0.0032%. An example of the FAP with respect to the S/N in *Kepler* data, calculated by FELIX, is shown on Fig. 2.2.

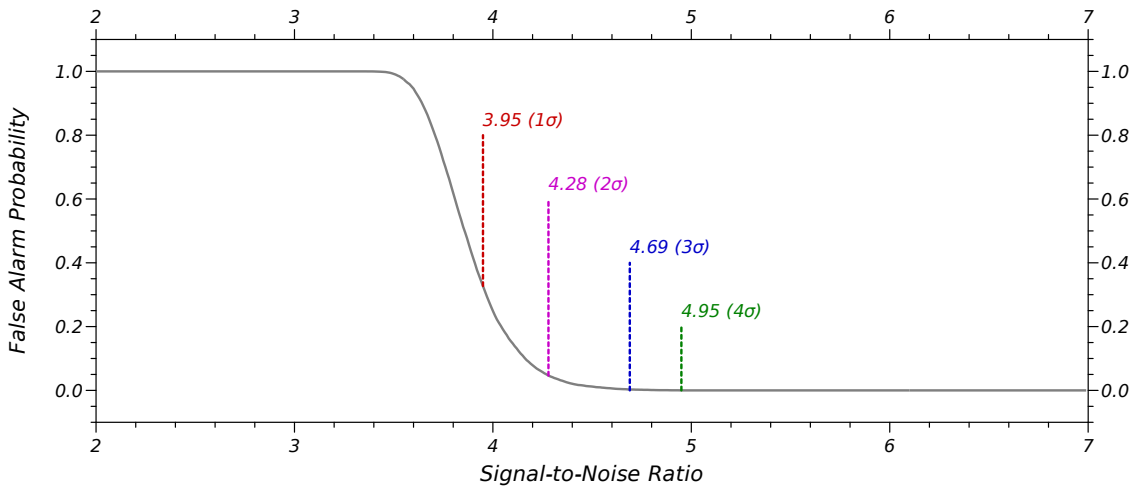

Figure 2.2: False alarm probability with respect to the S/N computed by FELIX corresponding to the LSP, for the Q12 data from *Kepler*, of the pulsating sdB KIC3527751.

The errors on the frequency, period, amplitude and phase are also estimated by FELIX. The code first measures the amplitude error σ_A directly in the LSP. To do so, the median amplitude value σ_A in a chosen window around each frequency is calculated [37]. Then, the phase error σ_ϕ and the frequency error σ_f are obtained from σ_A. They are given by the propagation of random and uncorrelated noise on a NLLS fit of a sinusoidal signal, demonstrated by Montgomery & O'Donoghue [38]:

$$\sigma_\phi = \frac{\sigma_A}{A} \text{ and } \sigma_f = \sqrt{3}\frac{\sigma_A}{\pi T A}\,, \tag{2.2}$$

where T is the total time baseline of the observations and A the amplitude.

When the prewhitening is finished, the frequency f, period P, amplitude A and phase ϕ of the detected peaks are listed, as well as their corresponding errors σ_f, σ_P, σ_A and σ_ϕ. Their S/N is also referenced. With this basis, the mode identification can start. From

the performed FFT, time-frequency maps are also extracted to help the identification. These maps provide an alternative visualization of the frequency content of the data by including its variation over time. Instead of computing a single LSP across the entire time domain, the signal is divided into multiple shorter time windows, for which a periodogram is calculated. Typically, the resulting maps are displayed as heatmaps, with frequency on the x-axis, time on the y-axis, and color indicating amplitude at each point. Using time-frequency maps is therefore useful for having a better idea of how the frequency spectrum evolves over time. In the case of a stable pulsation mode, it should appear as a clear vertical line in the time-frequency map.

2.3 Required steps for the identification of pulsation modes

To obtain an effective mode identification, several steps must be done on the list of extracted frequencies:

1. Removing the potential instrumental artifacts.
2. Removing the frequency modulations.
3. Identifying the rotationally-splitted pulsation frequencies, also known as rotational multiplets.
4. Performing a Kolmogorov-Smirnov test to deduce the period spacing of $\ell = 1$ and $\ell = 2$ pulsation modes, respectively.

Once these steps are done, the identification of pulsation modes from period spacing, which is the core of the mode identification, is carried out. We remind that mode identification means to obtain/derive the possible (k, ℓ, m) indexes of the pulsation modes present in the star. Mode identification is a necessary step of asteroseismic modeling, which aims at constraining models of the structure of the stars.

2.3.1 Instrumental artifacts

When dealing with space telescopes data, the associated LSP can present peaks not related to any pulsation mode or of astrophysical origin, instead originating from instrumental artifacts. All artifacts of *TESS* data are normally already removed by the MAST, so there should not be artifacts in the obtained data. It is not the case for *Kepler* data. The most common artifacts in *Kepler* SC data are linked with the LC readout time [39]. These artifacts are observed the LC sampling rate, $f_{\mathrm{LC}} = 566.4$ μHz and its harmonics:

$$f_{\text{artifact, LC}} = n \times 566.4 \ \mu\text{Hz, n} = 1, 2, 3, \ldots \tag{2.3}$$

In fact, the peak corresponding to the sampling rate is rarely visible in periodograms, contrarily to peaks at $n = 6$, 7 and 8 which are usually the most prominent [40]. As they are not varying much in frequency and amplitude, LC artifacts can easily be spotted [39, 40]. During the process of mode identification, it is thus important to verify if detected frequencies are close to known artifacts, in order to remove them.

Besides LC artifacts, another artifact at a frequency around 80-95 μHz was detected for Q0-Q2. The frequency peak is very likely to be due to the reaction wheel, having the same housing temperature variation [39]. Other spurious periodicities were analyzed by

Baran et al. (2013) [40], for Q0-Q14 SC data for four different stars. These spurious frequencies are also checked if a peak is detected near one of them in our list of extracted frequencies, and was removed in this case.

2.3.2 Frequency modulation clearing

Once extracted frequencies are known, they must be cleared from all frequency modulations. It has been found that amplitudes and periodicities of pulsation modes of sdB stars are varying with time, sometimes with a regular pattern and sometimes not [41, 42]. The most probable cause is the reminiscent of nonlinear weak mode interaction: under certain resonance conditions, pulsations may have temporal changes in their amplitude and frequency [41, 42]. It is thus important not interpreting frequency changes as independent pulsation modes. Frequency modulations $\Delta\nu$ are typically around 10-20 nHz for pulsating sdB stars [42].

The frequency clearing is done with a small algorithm, looping on all extracted modes, following these steps:

1. Selecting the peak with the highest SNR, denoted as $\nu_{\max}$.
2. Removing all frequencies detected within the range $(\nu_{\max} - \Delta\nu)$ to $(\nu_{\max} + \Delta\nu)$.
3. Proceeding to the next highest SNR peak in the updated frequency list, $\nu_{\max,\,\mathrm{new}}$.

In parallel, time-frequency maps of the pulsator are checked. The purpose of this check is to visually determine whether modulations above the initial limit (here 10-20 nHz) are more likely to be the result of a rotationally-splitted mode or a frequency modulation.

2.3.3 Identification of rotationally-splitted modes

In this work, rotationally-splitted modes are denoted multiplets or rotational multiplets. By definition (see Sec. 1.2.2), $\ell = 1$ multiplets, denoted triplets, have three m values: -1, 0 and $+1$. For $\ell = 2$ multiplets, the m number can take 5 values: -2, -1, 0, $+1$ and $+2$. Such modes are denoted quintuplets. When the star is not rotating, the splittings of a given mode are degenerated in m, having the same frequency. In the case of slow rotation, pulsation modes with the same k value can have m components spaced enough to be distinguishable in the list of extracted frequencies. This happens generally at another scale than the frequency modulations explained above, given the rotation periods of sdB stars being about a few days to a few dozens of days (see Sec. 3.3) [12, 32]. The principle is illustrated on Fig. 2.3.

For slow rotation, the frequency spacing of modes having a consecutive m number, but the same ℓ and k, can be obtained by neglecting higher-order terms [12]:

$$\Delta\nu_{k\ell} = \frac{1}{2\pi}\int_0^R K_{k\ell}(r)\Omega_{\mathrm{rot}}(r)dr \ , \tag{2.4}$$

where $\Omega_{\mathrm{rot}}(r) = 2\pi/P_{\mathrm{rot}}(r)$ is the spherically symmetric rotation law (expressed in units of angular frequency) and $K_{kl}(r)$, acting as a weight function, is the first order rotation kernel. It is given by

$$K_{k\ell}(r) = \frac{\xi_r^2 + [\ell(\ell+1)-1]\xi_h^2 - 2\xi_r\xi_h}{\int_0^R [\xi_r^2 + \ell(\ell+1)\xi_h^2]\rho r^2 dr}\rho r^2, \tag{2.5}$$

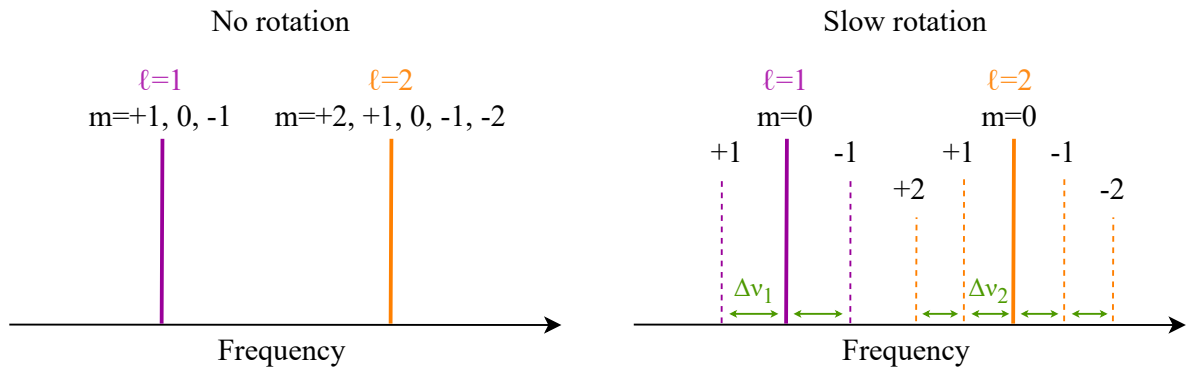

Figure 2.3: Illustration of the effects of slow rotation on pulsation modes [12].

where ξ_r and ξ_h are the real parts of the radial and the horizontal components of the displacement vector defined in Eq. (1.16). If a solid-body rotation is assumed, the $\Omega_{\rm rot}$ component is not dependent on r anymore and the frequency spacing of rotational splitting in Eq. (2.4) becomes

$$\Delta\nu_{k\ell} = \frac{\Omega_{\rm rot}}{2\pi}(1 - C_{k\ell}) \ , \tag{2.6}$$

where $C_{k\ell}$ is the first-order solid-body rotation coefficient, also known as the Ledoux coefficient and given by

$$C_{k\ell} = \frac{\int_0^R [\xi_h^2 + 2\xi_r\xi_h]\rho r^2 dr}{\int_0^R [\xi_r^2 + \ell(\ell+1)\xi_h^2]\rho r^2 dr} \ . \tag{2.7}$$

For p-modes, $C_{k\ell}$ is small enough to be neglected in Eq. (2.6), frequency spacing can be reduced and is given by

$$\Delta\nu_{k\ell} \simeq \frac{\Omega_{\rm rot}}{2\pi} = \frac{1}{P_{\rm rot}} \ , \tag{2.8}$$

independently of ℓ and k. Therefore, the frequency spacing in rotationally-splitted p-modes only depends on the rotation period of the star $P_{\rm rot}$.

For g-modes, $C_{k\ell} \simeq 1/[\ell(\ell+1)]$, which is a good approximation near the asymptotic limit $k \gg \ell$, corresponding to the observed g-modes in sdB stars. Contrarily to p-modes, the spacing changes with respect to ℓ. The frequency spacings of the rotational splitting for $\ell = 1$, $\ell = 2$, and $\ell = 4$ can be expressed as:

$$\Delta\nu_{k1} \simeq \frac{0.5}{P_{\rm rot}}, \ \Delta\nu_{k2} \simeq \frac{0.83}{P_{\rm rot}} \text{ and } \Delta\nu_{k4} \simeq \frac{0.95}{P_{\rm rot}} \ . \tag{2.9}$$

These typical spacings are also illustrated in Fig. 2.3, in the case of slow rotation. As the rotation period of both KIC5807616 and TIC441725813 are already known from previous studies [43, 32], the main purpose of the analysis of rotationally-splitted modes is to identify their ℓ values from the observed spacings. For KIC5807616, a new estimation of the period will be performed (see Sec. 4.2.1).

The second purpose of the rotational multiplets analysis is to determine the central frequency of each observed multiplets. In this work, when the multiplet is not clearly identified, the frequency of highest S/N is set to be the central one. The frequency list is then cleared from $m \neq 0$ observed modes, only retaining central frequencies.

2.3.4 Kolmogorov-Smirnov test

In the asymptotic regime $k \gg l$, the period spacing between consecutive g-mode radial orders k tends to be the same. This constant period spacing is given in Eq. (1.22), and reminded here:

$$\Delta P_\ell \approx \frac{\Pi_0}{\sqrt{\ell(\ell+1)}} \,, \tag{2.10}$$

where $\Delta P_\ell = |P_{\ell,k+1} - P_{\ell,k}|$ and Π_0 is the reduced period spacing in the asymptotic limit. The most probable period spacings in the extracted frequency list can be obtained by performing a Kolmogorov-Smirnov (KS) test. The KS test aims to give the probability that a set of given numbers is drawn from a particular distribution. Applied to a list of period, the term $r_i(\Delta P)$ can be defined as [44]

$$r_i(\Delta P) = k_i - \lfloor k_i \rfloor \,, \tag{2.11}$$

where i denotes the i^{th} value of the period list, $\lfloor k_i \rfloor$ is the floor value of k_i, defined as the greatest integer that is less than or equal to k_i, and k_i is given by

$$k_i = \frac{P_i - P_{\text{shortest}}}{\Delta P} \,. \tag{2.12}$$

The probability Q that $r_i(\Delta P)$ values are uniformly distributed is computed as a function of ΔP. A non-random period spacing distribution will be visible as a minima of Q, so the goal is to find period spacings for which the value of Q is minimum. Generally, the KS test is shown as the variation of $\log Q$ with respect to ΔP. An example of KS test for the KIC10553698 sdB star is shown on Fig. 2.4. More information about this star is available in Sec. 3.3.6.

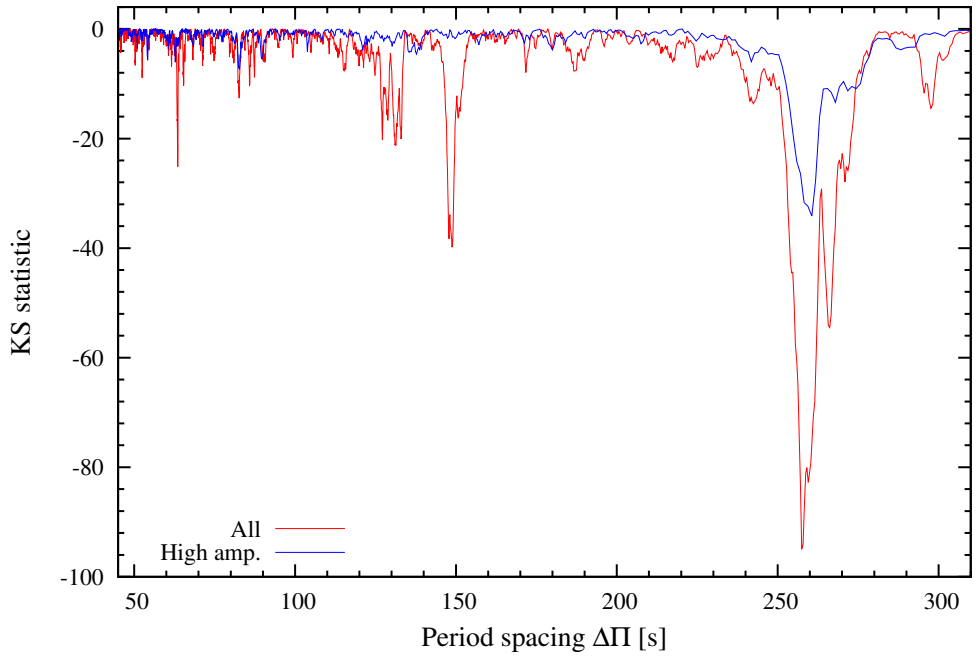

Figure 2.4: KS test performed for g-mode pulsations of KIC10553698 [17].

The period spacing of $\ell = 1$ and $\ell = 2$ modes can thus directly be estimated with the KS test, highlighted by minima of $\log Q$ [44]. From Eq. (2.10), the relation between $\ell = 1$

and $\ell = 2$ period spacings is given by

$$\Delta P_{\ell=2} = \frac{\Delta P_{\ell=1}}{\sqrt{3}} \,. \tag{2.13}$$

In the example of Fig. 2.4, the biggest peak around 260 s matches $\Delta P_{\ell=1}$ and the second peak around 150 s matches $\Delta P_{\ell=2}$, clearly showing the $\sqrt{3}$ relation between both. The period spacing derived from the KS test, together with the identification of rotationally-splitted modes, is the basis for the mode identification process.

2.4 Main identification from period spacing

From the telescope data, pulsations are extracted with FELIX by applying the prewhitening technique on the LSP associated to the data (see detail in Sec. 2.2). Then, after checking that extracted frequencies are not instrumental artifacts, the extracted spectrum is cleared of frequency modulations. A first attribution the ℓ number of rotational multiplets is done based on observed rotational splittings.

In parallel, the determination of the period spacing for $\ell = 1$ and $\ell = 2$ modes is determined from a KS test, performed on the list cleared of non-central frequencies. These steps all together constitute the basis of the identification from period spacing. A schematic overview of the identification of pulsation modes process, including the required steps just described, is presented on Fig. 2.5.

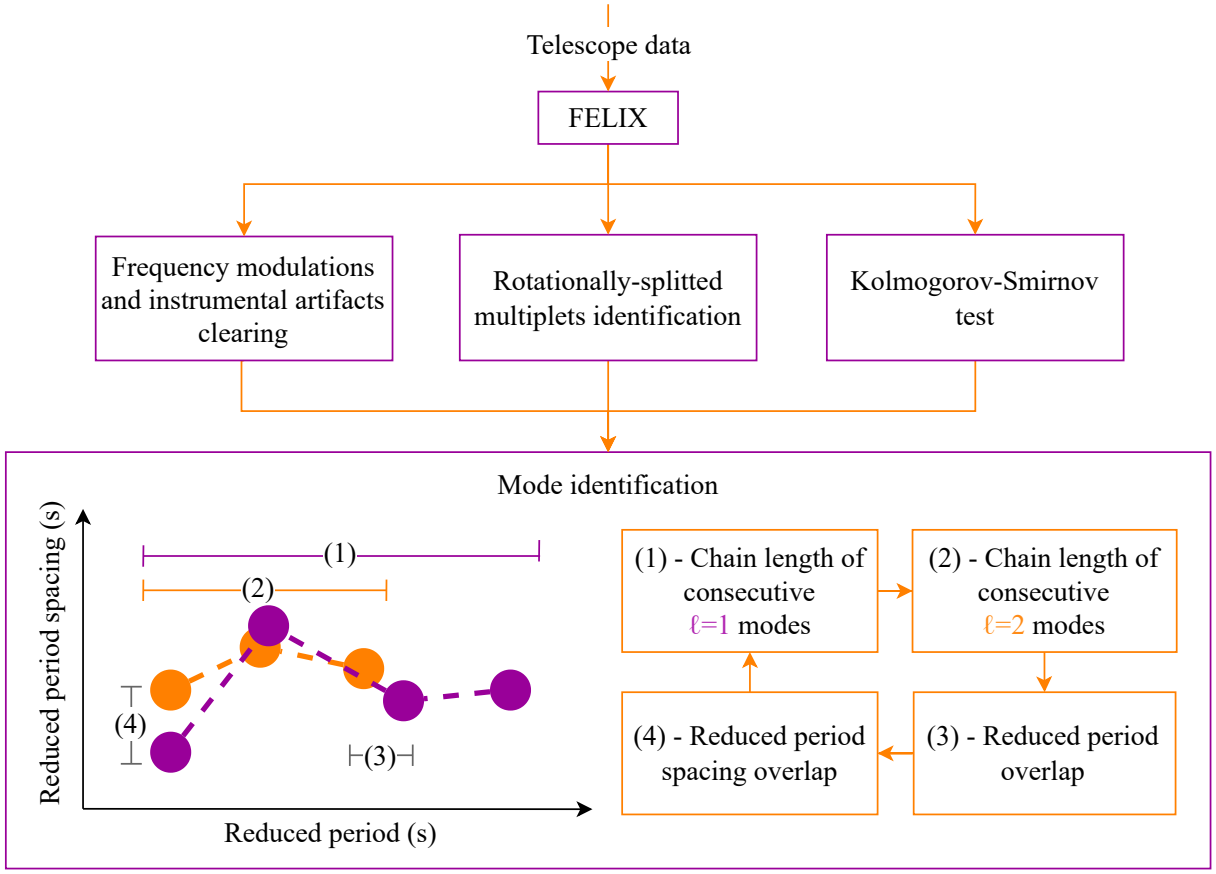

Figure 2.5: Summary of the process of mode identification.

In the literature, the identification with period spacing is the result of various trials-and-errors of k and l attributions based on the multiplet structures, until having a satisfactory model. In this work, it hinges on several quality criteria determined from important features visible in the period-spacing diagram. The period-spacing diagram is often used in theoretical papers. It consists in plotting the period difference between consecutive modes as a function of the period. Instead, reduced periods $\Pi_{n,\ell}$ are used to have an overlap between $\ell = 1$ and $\ell = 2$ modes of the same radial order k. Reduced periods are expressed as

$$\Pi_{k,\ell} = P_k \times \sqrt{\ell(\ell+1)} \ . \tag{2.14}$$

The reduced period spacing is thus given by

$$\Delta\Pi_{k,\ell} = |\Pi_{k+1,\ell} - \Pi_{k,\ell}| = \Delta P_\ell \times \sqrt{\ell(\ell+1)} \approx \Pi_0 \ , \tag{2.15}$$

so the observed reduced period spacings should be around Π_0. There is thus a vertical and a horizontal overlap of $\ell = 1$ and $\ell = 2$ modes in a diagram of reduced period spacing as a function of reduced periods.

The mode identification in this work aims to optimize four main criteria, believed to be hints of a good identification:

1. The length of the chain of consecutive $\ell = 1$ modes should be high enough.
2. The length of the chain of consecutive $\ell = 2$ modes should be high enough.
3. The overlap between $\ell = 1$ and $\ell = 2$ reduced period should be as good as possible.

   In the period-spacing diagram, it is translated as the horizontal distance between $\ell = 1$ and $\ell = 2$ modes of same radial order k, given by

   $$|\Delta\Pi_k| = |\Pi_{k,l=1} - \Pi_{k,l=2}| \ , \tag{2.16}$$

   where $\Pi_{k,l=1}$ and $\Pi_{k,l=2}$ are the reduced periods deduced after the $\ell = 1$ and $\ell = 2$ identification, given by Eq. (2.14). The smaller the value of $|\Delta\Pi_k|$, the better the reduced period overlap.
4. The overlap between $\ell = 1$ and $\ell = 2$ reduced period spacing should be as good as possible.

   In the period-spacing diagram, it is translated as the vertical distance between $\ell = 1$ and $\ell = 2$ modes of same radial order k, given by

   $$|\Delta\Pi_{k,l=1} - \Delta\Pi_{k,l=2}| \ , \tag{2.17}$$

   where $\Delta\Pi_{k,l}$ is the reduced period spacing given by Eq. (2.15).

The methodology proposed here aims to minimize the arbitrary nature of the mode identification process by establishing clear identification quality criteria. To obtain such consecutive $\ell = 1$ and $\ell = 2$ chains, a Python script is used (see Appendix A). This script is useful to have long consecutive chains but it does not take into account the vertical and horizontal overlaps, sometimes leading to long chains without overlaps. Concerning the list of reduced period overlaps, it is deduced directly by multiplying all periods by $\sqrt{\ell(\ell+1)}$, see Eq. (2.14). The last criterion is the only one harder to automatize and thus it is done by trying manually different identifications. From the reduced period overlaps list and the chains found with the code, a manual optimization is carried out. Once an identification presents both good overlaps and long chains, it is retained.

Once the identification is done, its general reliability can be evaluated. Generally, more $\ell = 1$ modes should be detected, and their associated S/N should be higher than $\ell = 2$ modes (see Sec. 1.2.2). If some modes remain unidentified, their S/N should be rather small and there should be few or no modes between consecutive chains.

Chapter 3

Overview of pulsating hot subdwarfs in the original *Kepler* field

This section aims to present a detailed overview of pulsating sdB stars observed in the original *Kepler* field. For each of the 18 pulsating stars, a complete state-of-the-art from the literature, acknowledging their main characteristics and comparing their pulsation behaviors is presented. This overview also presents the Lomb-Scargle Periodograms (LSPs) computed from *Kepler* light curves. The choice of KIC5807616 as the principal star studied in this master thesis is then justified.

3.1 Important criteria for the selection

The selection criteria for the main star to be studied in this work are:

- The pulsator should have enough but not too much g-modes.
- The pulsation spectrum should have rather have low amplitude and frequency modulations (see Sec. 2.3.2).
- The mode identifications available in the literature should be neither complete nor fully convincing.

The main classification of pulsating sdBs is based on the presence of g-modes, p-modes or both in their pulsation spectrum. In case of both g- and p-modes, they are denoted as hybrid pulsators, generally dominated by one type or the other. The best way to identify p-mode, g-mode or hybrid pulsators is by analyzing the LSP associated to their observed light curves. Tab. 3.1 presents the typical period and frequency ranges of p-modes and g-modes in sdB stars.

Table 3.1: Typical period and frequency ranges of p- and g-modes in sdB stars [45].

	Period	**Frequency**
p-modes	1-10 min	1667-16667 μHz
g-modes	∼1-4 h	∼70-300 μHz

The determination of their atmospheric parameters, such as the effective temperature $T_{\rm eff}$ and the surface gravity $\log g$, defined in Eq. (1.1), give hints about the nature of sdBs pulsations. This is illustrated in Fig. 3.1, where p-mode pulsators are hotter and more compact, g-mode pulsators are cooler and less compact and hybrid pulsators are at the boundary between them. It is also worth to mention that some of the presented sdB stars in this figure are not pulsating.

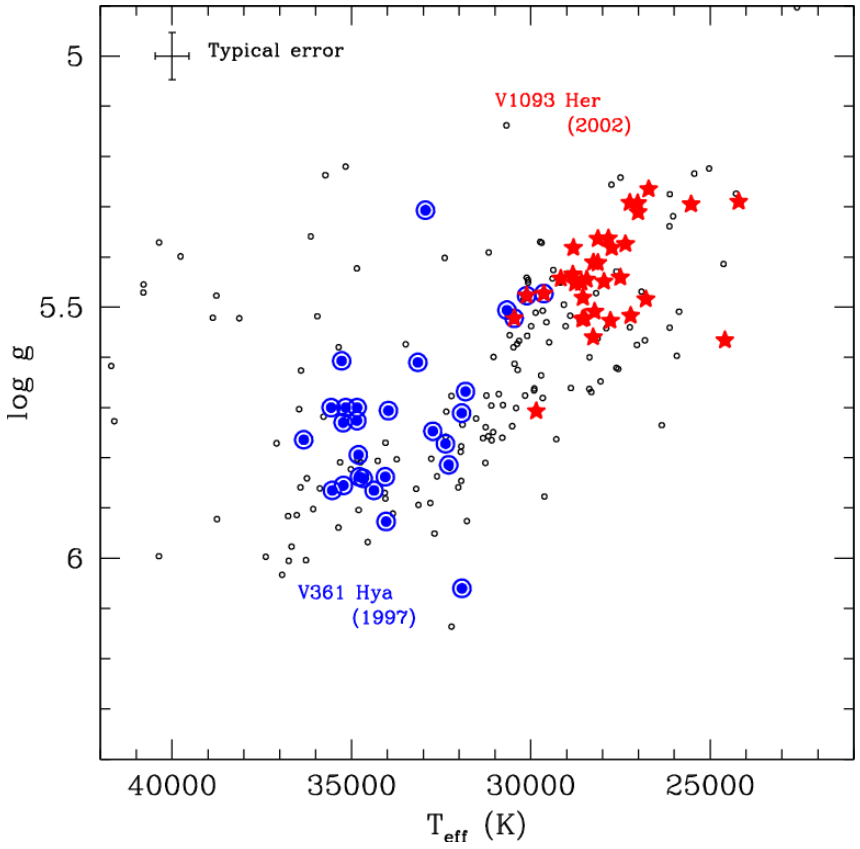

Figure 3.1: Log g - $T_{\rm eff}$ diagram of p-mode pulsators (blue circles with annulus) and g-mode pulsators (red stars). Overlaps are hybrid pulsators [45].

As the main objective of this work is to derive a detailed mode identification for one g-mode pulsator, it is important to choose a pulsator presenting a rich and clear pulsation spectrum in the g-mode region. Due to the rotation of the star, so called rotational multiplets can be visible in the pulsation spectrum. As described in Sec. 2.3.3, the study of frequency splittings of rotational multiplets in a star can lead to an estimate of its rotation period. In this work, we seek for a star with a rather slow rotation period, to avoid overlapping rotational multiplets from different modes, which would greatly complicate the mode identification. Most sdB stars are slow rotators, except those in close binaries.

3.2 Available data

Light curves corresponding to each star is firstly downloaded from the *MAST* [26] observational data and processed with FELIX. It is necessary to have a sufficient observational cadence to ensure a good sampling of both g-modes and p-modes. As already mentioned in Sec. 2.1.1, observations from *Kepler* are available in short cadence (SC) and long cadence (LC), which correspond to a data point every 1 and 30 min, respectively [29].

According to the Nyquist theorem, the Nyquist frequency is equal to half the sampling frequency, hence $f_{\mathrm{Nyq,\,SC}} \simeq 8333$ μHz and $f_{\mathrm{Nyq,\,LC}} \simeq 277$ μHz. Based on Tab. 3.1, the SC data are thus preferred to have a classification between g-modes and p-modes. Known pulsating sdBs of the original *Kepler* field are listed in Tab. 3.2. This table also includes relevant observational parameters such as the observation quarters in SC, defined in Sec. 2.1.1, and its apparent magnitude seen from *Kepler* K_p.

Table 3.2: List of the studied sdBs and their corresponding observational parameters [29].

sdB pulsator	**Other name**	$\mathbf{K_p}$	**Available quarters (SC)**
KIC9472174	2M1938+4603	12.3	Q0, Q5-Q17.2
KIC2437937	B5 (NGC6791)	13.9	Q11.X
KIC3527751	J19036+3836	14.8	Q2, Q5-Q17.2
KIC11558725	J19265+4930	14.9	Q3.3, Q6-Q17.2
KIC5807616	KPD 1943+4058	15.0	Q2.3, Q5-Q17.2
KIC10553698	J19531+4743	15.1	Q4.1, Q8-Q10, Q12-Q14, Q16-Q17.2
KIC2697388	J19091+3756	15.4	Q2.3, Q5-Q17.2
KIC7668647	FBS1903+432	15.4	Q3.1, Q6-Q17.2
KIC10001893	J19095+4659	15.8	Q3.2, Q6-Q17.2
KIC10139564	J19249+4707	16.1	Q2.1, Q5-Q17.2
KIC8302197	J19310+4413	16.4	Q3.1, Q5-Q17.2, except Q12
KIC7664467	J18561+4319	16.4	Q2.3, Q5-Q17.2, except Q12
KIC10670103	J19346+4758	16.5	Q2.3, Q5-Q17.2
KIC11179657	J19023+4850	17.1	Q2.3, Q5-Q17.2, except Q8 and Q12
KIC2991403	J19272+3808	17.1	Q1, Q5-Q17.2
KIC2991276	J19271+3810	17.4	Q2.1, Q6-Q17.2, except Q12
KIC2569576	B3 (NGC6791)	18.1	Q11.3, Q14-Q17.2
KIC2438324	B4 (NGC6791)	18.3	Q6-Q17.2

All periodograms presented in this work follow a consistent format, displaying the frequency spectrum, known artifacts from the *Kepler* space telescope [39], and the 4σ detection threshold. This detection threshold is derived from the FAP calculation performed by FELIX, following the methodology described in Sec. 2.2. It is important to note that, due to the computational demands when it comes to do it with several quarters, the FAP calculation was conducted for only one quarter. More information is available in Tab. B.1 of Appendix B, showing all obtained SNR values after the FAP calculation. Generally, a SNR limit around 5 describes well the 4σ limit in the different stars, which corresponds to a probability of less than 0.01% that a peak could be due to a noise fluctuation.

3.3 Overview

3.3.1 KIC9472174

The first star analyzed here is KIC94721740, also known as 2M1938+460. Its effective temperature and surface gravity are respectively $T_{\rm eff} = 29564 \pm 106$ K and $\log g = 5.425 \pm 0.009$ dex [46]. This star is an eclipsing sdB + dM system with a pulsating primary, which is very rare because only one another sdB + dM eclipsing binary with the sdB pulsating is known (NY Vir or PG 1336-018) [47]. Observed light curves show a strong reflection effect, as it can be seen in Fig. 3.2. The primary eclipse (dM in front of the sdB) and the secondary eclipse (dM behind the sdB) are also visible in the figure.

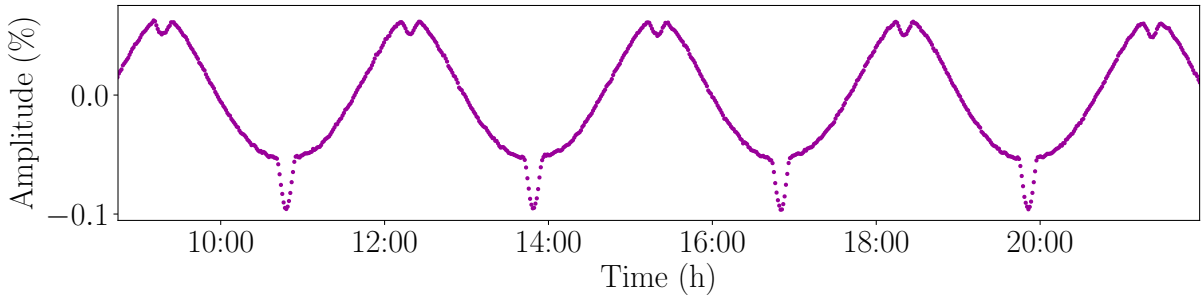

Figure 3.2: Part of a prewhitened KIC9472174 light curve, prewhitened by FELIX, April 30th 2011 (Q9).

This effect makes the star difficult to study in practice from its strong effect on the LSP, represented on Fig. 3.3. The main frequency peak at ~ 92 μHz visible in the LSP is the orbital period of the system $P_{\rm orb} = 0.125765300 \pm 0.000000021$ days. [46]. Most of the other visible peaks are harmonics related to the binary.

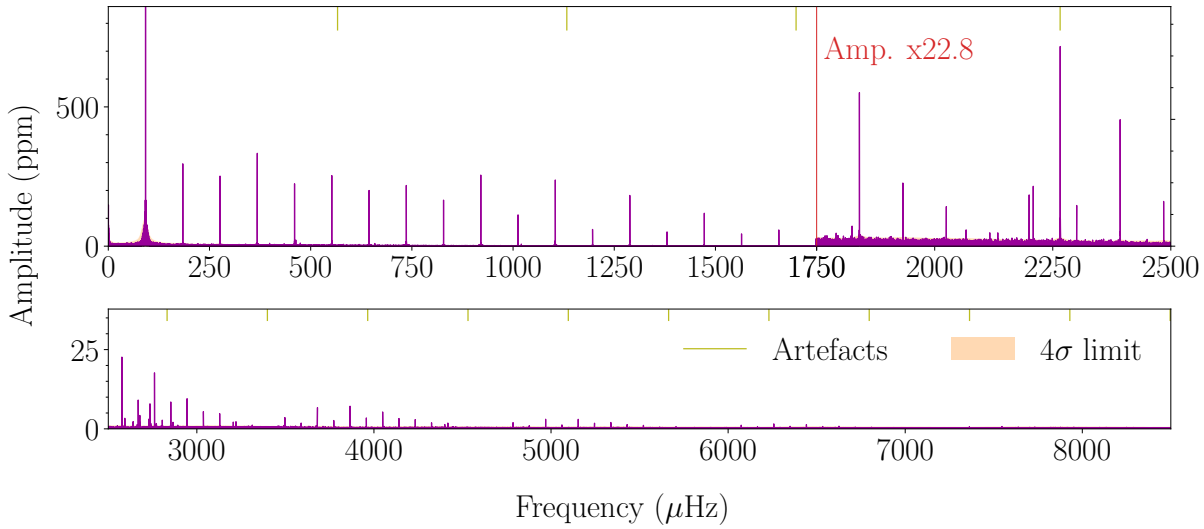

Figure 3.3: LSP of KIC9472174 light curves from FELIX.

To be able to analyze the pulsation spectrum of this sdB, the effect of the binary must be removed from the light curves. This clean out can be done by folding light curves with the orbital period of the companion [46, 48]. However, the sdB star probably has a fast

rotation, synchronized or not. Consequently, rotational multiplets assigned to different modes are mixed and an identification in this case is very difficult, and this star was then dismissed for the purposes of this work.

3.3.2 KIC2437937

KIC2437937 is a pulsating sdB star located in the open cluster NGC6791, and is named B5 inside the cluster. Its effective temperature is $T_{\rm eff} = 24860 \pm 270$ K and its surface gravity is $\log g = 5.348 \pm 0.052$ dex [49]. The very low available observation data, only 1 month, makes this star not suitable for our purposes. The LSP of obtained light curves is nevertheless shown in Fig. 3.4. The 3 peaks visible between ∼4000 and 5000 μHz are very likely to only be artifacts, thus no pulsation is observed for Q11 in SC. With LC *Kepler* data, also for Q11, four g-modes periodicities were detected [50].

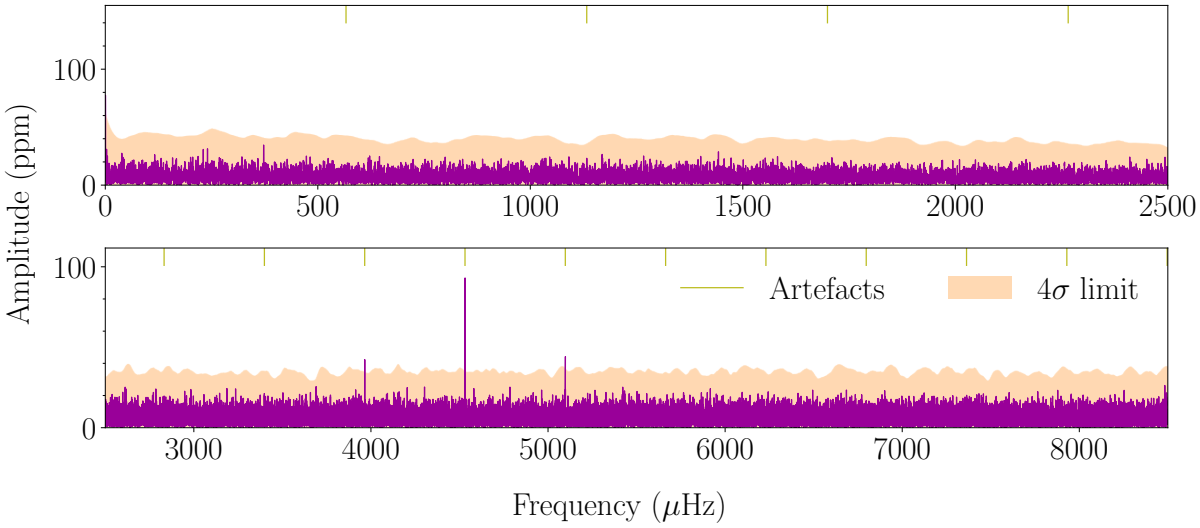

Figure 3.4: LSP of KIC2437937 light curves from FELIX.

In the NGC6791 open cluster, two other pulsating sdBs are also present: B3 and B4, analyzed in Secs. 3.3.17 and 3.3.18; and one non pulsating sdB, B6 (KIC2569583) [49]. With the objective to enlarge the available data to analyze for B3, B4 and B5, Sanjayan et al. (2022) [49] performed an analysis of the *Kepler* superaperture LC data. The idea was to check all pixels of the field of view to detect the three pulsating stars. In the case of B5, they detected 26 possible g-mode frequencies. The rotation period of the star was determined from rotational splittings [49]: $P_{\rm rot} = 71.0 \pm 1.8$ days.

3.3.3 KIC3527751

KIC3527751, also referred to as J19036+3836, has sufficient observational data to enable a detailed analysis of its pulsation spectrum. It is characterized by an effective temperature and a surface gravity of respectively $T_{\rm eff} = 27818 \pm 163$ K and $\log g = 5.35 \pm 0.03$ dex [51]. As shown in Fig. 3.5, the star presents a rich g-mode spectrum. Additionally, the presence of p-modes confirms earlier studies identifying KIC3527751 as a hybrid pulsator [51].

From *Kepler* data, Foster et al. (2015) [51] deducted a potential differential rotation in the radial direction from differences in the rotation period calculated from p-mode

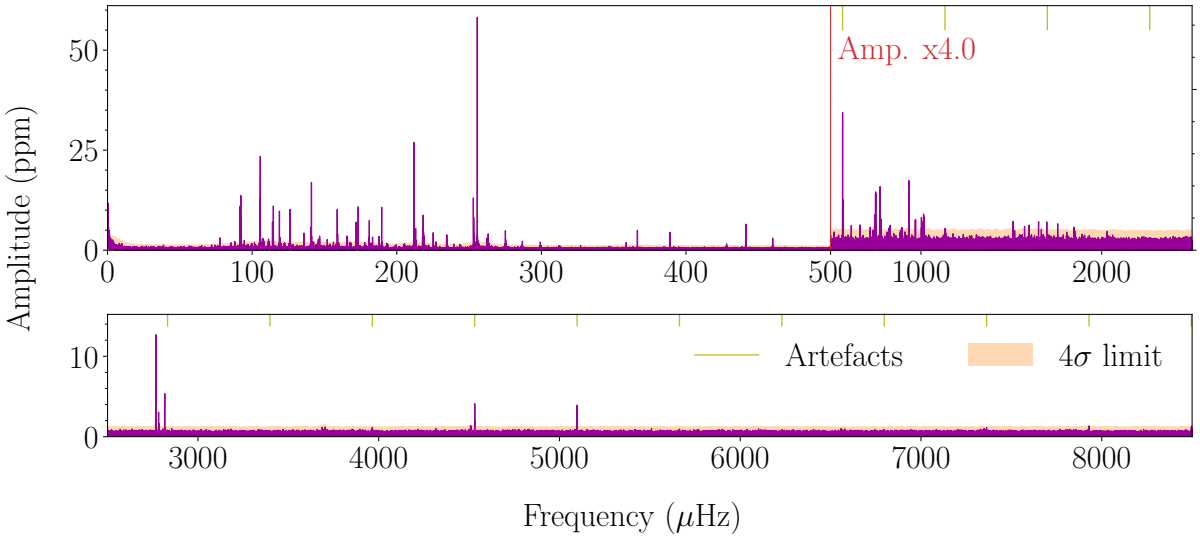

Figure 3.5: LSP of KIC3527751 light curves from FELIX.

and g-mode rotational splittings [51]. The rotation period is estimated to be $P_{\text{rot, core}} = 15.3 \pm 0.7$ days and $P_{\text{rot, envelope}} = 42.6 \pm 3.4$ days. Therefore, the star would rotate more slowly in the core, where g-modes are located, than in the envelope, where p-modes are located. In the same paper, a mode identification involving mode trapping in the g-mode region is suggested. However, Zong et al. (2018) [41] questioned the existence of a differential rotation in KIC3527751, as they could not retrieve the p-mode multiplets seen by Foster et al. (2015) [51]. Their analysis indicated that certain modes lack sufficient S/N, making them highly likely to be noise fluctuations. The rotation period of the core is nevertheless likely to be 15.3 ± 0.7 days, as mentioned before.

3.3.4 KIC11558725

KIC11558725, also known as J19265+4930, is a binary system composed of a sdB and a white dwarf (WD) with an orbital period of 10.0545 ± 0.0048 days [52]. This corresponds to a frequency of ~ 1.2 μHz, too small to affect the LSP spectrum in regions of interest. As shown on the LSP hereafter, the star shows a rich g-mode spectrum with also clear p-modes to be classified as a hybrid pulsator.

The values of its effective temperature and surface gravity are $T_{\text{eff}} = 27910 \pm 210$ K and $\log g = 5.410 \pm 0.015$ dex [52]. The clear presence of multiplets in both p-modes and g-modes allowed to determine a rotation period for the sdB component from their rotational splittings $P_{\text{rot, core}} = 45.1 \pm 7.8$ days and $P_{\text{rot, envelope}} = 40.2 \pm 3.3$ days [19]. Thus, the star is interpreted to be a solid-body, or almost, rotator with $P_{\text{rot}} \simeq 44$ days [19]. So this star is a slow rotator. Its modes have also been identified, revealing potential trapping in the g-mode region [19].

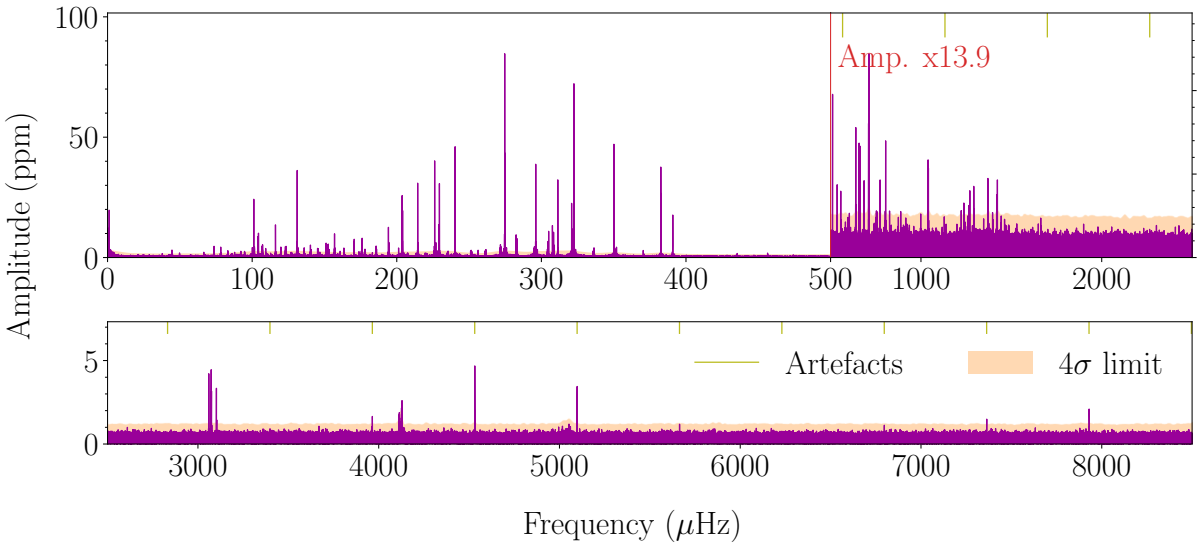

Figure 3.6: LSP of KIC11558725 light curves from FELIX.

3.3.5 KIC5807616

KIC5807616 mostly known as Kepler-70 (or KPD 1943+4058) is a rich hybrid pulsator, dominated by g-modes, as shown in Fig. 3.7. Effective temperature and surface gravity values of KIC5807616 are $T_{\rm eff} = 27730 \pm 270$ K and $\log g = 5.52 \pm 0.03$ dex [53]. This star is not a binary but Charpinet et al. (2011) [54] claimed the presence of Earth-sized bodies with orbital periods of 5.7625 and 8.2293 hours, so respectively ∼48.2 μHz and ∼33.8 μHz, as very low-amplitude peaks visible in the LSP.

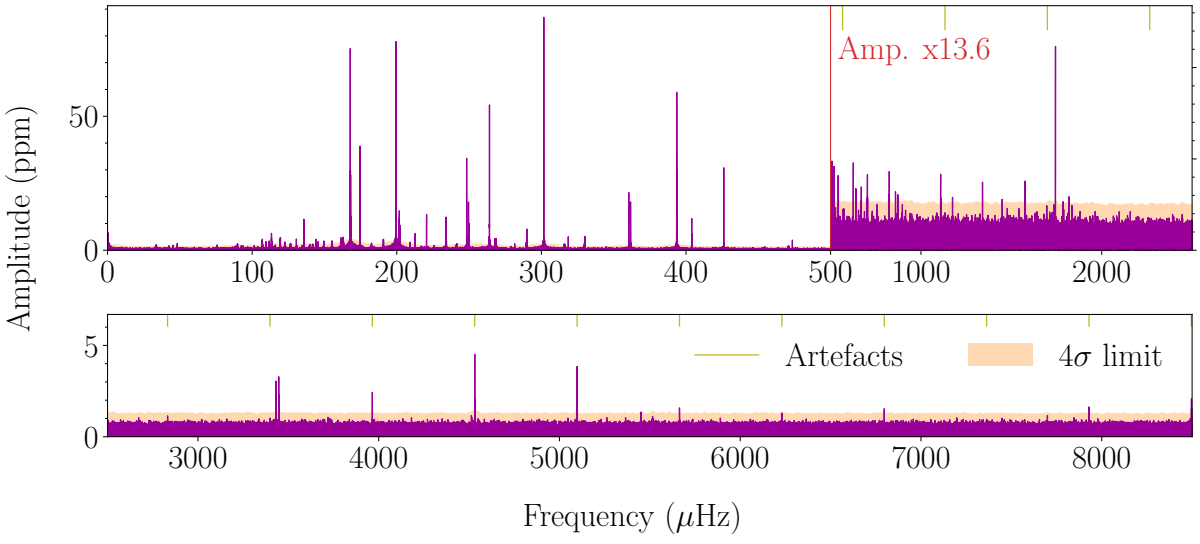

Figure 3.7: LSP of KIC5807616 light curves from FELIX.

The number of clear multiplets is low in the g-mode region [55], but the rotation period on the star could be determined from p-mode rotational splittings: $P_{\rm rot,\ envelope} \simeq 39.2341$ days [54] (based on Q5 and Q6). Another estimate based on all available quarters has been done and resulted to a period of 44.9 ± 1.1 days [55]. KIC5807616 is thus a slow rotator.

3.3.6 KIC10553698

For this star, also known as J19531+4743, observations are slightly more fragmented in terms of quarters than other stars but still of sufficient quality. Associated effective temperature and surface gravity are $T_{\rm eff} = 27423 \pm 293$ K and $\log g = 5.436 \pm 0.024$ dex [17]. Its corresponding LSP is shown in Fig. 3.8. KIC10553698 is again a hybrid pulsator presenting a rich g-mode spectrum and some p-modes with a well above-threshold S/N.

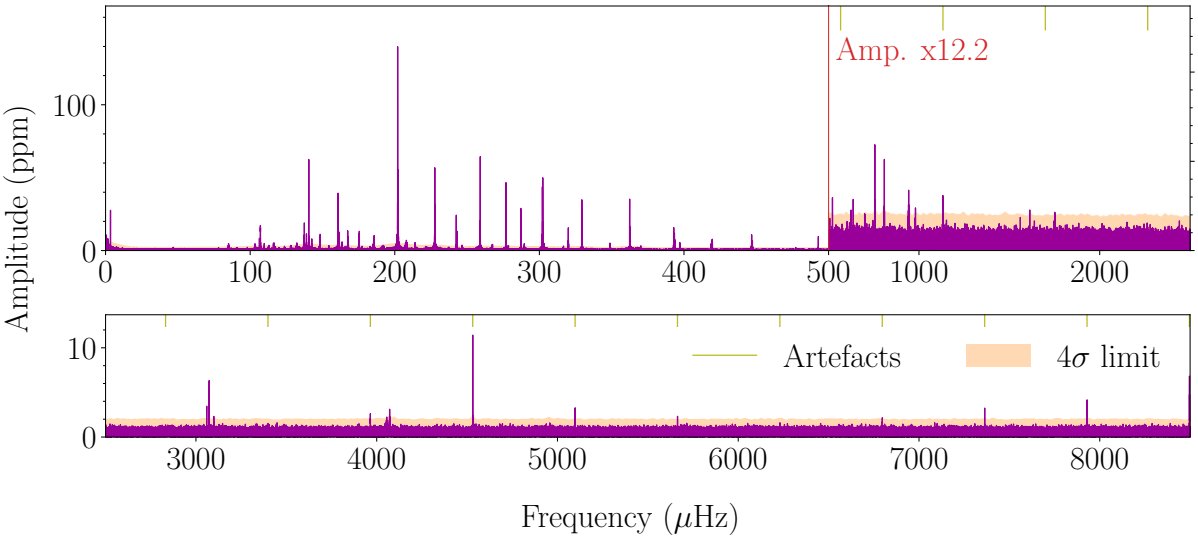

Figure 3.8: LSP of KIC10553698 light curves from FELIX.

A peak around ∼3.42 μHz , corresponding to a period of 3.387 days led Østensen et al. (2014) [17] to suggest the existence of an unseen companion, probably a white dwarf. The *Kepler* data displays rotational multiplets and the rotation period has already been estimated from their frequency splittings: $P_{\rm rot} = 41 \pm 3$ days [17]. This star is thus a slow rotator. Contrarily to the previously mentioned pulsators with potential trapping, there is here a clear indication of mode trapping in its spectrum [17]. This star is probably the best known case of modes trapping in pulsating sdBs of the original *Kepler* field.

3.3.7 KIC2697388

Concerning KIC2697388, also known as J19091+3756, the LSP shown in Fig. 3.9 presents a rich g-mode spectrum and some p-modes. This is a hybrid pulsator, dominated by g-modes. Concerning atmospheric parameters, $T_{\rm eff} = 25395 \pm 227$ K and $\log g = 5.5 \pm 0.031$ dex [43].

Analyses realized on KIC2697388 based on rotational splittings show that the star is a slow rotator, with a rotation period of $P_{\rm rot} \simeq 45$ days [56]. Again, mode identification attempts resulted in the possibility of having trapping in the g-mode region [57].

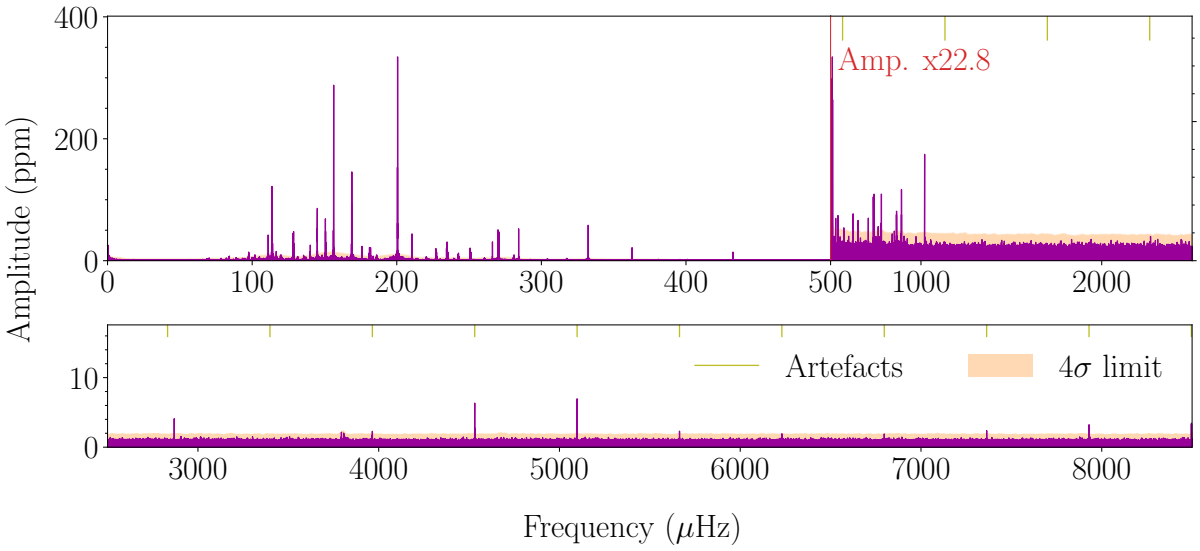

Figure 3.9: LSP of KIC2697388 light curves from FELIX.

3.3.8 KIC7668647

This star is also referenced as FBS1903+432, and is a sdB + WD binary system [58]. A peak around 0.81 μHz in the LSP translated the presence of an unseen companion with an orbital period of $\sim$ 14.2 days [58]. This LSP is presented on Fig. 3.10, showing a rich g-mode pulsation spectrum and a few p-modes in the higher frequencies region. This kind of spectrum, i.e. a hybrid pulsator dominated by g-modes, seems to be the most common one for pulsating sdB in the original *Kepler* field. Its effective temperature and surface gravity are given by $T_{\rm eff} = 27700 \pm 300$ K and $\log g = 5.5 \pm 0.03$ dex [58].

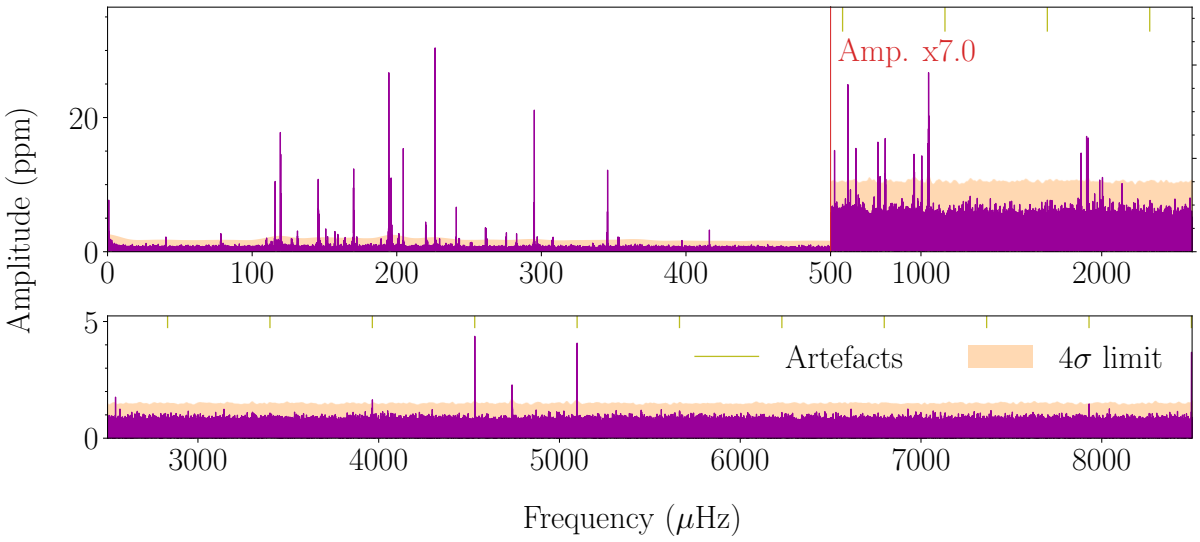

Figure 3.10: LSP of KIC7668647 light curves from FELIX.

A first derivation of the rotation period of this pulsator was done by Telting et al. (2014) [58], who analyzed g-modes rotational splittings to estimate it to be $P_{\rm rot,\,core} \simeq$ 46 to 48 days, it is thus a slow rotator. The low amount of p-modes made the rotation period estimation at the envelope not possible. Authors nevertheless suggested that the

envelope could be slower from differences in the main rotational splittings. The presence of trapping is discussed in the same paper [58], but no clear conclusion is made.

3.3.9 KIC10001893

The hybrid nature, with a rich g-mode spectrum, of KIC10001893 (or J19095+4659) is visible in the LSP shown in Fig. 3.11. Concerning atmospheric parameters, its effective temperature is $T_{\rm eff} = 27500 \pm 500$ K and its surface gravity is $\log g = 5.35 \pm 0.05$ dex [59].

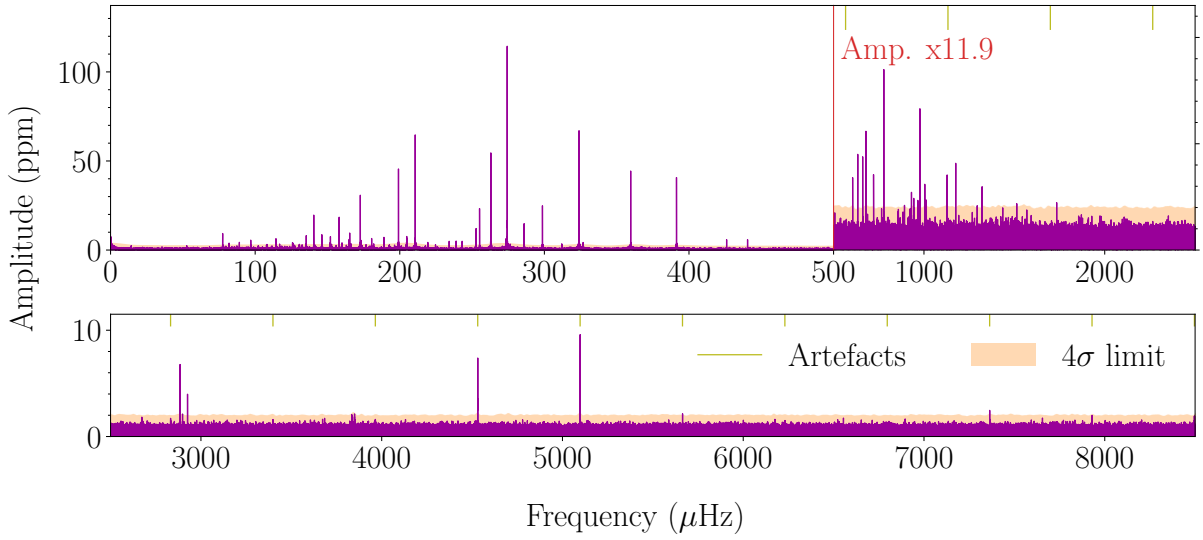

Figure 3.11: LSP of KIC10001893 light curves from FELIX.

No rotation period has been found so far, due to the absence of rotational splittings in the data [18]. Two possible explanations were proposed [18]: either the rotation is too slow to be detected, either the rotation axis is oriented towards the observer, suppressing the side components. A mode identification was attempted only from period spacings and resulted to probable mode trapping, even if several modes were not attributed [18].

3.3.10 KIC10139564

KIC10139564, also known as J19249+4707, is, contrarily to all other pulsating sdBs of the original *Kepler* field, a hybrid pulsator dominated by p-modes. This characteristic is visible in the LSP obtained with FELIX shown in Fig. 3.12. Its effective temperature is $T_{\rm eff} = 31859 \pm 126$ K and its surface gravity is $\log g = 5.673 \pm 0.026$ dex [60], which are values higher than the ones already mentioned, confirming its p-mode domination.

In this star, nearly all frequencies are splitted into multiplets, making a rotation period estimate possible: $P_{\rm rot} = 25.6 \pm 1.8$ days [60]. Due to the variety of multiplets presents in its spectrum, frequency and amplitude modulations have been studied in detail [37]. This study aimed to improve predictions from current nonlinear theoretical models, as some multiplets of this star are not well reproduced by these frameworks.

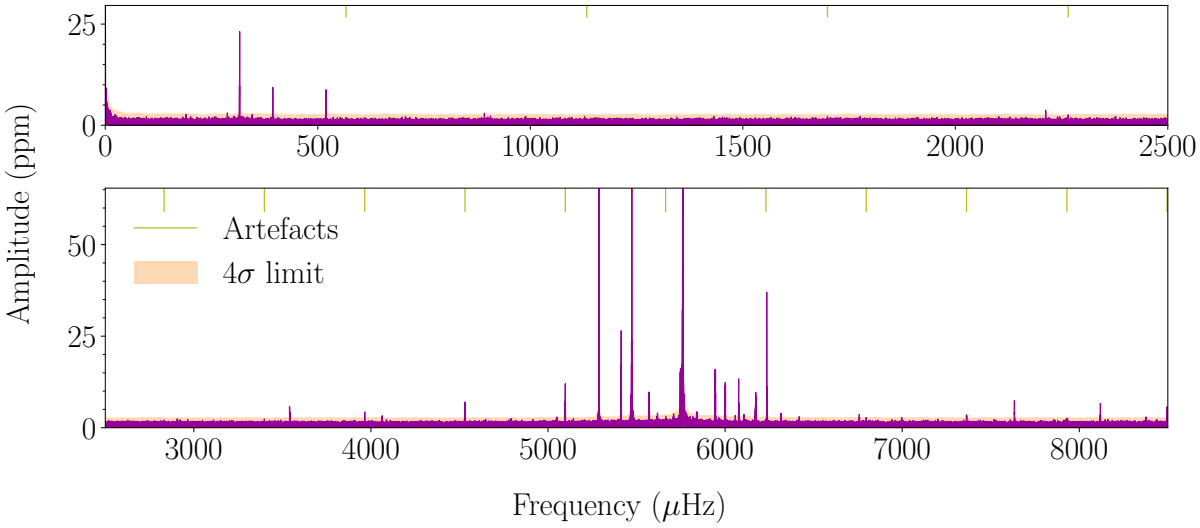

Figure 3.12: LSP of KIC10139564 light curves from FELIX.

3.3.11 KIC8302197

This star, also known as J19310+4413, seems not having any p-modes in its corresponding LSP, as shown in Fig. 3.13. This star is therefore a pure g-mode pulsator. As for KIC10001893 (in Sec. 3.3.9), KIC8302197 has surprisingly no multiplets, suggesting this star to be a very slow rotator or that the orientation of the pulsation axis is pole-on [61].

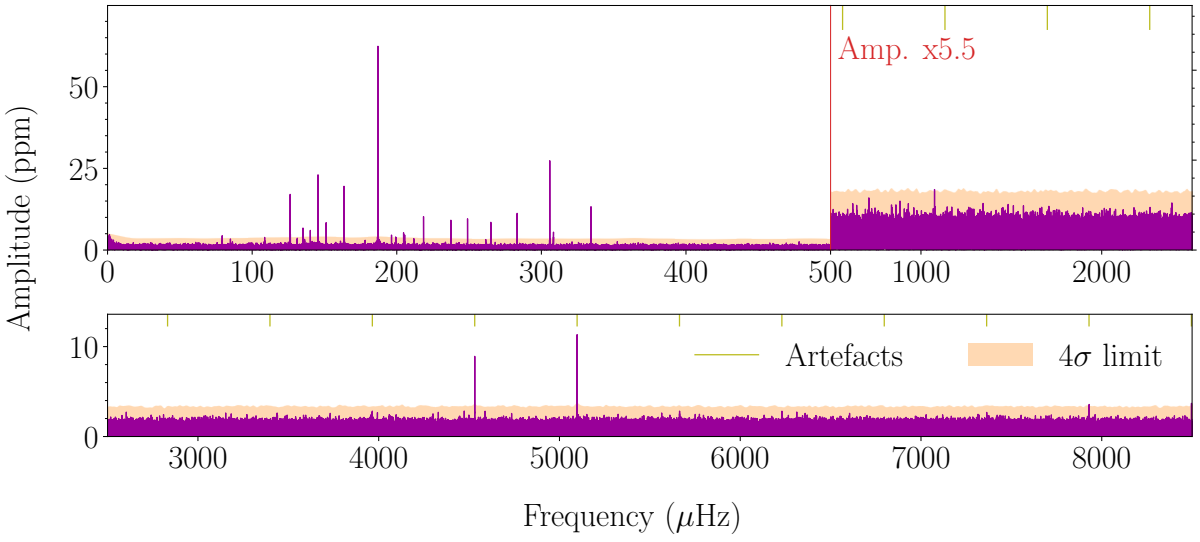

Figure 3.13: LSP of KIC8302197 light curves from FELIX.

Values of effective temperature and surface gravity of the star have been derived: $T_{\rm eff}$ = 27450 ± 200 K and $\log g$ = 5.438 ± 0.033 dex [61]. Its amplitude spectrum is sparse compared to other pulsators, and this combined with the lack of rotational splittings make the identification process difficult. An identification has been made by Baran et al. (2015) [61], and suggested the presence of mode trapping.

3.3.12 KIC7664467

The LSP of KIC7664467, also known as J18561+4319, as the previously mentioned pulsator, has no p-modes. So this pulsator is also a g-mode sdB, as shown in Fig. 3.14. Its effective temperature and surface gravity reach $T_{\rm eff} = 27440 \pm 120$ K and $\log g = 5.38 \pm 0.02$ dex [62]. It has been found that KIC7664467 is a binary system with a white dwarf, where the estimated orbital period of the companion is $P_{\rm orb} = 1.559049 \pm 0.0000027$ days (peak at ~ 7.42 μHz in the LSP) [62].

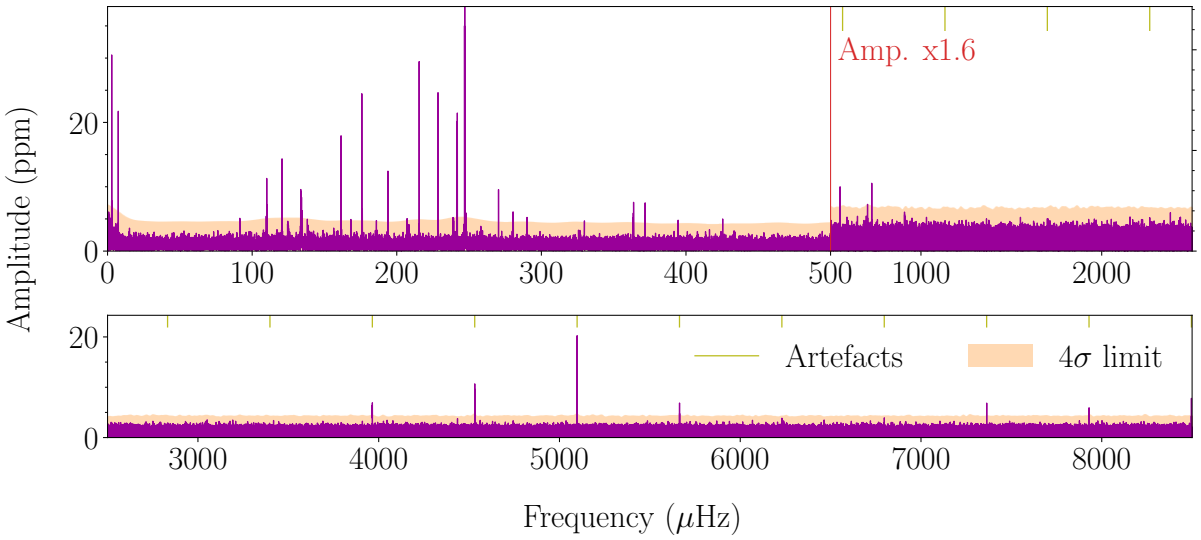

Figure 3.14: LSP of KIC7664467 light curves from FELIX.

From rotational splittings, the rotation period of the star has already been estimated: $P_{\rm rot} = 35.1 \pm 0.6$ days [62]. It is thus a slow rotator. Finally, this pulsator could also present some trapping, as suggested by Baran et al. (2016) [62]. The number of modes above the noise level is however lower than in other sdBs of the original *Kepler* field.

3.3.13 KIC10670103

KIC10670103 (or J19346+4758) is the sdB pulsator with the highest amount of frequencies that could be detected [63]. Concerning the nature of its pulsations, only g-modes are present in the LSP, shown in Fig. 3.15. The star is thus a very rich g-mode pulsator. Concerning atmospheric parameters, the star has an effective temperature of $T_{\rm eff} = 21485 \pm 540$ K and a surface gravity of $\log g = 5.14 \pm 0.05$ dex [63].

The study of rotational splittings by Reed et al. (2014) [63] led to a rotation period of $P_{\rm rot} = 88 \pm 8$ days, making this star one of the slowest rotator (with known period) of the original *Kepler* field. The mode identification also suggested the presence of trapping [63]. The very high number of detectable modes could make the identification process difficult.

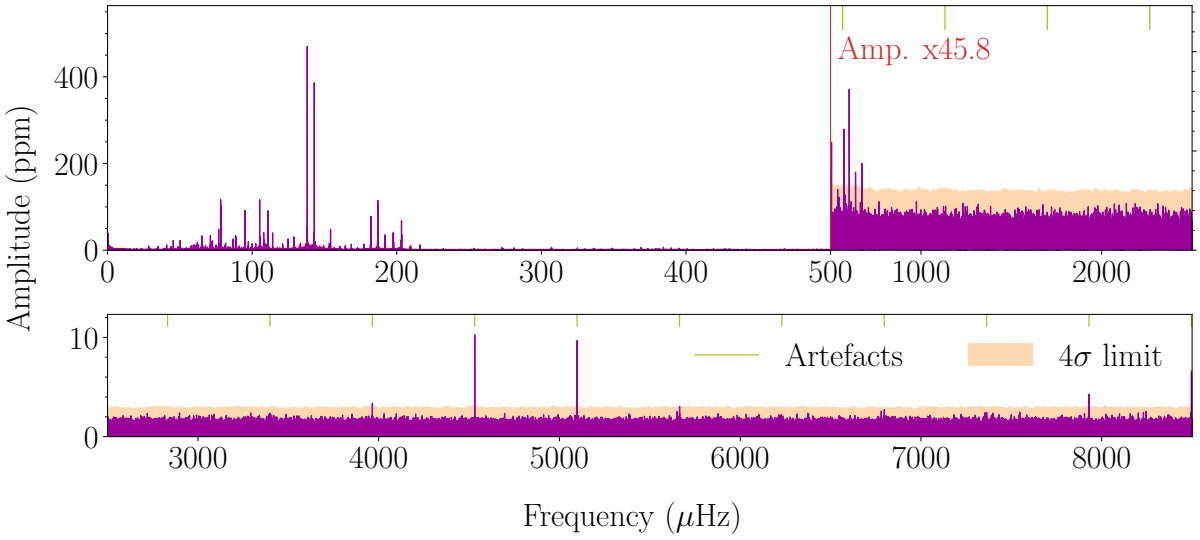

Figure 3.15: LSP of KIC10670103 light curves from FELIX.

3.3.14 KIC11179657

The KIC11179657 system (or J19023+4850) is a binary system composed of a pulsating sdB and a dM companion. This star is characterized by an effective temperature and a surface gravity of respectively $T_{\rm eff} = 26000 \pm 800$ K and $\log g = 5.14 \pm 0.13$ [64]. From a frequency peak around $\sim 29\mu$Hz, an orbital period of $P_{\rm orb} \simeq 0.394$ days [64] has been found for the second component. This frequency peak can be seen in the LSP of KIC11179657 in Fig. 3.16. Once again, this sdB does not show any p-modes in its pulsation spectrum.

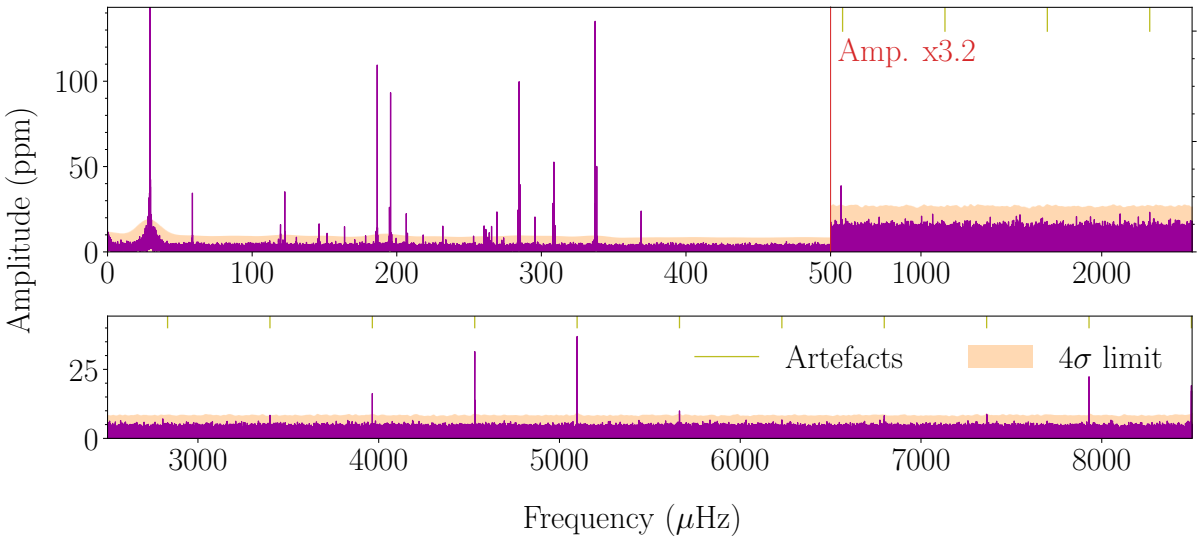

Figure 3.16: LSP of KIC11179657 light curves from FELIX.

Rotational splittings have already been studied to have an estimate of the rotation period of the star [65]: $P_{\rm rot} \simeq 7.4$ days, which is quite fast compared to other studied sdBs of *Kepler*. This is explained by the fact that it is a sdB in a close binary, hence tides "increases" the rotation of the star. KIC11179657 frequency and amplitude modulation patterns have been studied in detail, as well as those of KIC2438324 (see Sec. 3.3.18) [42].

3.3.15 KIC2991403

KIC2991403, also known as J19272+3808, has an effective temperature of $T_{\rm eff} = 27300 \pm 200$ K and a surface gravity of $\log g = 5.43 \pm 0.03$ [64]. It is also a binary system composed of a pulsating sdB and a dM companion. The LSP of this star presented hereafter in Fig. 3.17 clearly shows two high peaks at the very low frequency part of the LSP. These peaks correspond to the orbital period of the binary and its first harmonic [64]. The orbital period is estimated to be $P_{\rm orb} \simeq 0.417$ days, from a peak at $\sim 27.8 \mu$Hz in the LSP [65]. Concerning other visible peaks, KIC2991403 seems to be only pulsating in the g-mode region.

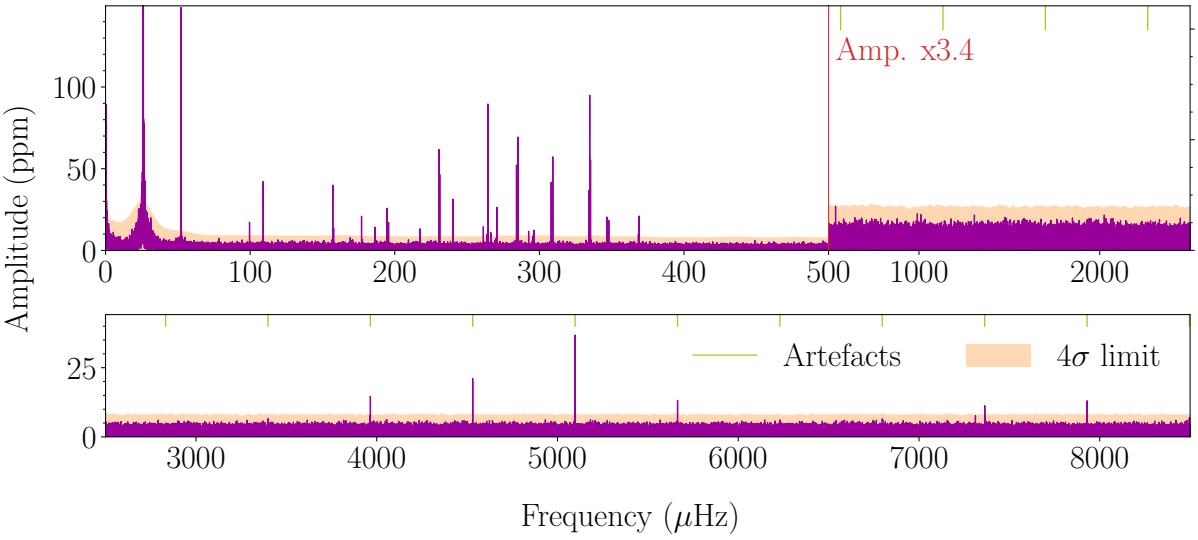

Figure 3.17: LSP of KIC2991403 light curves from FELIX.

A rotation period estimate was made by Baran et al (2012) [64] based on rotational splittings, leading to a value of $P_{\rm rot} \simeq 10.46$ days. which is a value close to the ones of KIC11179657 and KIC2438324, and also due to its close companion. Even if the g-mode spectrum is not very rich, mode identification on this star have been made [64], also discussing the presence of trapping.

3.3.16 KIC2991276

The corresponding LSP of KIC2991276 (or J19271+3810) is shown in Fig. 3.18. Unlike other stars mentioned in this report, this sdB periodogram shows no frequency peak in the g-mode region. A few p-modes can be detected, making this star probably a pure p-mode pulsator. The effective temperature and the surface gravity of this star, $T_{\rm eff} = 33900 \pm 200$ K and $\log g = 5.82 \pm 0.04$ dex [66], which are similar to values obtained for KIC10139564 (see Sec. 3.3.10) tend to confirm that.

A possible explanation behind this feature is the high variability observed in the different observation quarters of the star. In other words, some modes clearly visible tend to change quite much in frequency and amplitude, or disappear completely, in about a month [66]. This behavior is typical for solar-like pulsators, driven by convection in the outer layers, and causes are not completely well understood yet [66]. This star will be referenced as a p-mode pulsator in this work but a further investigation is needed.

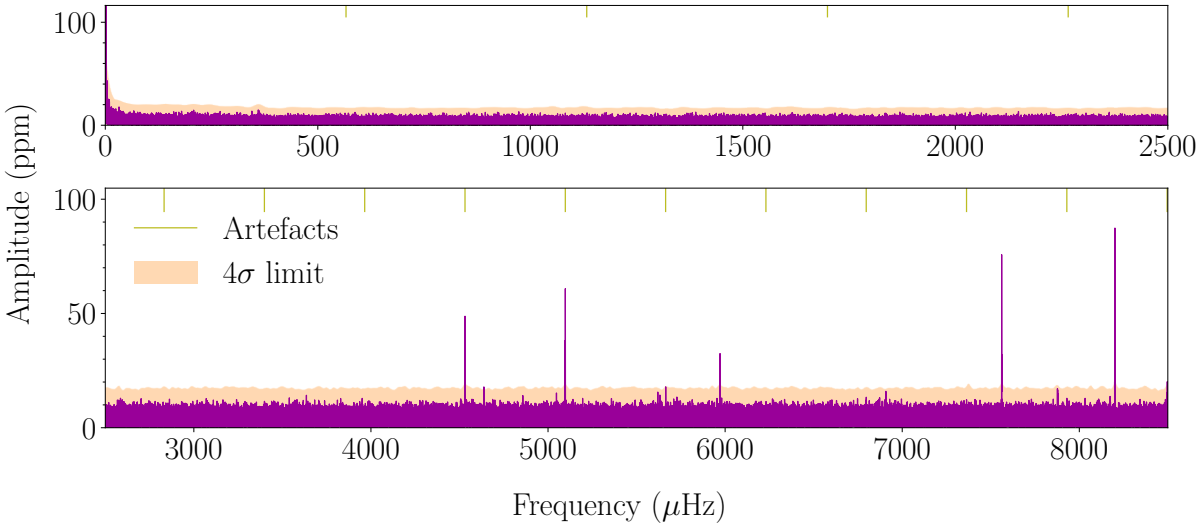

Figure 3.18: LSP of KIC2991276 light curves from FELIX.

3.3.17 KIC2569576

KIC2569576 is the second mentioned star of the NGC6791 cluster, denoted B3. A small amount of observation quarters are available for this pulsator, its LSP is presented on Fig. 3.19. The star is likely to be only pulsating in the g-mode region, as also suggested by its derivated atmospheric parameters: $T_{\rm eff} = 23540 \pm 210$ K and $\log g = 5.311 \pm 0.035$ dex [49].

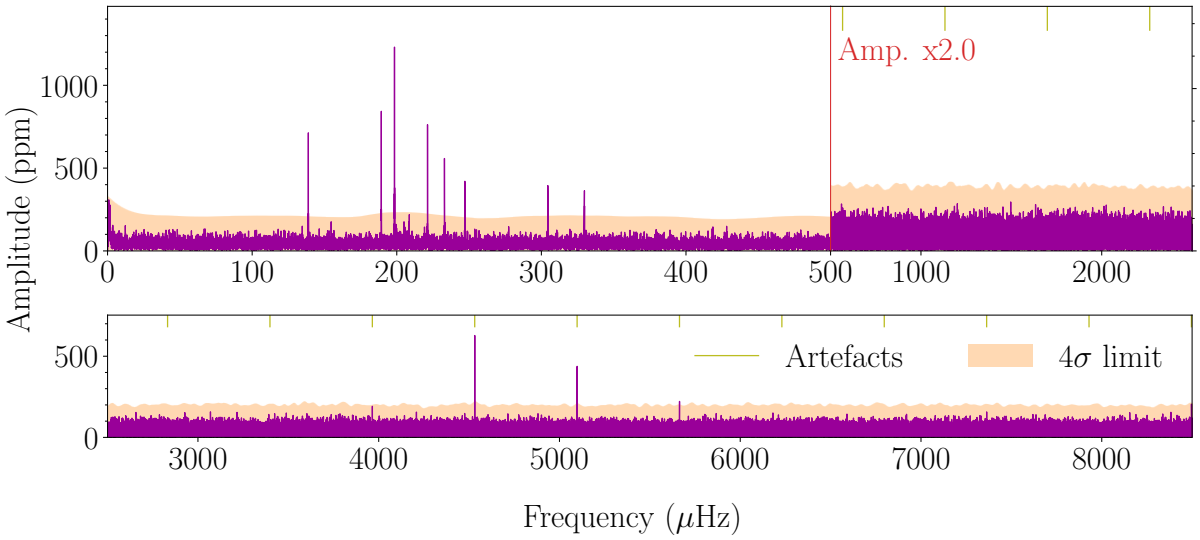

Figure 3.19: LSP of KIC2569576 light curves from FELIX.

As described in more detail in Sec. 3.3.2 for KIC2437937, an analysis of the *Kepler* super-aperture LC data is available [49]. In this analysis, much more g-mode frequencies were detected and led to an estimate of the rotation period: $P_{\rm rot} = 64.2 \pm 1.1$ days [49], from rotational splittings. However, splittings used for this estimate are varying quite much, as the difference between the maximum and minimum rotation estimated is around 22 days. Even if the mentioned paper detects more modes than what is visible in the presented LSP, there are still not much detectable modes for this pulsator.

3.3.18 KIC2438324

The last pulsator mentioned in this work is also the last pulsating sdB of the NGC6791 cluster to be studied, B4. Derivated atmospheric parameters are $T_{\rm eff} = 25290 \pm 300$ K and $\log g = 5.510 \pm 0.043$ dex [49]. As for other pulsating sdBs of the cluster, KIC2438324 seems to be a pure g-mode pulsator, as it can be seen in Fig. 3.20. Unlike B3 and B5, there are enough available quarters in *Kepler* to have a clear frequency spectrum. KIC2438324 is also known to be a binary system with a white dwarf (dM) orbiting at an orbital period of around 0.40 days, resulting in a visible high amplitude peak around 29 μHz [49].

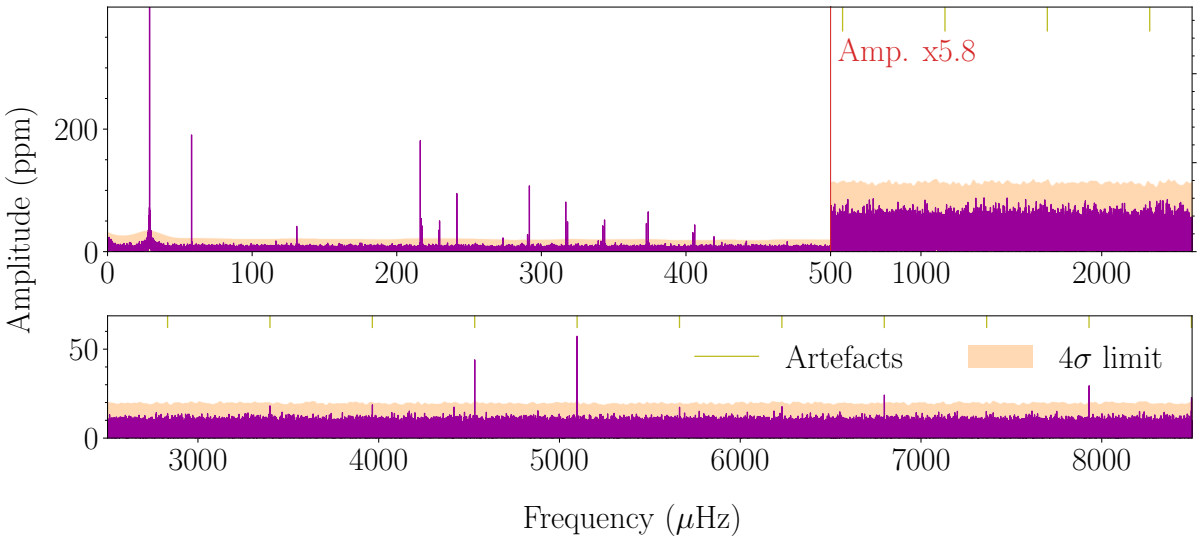

Figure 3.20: LSP of KIC2438324 light curves from FELIX.

This star is rich in multiplets and its frequency and amplitude modulations have been studied, as KIC11179657 and KIC3527751 [42, 41]. From rotational splittings, the rotation period has already been found and is $P_{\rm rot} \simeq 9.63$ days [67], which is also faster than typical values found for pulsating sdBs in the original *Kepler* field.

3.4 General comparison and selection

Among all 18 pulsating sdBs of the original *Kepler* field, only 2 are dominated by p-modes: KIC10139564 (hybrid) and KIC2991276 (pure p-mode pulsator). For two other pulsators, their LSP was not showing any detectable mode in our investigation, either from a lack of observational data (KIC2437937) or either from the contamination of the spectrum by binary harmonics (KIC9472174). In the remaining sdBs, 7 are hybrid but largely dominated by g-modes, and 7 others seems not having pulsations in the p-mode region, and are hence pure g-mode pulsators. From their atmospheric properties mentioned earlier, it is also possible to insert them in a log g - $T_{\rm eff}$ diagram, presented on Fig. 3.21.

It can be clearly seen that, as represented on Fig. 3.1, g-mode pulsators tend to have smaller effective temperature and surface gravity than p-mode pulsators. There is also the transition region where most of hybrid pulsators are. Analyzing its position on the graph, KIC9472174 could be a hybrid pulsator, certainly dominated by g-modes. Concerning KIC2437937, its position suggests either a pure g-mode pulsator, either a hybrid pulsator,

largely dominated by g-modes. This possibility fits well with the analysis of Sanjayan et al. (2022) [49] described for KIC2437937.

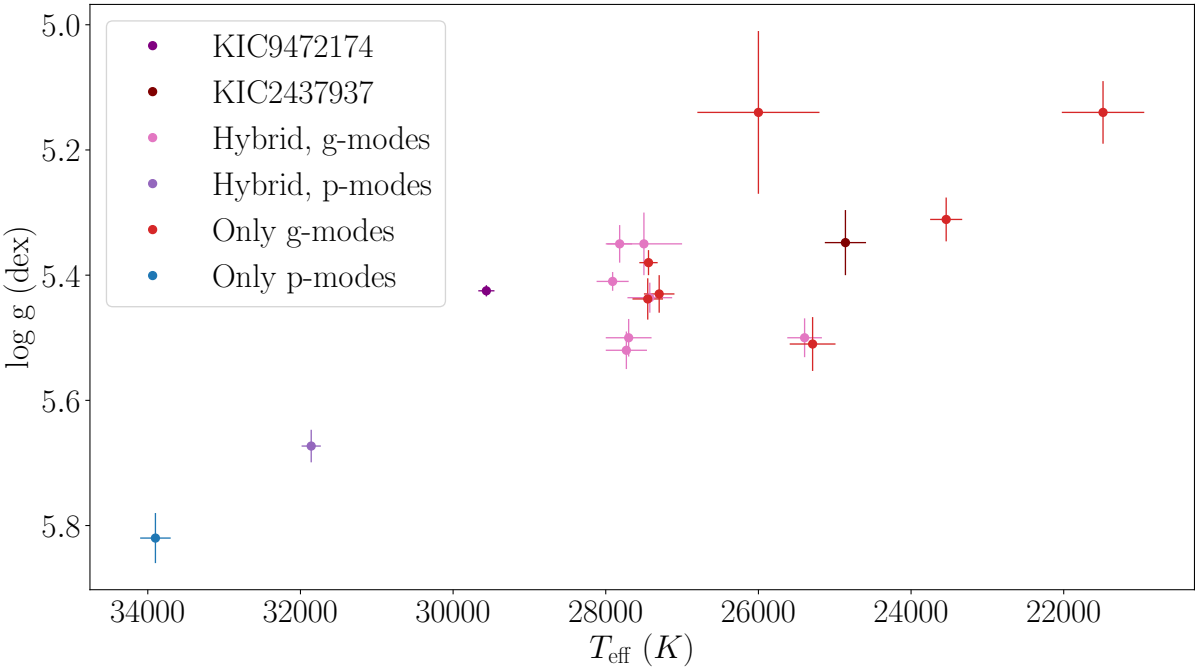

Figure 3.21: Log g - $T_{\rm eff}$ diagram of the 18 pulsating hot subdwarfs in the original *Kepler* field.

P-mode dominated sdBs, KIC9472174 and KIC2437937 are not going to be investigated further for mode identification. Note that this work aims to analyze g-modes, which are of main interest for seismic modeling. Concerning the others, some of them do not have enough g-modes being above the 4σ amplitude threshold such as KIC8302197, KIC7664467, KIC11179657, KIC2991403, KIC2569576 and KIC2438324. To this list must be added KIC10670103, presenting too many g-modes and thus making the identification more challenging.

Concerning mode trapping, many sources suggested trapping but only two are complete enough to have a basis for a possible mode identification: KIC10553698 and KIC10001893. KIC5807616 is the only remaining pulsator for which trapping has not been discussed in the literature, making it interesting to study. Therefore, a choice has to be made for this master thesis between KIC10553698, KIC10001893 and KIC5807616. At the end, KIC5807616 was chosen, essentially because no complete and convincing mode identification were available in the literature. It is also a very promising star for asteroseismology [53].

To conclude, Tab. 3.3 summarizes the important properties discussed in this section, where the chosen pulsator to study is highlighted in bold. A complete overview of each pulsator has been done. After a brief comparison, the choice finally converged to KIC5807616. The next sections are thus dedicated to the mode identification of the pulsation modes in KIC5807616.

Table 3.3: Overview of pulsating hot subdwarfs in the original *Kepler* field, summary table.

Sdb pulsator	**Binary**	**Pulsator type**	**P_{rot} (d)**	**Err (d)**	**Trapping**
KIC9472174	dM	/	/	/	/
KIC2437937	/	/	71.0	±1.8	No
KIC3527751	/	Hybrid, g-modes	15.3	±0.7	Probable
KIC11558725	WD	Hybrid, g-modes	∼44	/	Probable
KIC5807616	/	**Hybrid, g-modes**	∼ 39.2341	/	**No**
KIC10553698	WD	Hybrid, g-modes	41	±3	Yes
KIC2697388	/	Hybrid, g-modes	∼45	/	Probable
KIC7668647	WD	Hybrid, g-modes	∼ 46 to 48	/	Probable
KIC10001893	/	Hybrid, g-modes	/	/	Probable
KIC10139564	/	Hybrid, p-modes	25.6	±1.8	/
KIC8302197	/	Only g-modes	/	/	Probable
KIC7664467	/	Only g-modes	35.1	±0.6	Probable
KIC10670103	/	Only g-modes	88	±8	Probable
KIC11179657	dM	Only g-modes	∼7.4	/	No
KIC2991403	dM	Only g-modes	∼10.46	/	Probable
KIC2991276	/	Only p-modes	/	/	/
KIC2569576	/	Only g-modes	64.2	±1.1	No
KIC2438324	WD	Only g-modes	∼9.63	/	No

Chapter 4

Results of mode identification

The first main step before diving into the mode identification was to select the star to be studied. But to practice and get used with the identification of g-modes in sdB stars, TIC441725813 is first studied from the observations of the *TESS* space telescope. This pulsator has already been studied very recently in 2024 by Su et al. (2024) [32], also by using FELIX to extract the pulsation properties. The purpose of doing a second identification for TIC441725813 is thus to check the methodology used in this work and to have a comparison with the results given in the literature.

The second studied pulsator is KIC5807616, also known as Kepler-70 or KPD 1943+4058, a pulsating sdB observed in the original *Kepler* field. It is a hybrid pulsator with a rich g-mode spectrum. It presents rotational multiplets, indicating that it is a slow rotator. The selection of KIC5807616 to be the main studied star was done in the previous chapter, with a description of KIC5807616 presented in Sec. 3.3.5. In this chapter, the mode identification obtained for this pulsator will be presented in Sec. 4.2, following the methodology described in Chap. 2.

4.1 First pulsator: TIC441725813

TIC441725813, also known as TYC 4427-1021-1, has been classified as a sdB star only recently and is among the brightest known stars of this type, with an apparent magnitude V of 10.90 [68]. Its effective temperature and surface gravity reach $T_{\rm eff} = 27827 \pm 177$ K and $\log g = 5.463 \pm 0.028$ dex [32].

This star has been observed with *TESS* in a total of 26 sectors with four main datasets of consecutive sectors. In the primary mission, it has been observed from S14 to S25 in SC with a sampling of 2 min. In the extended mission, additional observations in S40-41, S47-52 and S55-60 are also available in SC but also in ultrashort cadence with a sampling of 20 s (see Sec. 2.1.2). The Nyquist frequencies associated to these cadences are $f_{\rm Nyq,\ SC} \simeq 4167$ μHz and $f_{\rm Nyq,\ ultrashort} \simeq 25000$ μHz. The ultrashort cadence data is preferred when available to catch higher frequencies, but both Nyquist frequencies are high enough to study efficiently all g-modes of the star. These four datasets are denoted G1, G2, G3 and G4 in this work, respectively.

The LSP of each dataset is displayed in Figs 4.1, 4.2, 4.3 and 4.4 and their frequency resolution is indicated in Tab. 4.1. The 4σ detection threshold corresponding to each dataset is obtained from the FAP calculation performed by FELIX and is also shown on

Tab. 4.1. Unlike with *Kepler* data, the calculation has been performed for all sectors. As can be observed in these LSPs, TIC441725813 is a hybrid pulsator, with a clear dominance of g-modes.

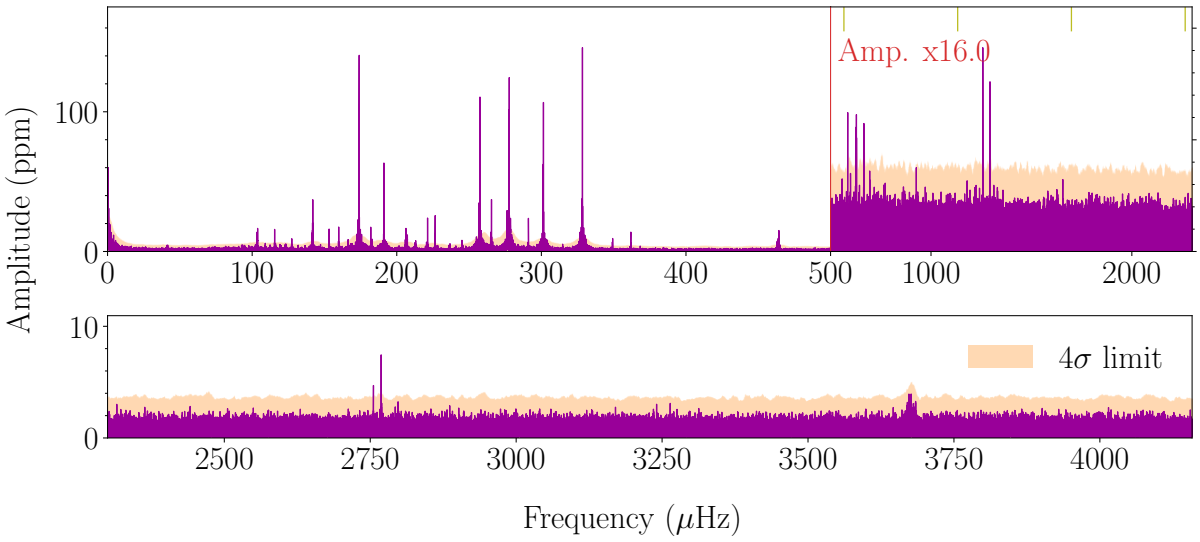

Figure 4.1: LSP of the TIC441725813 light curves, for the G1 dataset, from FELIX.

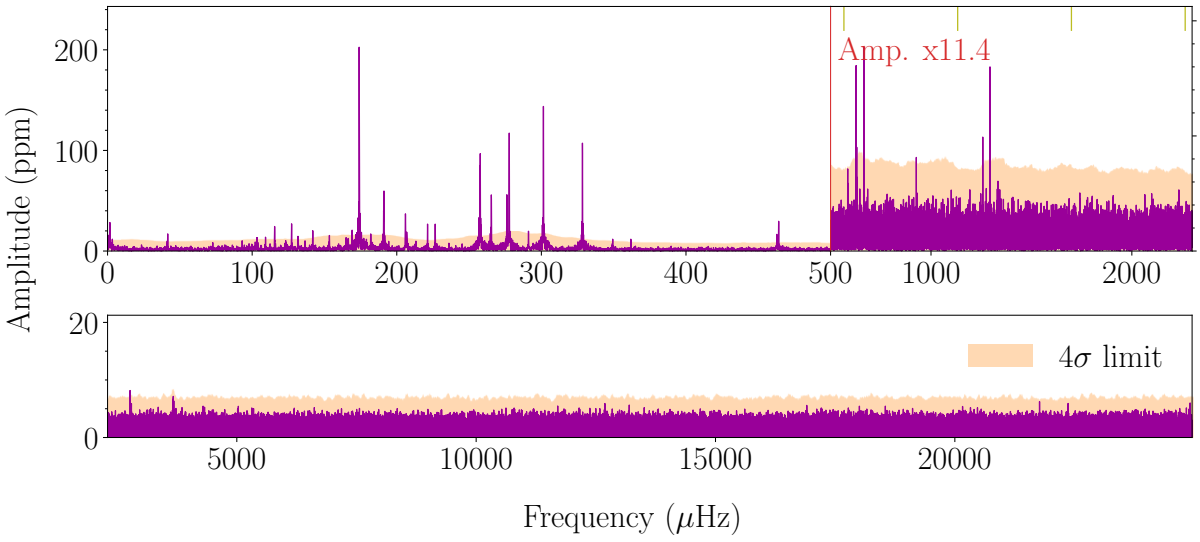

Figure 4.2: LSP of the TIC441725813 light curves, for the G2 dataset, from FELIX.

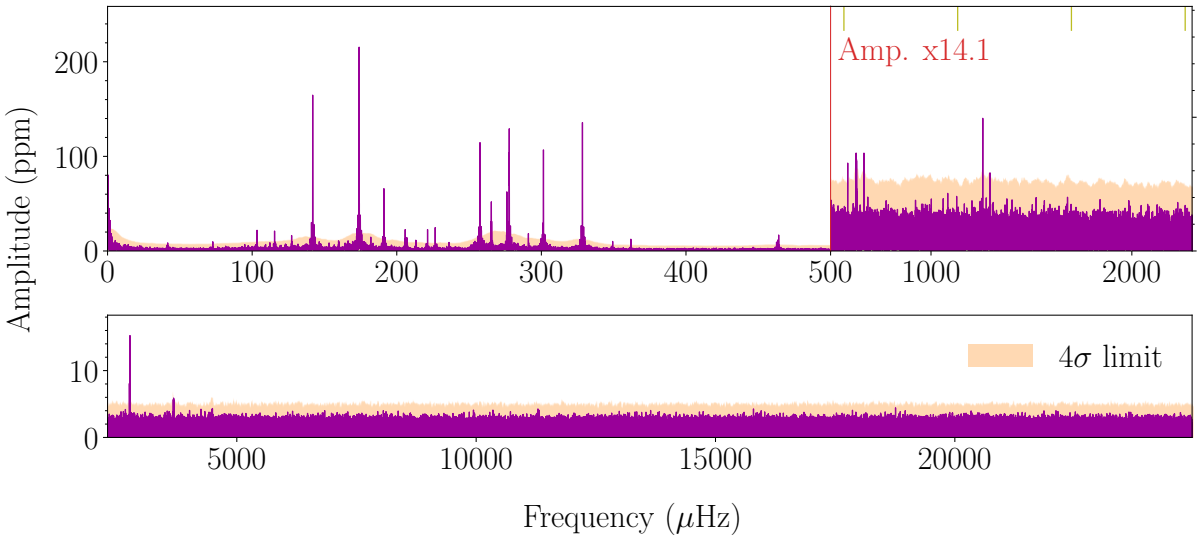

Figure 4.3: LSP of the TIC441725813 light curves, for the G3 dataset, from FELIX.

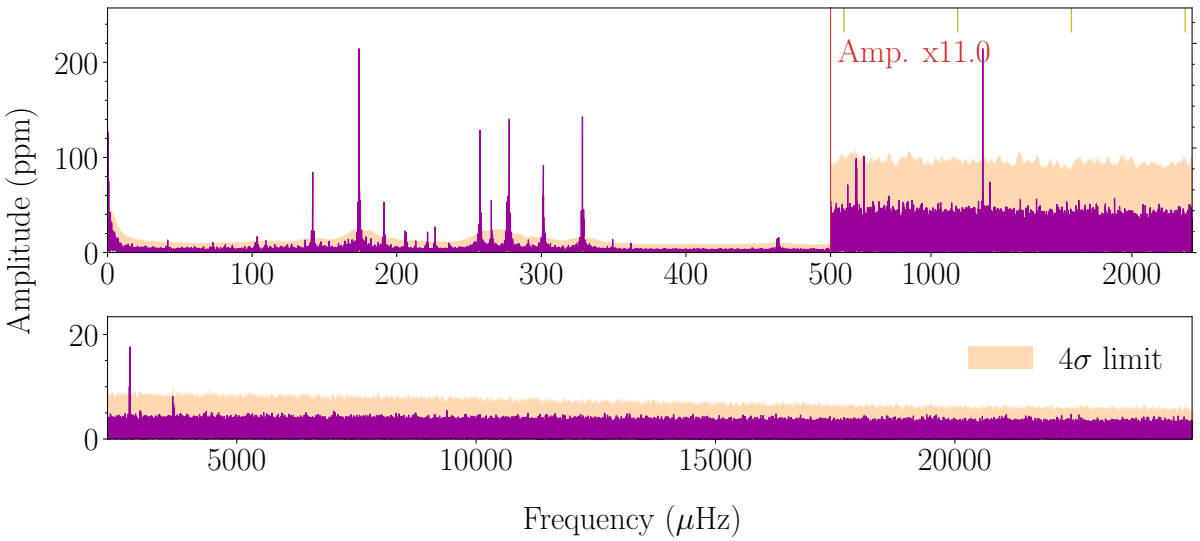

Figure 4.4: LSP of the TIC441725813 light curves, for the G4 dataset, from FELIX.

Table 4.1: SNR thresholds computed from the FAP calculation for frequency peaks detection in the LSP of G1, G2, G3 and G4 datasets of TIC441725813. The resolution of the LSP is also indicated.

Dataset	**Sectors**	**LSP resolution**	4σ	3σ	2σ	1σ
G1	S14-25	36 nHz	5.34	4.89	4.51	4.20
G2	S40-41	207 nHz	5.25	4.71	4.26	3.92
G3	S47-52	71 nHz	5.39	4.86	4.42	4.10
G4	S55-60	70 nHz	5.42	4.81	4.41	4.08

The analysis of Su et al. (2024) [32] included a discussion about the possible orbital signature of a companion from frequency peaks around ∼41 μHz. In this work, the goal of the analysis of TIC441725813 is to get used with the identification of g-modes. On this basis, the extraction with FELIX is done for frequencies ranging between 50 and 700 μHz. The extraction is done with the 4σ threshold independently on G1, G2, G3 and G4. In total, 134 (G1), 55 (G2), 80 (G3) and 65 (G4) frequencies were detected above the 4σ threshold. The list of frequencies extracted at 4σ for TIC441725813 is presented in Appendix C, for each dataset (Tabs. C.1, C.2, C.3 and C.4).

The resolution of the LSP of all datasets is higher than the typical range of frequency modulations of 10-20 nHz (see Tab. 4.1). Thus, the distinction between potential multiplets and frequency modulations is done visually by inspecting the time-frequency maps in FELIX. The clearing of modulations is done for all datasets, following the methodology described in Sec. 2.3.2. Tab. 4.2 presents the number of remaining frequencies after the frequency modulation clearing for each dataset.

Table 4.2: Number of frequencies before and after the frequency modulation (FM) clearing and resolution of the LSP in the different analyzed datasets of TIC441725813.

Parameter	**G1**	**G2**	**G3**	**G4**
Nb. of modes before FM clearing	134	55	80	65
Nb. of modes after FM clearing	56	38	51	43

4.1.1 Rotationally-splitted modes

The identification of rotationally-splitted modes observed by *TESS*, and cleared from the frequency modulations, is performed by following the methodology described in Sec. 2.3.3. In the analysis of Su et al. (2024) [32], the rotation period of the envelope was estimated from relevant rotationally-splitted p-modes for the G1 dataset. They estimated it to be 17.9 $\pm$ 0.7 days. However, their estimation of the rotation period of the core, based on identified $\ell = 1$ multiplets, revealed a rotation period of the core of 85.3 $\pm$ 3.6 days. Hence, the core would be rotating much more slowly than the envelope. Based on the rotation period of the core and by using Eq. (2.9), the frequency spacing between g-modes of consecutive m and same k is given by

$$\Delta\nu_{k1} \simeq 0.067 \pm 0.001 \ \mu\text{Hz and } \Delta\nu_{k2} \simeq 0.111 \pm 0.005 \ \mu\text{Hz}. \tag{4.1}$$

The number of potential multiplets appeared to be the highest for the G1 dataset with 7 potential multiplets detected. No new potential multiplets were found in other datasets, which are just confirming the multiplets found in G1 (3 for G2, 6 for G3 and 6 for G4). Indeed, the G1 dataset is the dataset with the best frequency resolution, due to its longer observation time baseline. Therefore, for the identification of rotational multiplets, only the G1 dataset is used. From Eq. (4.1), the identification of the potential multiplets of the G1 dataset is performed. After the identification, 5 out of 7 multiplets have been identified, the others not being complete enough. All 5 modes appeared to be $\ell = 1$ multiplets, and their identification is presented in Tab. 4.3.

Table 4.3: Rotationally-splitted g-modes identification of TIC441725813. Associated errors are indicated next to the value. Central frequencies ($m = 0$) are highlighted in bold.

ID	Frequency (μHz)		$\Delta\nu$ (μHz)		Amplitude (%)		S/N	m	ℓ
	190.9852	5.19E-04			0.0355	9.42E-04	37.71	-1	
			0.063	8.52E-04					
f24	**191.0478**	**6.75E-04**			**0.0273**	**9.40E-04**	**29.00**	0	1
			0.066	7.32E-04					
	191.1138	2.82E-04			0.0654	9.42E-04	69.43	+1	
	213.0797	1.91E-03			0.082	7.97E-04	10.25	-1	
			0.076	3.84E-03					
f22	**213.1560**	**3.33E-03**			**0.0047**	**7.95E-04**	**5.88**	0	1
			0.064	4.20E-03					
	213.2203	2.56E-03			0.0061	7.94E-04	7.63	+1	
	257.5512	1.45E-04			0.1082	8.03E-04	134.84	-1	
			0.067	3.55E-04					
f15	**257.6185**	**3.24E-04**			**0.0484**	**8.01E-04**	**60.47**	0	1
			0.070	3.63E-04					
	257.6885	1.63E-04			0.0958	7.99E-04	120.02	+1	
	277.6765	1.58E-04			0.1007	8.14E-04	123.78	-1	
			0.064	2.85E-04					
f12	**277.7402**	**2.38E-04**			**0.0670**	**8.13E-04**	**82.40**	0	1
			0.065	2.69E-04					
	277.8048	1.27E-04			0.1251	8.12E-04	154.16	+1	
	301.3637	2.74E-04			0.0569	7.96E-04	71.55	-1	
			0.066	3.10E-04					
f9	**301.4298**	**1.46E-04**			**0.1066**	**7.94E-04**	**134.21**	0	1
			0.066	9.92E-04					
	301.4955	9.82E-04			0.0158	7.92E-04	19.94	+1	

Table 4.3 continued from previous page

ID	Frequency (μHz)		$\Delta\nu$ (μHz)		Amplitude (%)		S/N	m	ℓ
	328.3312	5.08E-04			0.0273	7.10E-04	38.50	-1	
			0.074	5.18E-04					
f7	**328.4050**	**9.67E-05**			**0.1446**	**7.14E-04**	**202.46**	0	1
			0.074	1.02E-03					
	328.4791	1.01E-03			0.0138	7.15E-04	19.30	+1	

Multiplets found in this analysis are the same as the ones presented in the analysis of Su et al. (2024) [32]. From Tab. 4.3, the mean frequency spacing of $\ell = 1$ multiplets is estimated: $\Delta\nu_{\ell=1} = 0.068 \pm 0.005$ μHz, which is very close to the one estimated by Su et al. (2024) [32] in Eq. (4.1). Thus, this work also suggests that the core of TIC441725813 is rotating much more slowly than its envelope. This feature was claimed for other known sdB pulsators in the past, all potentially being a binary star. The link between tidal interactions of sdB stars with their companion star and their observed differential rotation is nevertheless still hypothetical [32].

4.1.2 Final identification

In this master thesis, instead of doing an identification independently for each dataset, the choice is made to derive a single frequency list from all datasets and to perform the identification on this list. Most of the pulsation modes are present in all datasets, but some modes are sometimes missing in one or several of them. Modes cleared from frequency modulations and rotational splitting obtained from G1, G2, G3 and G4 datasets are thus merged, following this methodology:

- In the case of a mode present in one or more datasets, the mode of the highest S/N is taken. Note that because the G2 dataset is lacking frequency resolution compared to the others, the mode is taken only if it is not present in other datasets.
- In the case of a multiplet, the central frequency having the highest S/N is taken.

This merged dataset is denoted G1234 in this work. After the merging, the G1234 dataset contains a total of 47 modes. The KS test is performed on the G1234 dataset, and compared to the modes obtained only with the G1 dataset. The resulting KS tests are shown on Fig. 4.5.

The period spacing between two $\ell = 1$ modes of consecutive k is given by the minimum value of $\log Q$ (see Sec. 2.3.4). For the G1 dataset, there is a minimum at ~ 271.7 s. For the G1234 dataset, the peak is more visible, at ~ 266.7 s. The period spacing between two consecutive $\ell = 2$ modes can be obtained from Eq. (2.13), and is also visible in the KS tests. For both G1 and G1234 datasets, a second minimum is present at ~ 151.05 and ~ 155.75 s, respectively, confirming the $\sqrt{3}$ relation. The deeper peaks observed in the G1234 analysis make this dataset more reliable for identification based on period spacing. Thus, used period spacings in this analysis are $\Delta P_{\ell=1} = 266.7$ s and $\Delta P_{\ell=2} = 155.75$ s.

From $\ell = 1$ and $\ell = 2$ spacings found with the KS test, the identification is performed in the same way than described in Sec. 2.4. The identification of TIC441725813 resulted in

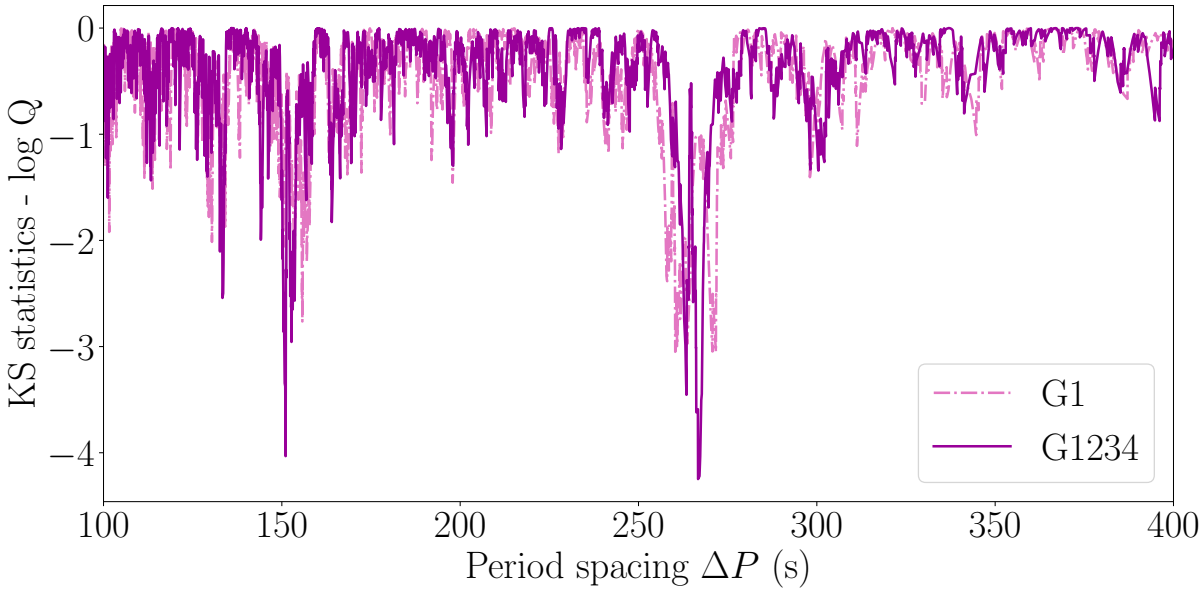

Figure 4.5: KS test of TIC441725813 extracted frequencies, for G1 and for G1234.

a total of 44 identified modes out of 47, ranging from ∼1500 to ∼14000 s. Among them, 28 modes of $\ell = 1$ and 16 modes of $\ell = 2$ were identified. Concerning k values, they are attributed such that the relation of Eq. (2.14) is respected for both $\ell = 1$ and $\ell = 2$ modes. The final identification of the ℓ and k values of each observed mode is available in Tab. D.1 in Appendix D. Note that the values of k are valid within Δk. The dataset from which each modes was taken and the occurrence in other datasets are also indicated.

The $\ell = 1$ and $\ell = 2$ chains are mostly localized at reduced periods between ∼4000 to ∼13000 s, which is also the case for other sdB stars. The associated period-spacing diagram is shown on Fig. 4.6. There is no trapping in this configuration, and all identified modes enter well in the asymptotic spacing sequence. The reliability of main $\ell = 1$ and $\ell = 2$ chains is enhanced by the different overlaps, as defined in Sec. 2.4, but some gaps are present along the chain, visible in the diagram. Some $\ell = 2$ modes are nevertheless not overlapping horizontally the $\ell = 1$ mode having the same reduced period. Not having a perfect overlap can be due to several factors. First, the identification is affected by choices in the frequency modulation clearing and the attribution of central frequencies for multiplets. Also, theoretical models of sdB stars do not necessarily predict a perfect overlap in the period ranges studied here [8]. A possible explanation is the slightly different influence of the convective superficial zone (see Fig. 1.5b) on the $\ell = 1$ and $\ell = 2$ modes, for a small range of k orders.

The S/N of the modes as a function of their period is shown on Fig. 4.7. It can directly be seen that all modes having a high S/N are identified. In the 10 modes of highest S/N, there are 6 $\ell = 1$ modes and 4 $\ell = 2$ modes, and surprisingly, their mean S/N is higher than for $\ell = 1$ modes in general (S/N $\sim$ 56 for $\ell = 1$ and S/N $\sim$ 90 for $\ell = 2$). This difference of S/N is due to the *f13* and *f14* $\ell = 2$ modes (see Tab. D.1), having very high S/N compared to other $\ell = 2$ modes. Looking at the 20 modes of highest S/N, the number of $\ell = 1$ modes increases to 14, with five $\ell = 2$ modes and an unidentified one, which is more compliant with expectations.

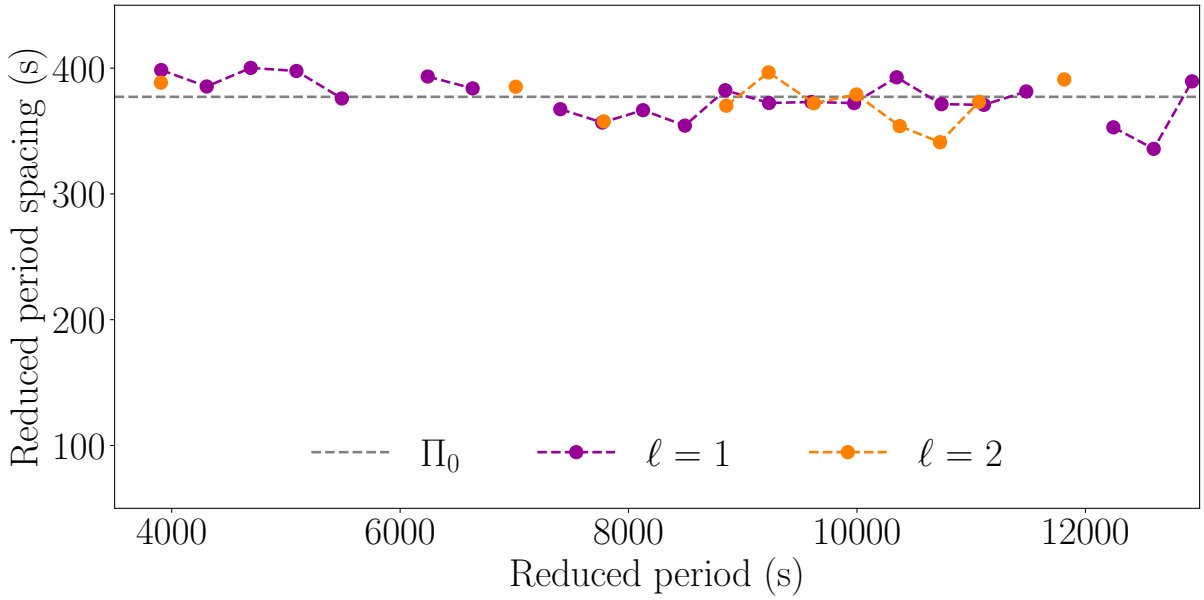

Figure 4.6: Period-spacing diagram for the TIC441725813 mode identification.

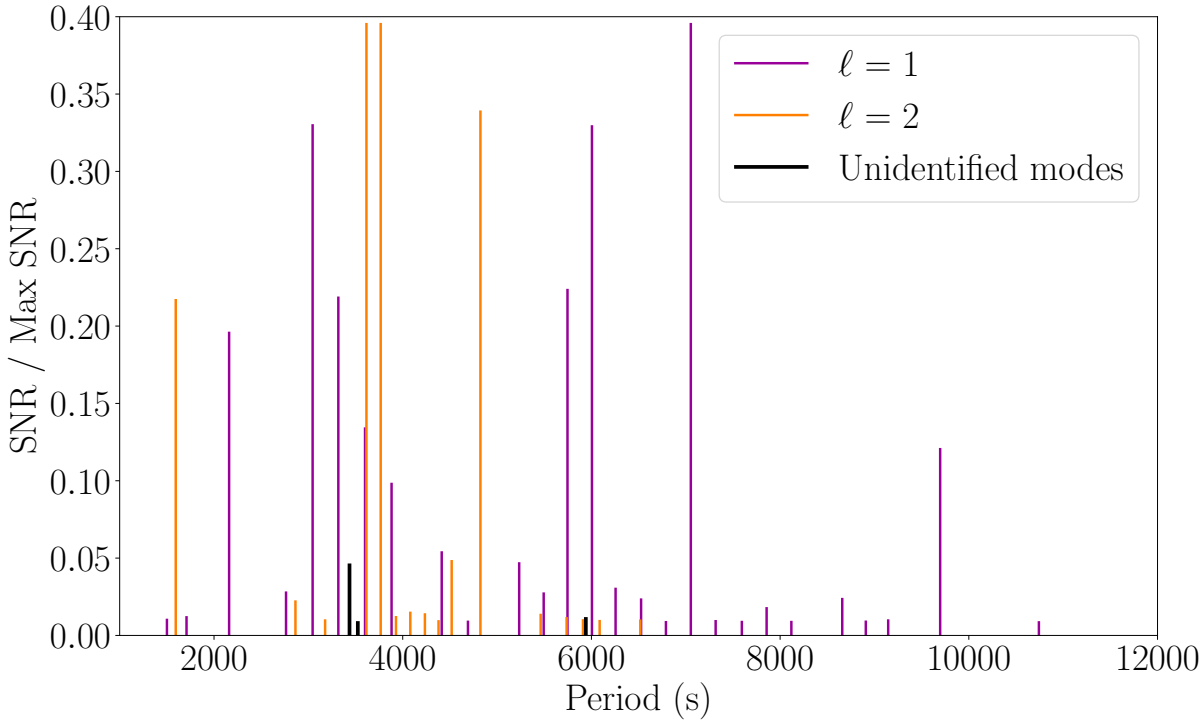

Figure 4.7: S/N diagram TIC441725813 mode identification. Unidentified modes are highlighted in black.

Among all modes, 3 modes remained unidentified: *f10* = 291.037 μHz, *f11* = 283.761 μHz and *f30* = 168.330 μHz (see Tab. D.1). For *f30* and *f11*, they are only localized in the G1 dataset, which is not surprising as it is the dataset with the best frequency resolution. The analysis of the time-frequency maps before prewhitening showed that *f30* and *f11* are not visible. However, after prewhitening nearby frequencies with high S/N, the local noise level is reduced, allowing the S/N of *f11* and *f30* to increase sufficiently to have a S/N above the detection threshold. In the case of *f11* and *f30*, they only show some hints of being pulsation modes in their time-frequency map, as shown on Figs. 4.9 and 4.10. Therefore, they also possibly due to noise fluctuations. Concerning *f10*, its S/N is much higher and it is clearly visible in the time-frequency maps, as shown on Fig. 4.8 for the G1 dataset. The paper of Su et al. (2024) [32] does not mention this mode even if they detected it with similar S/N values [32, 69].

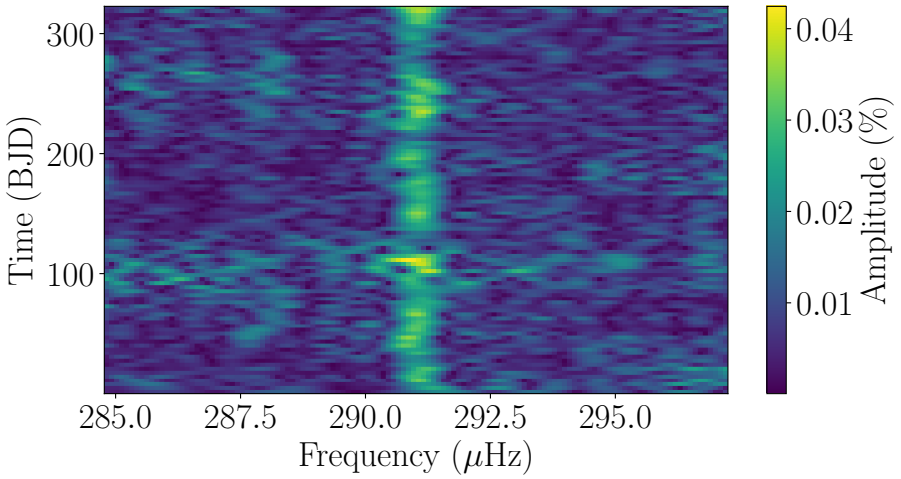

Figure 4.8: Time-frequency map of *f10* in the G1 dataset for TIC441725813.

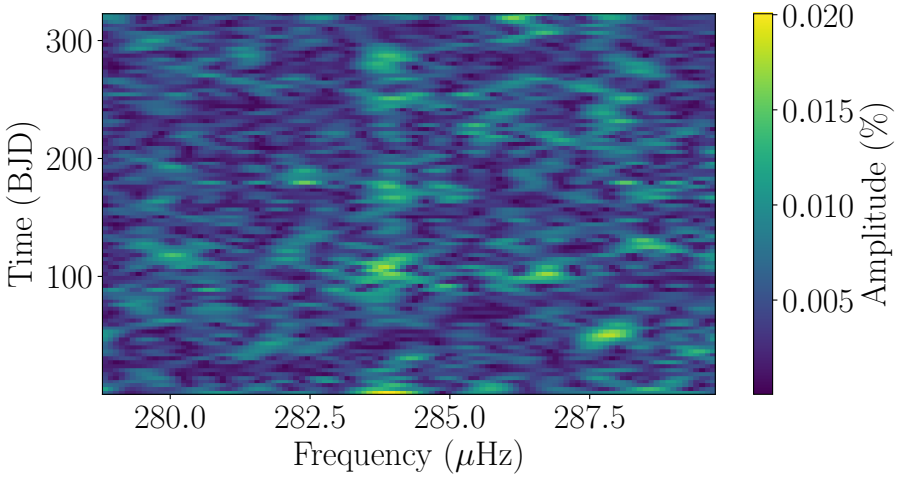

Figure 4.9: Time-frequency map of *f11* after the prewhitening of nearby frequencies in the G1 dataset for TIC441725813.

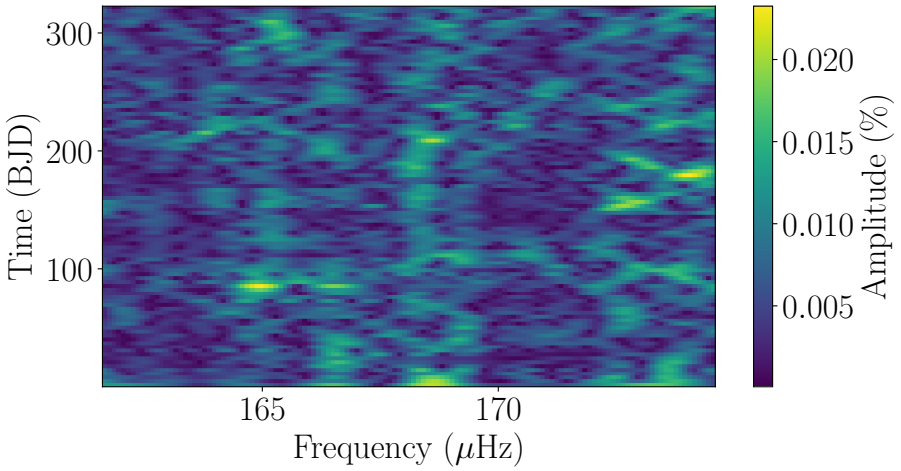

Figure 4.10: Time-frequency map of *f30* after the prewhitening of nearby frequencies in the G1 dataset for TIC441725813.

The possibility that unidentified modes are $\ell = 4$ modes has also been investigated. However, no reduced period overlap could was found. The only hint going in the sense of a $\ell = 4$ identification is that the period spacing between *f10* and *f11* is actually close to what can be expected between two consecutive $\ell = 4$ modes. The latter is obtained from Eq. (2.10), and is given by

$$\Delta P_{\ell=4} = \frac{\Delta P_{\ell=1}}{\sqrt{5}} \simeq 84 \text{ s}, \tag{4.2}$$

while the period spacing between *f10* and *f11* is equal to 88.10 s. This is not sufficient to have any conclusion regarding the $\ell = 4$ identification of *f10* and *f11*, but it is kept as a possibility.

It is also possible that these unidentified modes, and especially *f10*, are trapped modes. An alternative representation of the period-spacing diagram by identifying *f10* and *f30* as trapped $\ell = 1$ modes is shown on Fig. 4.11. In this configuration, the reduced period spacing between the two trapped modes would be around 5000 s, which is twice the typical spacing observed in KIC10553698 [17]. However, the amount of detected modes in TIC441725813 limits the possibility to investigate further this possible trapping, and no overlapping potential $\ell = 2$ trapped modes could be associated. This configuration can thus also be a possibility, but the main identification is more reliable.

Except for the mentioned unidentified modes, this identification is very similar to the one proposed by Su et al. (2014) [32]. Slight differences can be retrieved in the identified frequencies but at the order of frequency modulations, witnessing maybe another way of determining relevant frequencies from the raw data.

To conclude, the analysis of TIC441725813 led to the identification of most of the pulsation modes, confirming the available identification in the literature. An alternative identification with trapping was proposed based on unidentified modes and should be kept in mind for further investigation or when integrating the identification in seismic modeling.

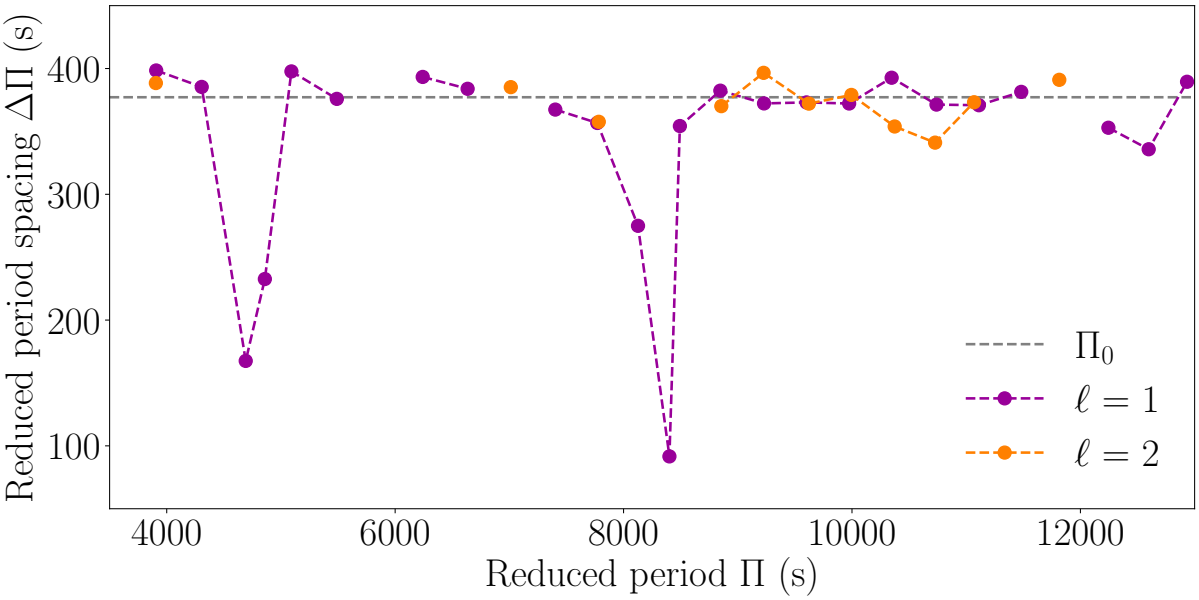

Figure 4.11: Period-spacing diagram including *f10* and *f30* as possible trapped modes for TIC441725813 mode identification.

4.2 Second pulsator: KIC5807616

The choice is made in this work to analyze the whole observed dataset, corresponding to the quarters Q2.3 and Q5 to Q17.2, to have a complete overview of all the potential modes of the star. The LSP for the whole dataset was already shown on Fig. 3.7. The FAP calculation performed by FELIX resulted in a 4σ threshold with a S/N of 5.14, for Q10 and Q11 data together, as shown on Fig. 4.12.

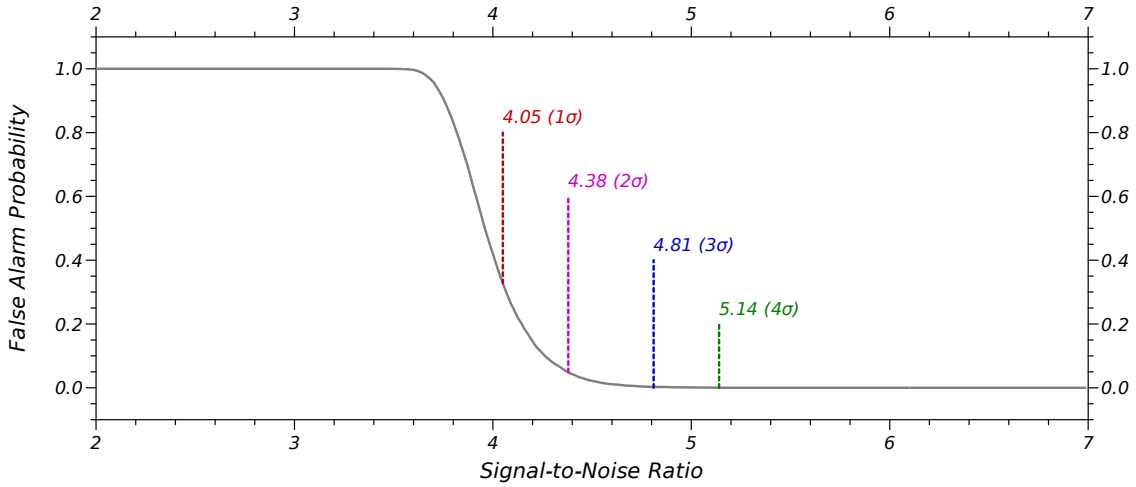

Figure 4.12: False alarm probability with respect to the S/N computed by FELIX corresponding to the LSP of KIC5807616, for Q10 and Q11.

The two available estimations of the rotation period for this star are based on the mean frequency spacing observed in two p-mode multiplets detected around 3447.2 and 3431.8 μHz. Including them in the analysis would allow us to obtain an independent estimate of

$P_{\rm rot}$. Therefore, the frequency extraction is done for frequencies ranging from 0 to ∼4000 μHz to be sure to catch all the g-mode spectrum of the star and relevant p-modes for the rotation period estimation. In the literature, planetary candidates were derived by the detection of peaks in the very low-frequency region around 48.2 μHz and 33.8 μHz [54]. Even if it is not the goal of this work, including this region is the identification can give hints about the real nature of these peaks.

Concerning the extraction, it is done with the 4σ (S/N = 5.14) threshold, but only frequencies with a S/N higher than 6.0 are used for the analysis to be sure that no frequency is due to the noise fluctuations. However, during the identification from period spacing, the 4σ list is used to possibly include modes that could enter well in the $\ell = 1$ or $\ell = 2$ chains. In total, 508 frequencies were detected above the 4σ threshold, including 420 frequencies with a S/N above 6.0. The list of frequencies extracted at 4σ for KIC5807616 is presented in Tab. C.5 of Appendix C.

The analysis of frequency modulations showed that the initial limit of 10-20 nHz is not sufficient to eliminate the majority of them. Instead, the limit is increased to 40 nHz. Even with this new limit, the boundary between frequency modulation and rotational splitting is difficult to determine for several modes and the analysis is done visually, based on their time-frequency maps. After the frequency modulation clearing, 139 frequencies remained.

4.2.1 Rotationally-splitted modes

In the list of 139 frequencies resulting from the frequency modulation clearing, 34 modes appeared to be potential multiplets, with the presence of rotational splitting. We remind that estimated values for the rotation period are $P_{\rm rot,\ Q5\text{-}Q6} = 39.2341$ days by Charpinet et al. (2011) [54] and $P_{\rm rot,\ all\ Q} = 44.9 \pm 1.1$ days by Krzesinski (2015) [55]. Among the potential rotational multiplets of this work, the two same p-modes used to determine $P_{\rm rot,\ Q5\text{-}Q6}$ and $P_{\rm rot,\ all\ Q}$ are present. The splittings between frequencies of those 2 p-modes are calculated and shown on Tab. 4.4. An identification is also provided, based on the number of observed splitted frequencies in the mode.

To determine the rotation period of the star, Eq. (2.8) is used. The mean spacing between p-mode multiplets can be obtained from Tab. 4.4:

$$\Delta\nu_{\rm p\text{-}modes} = 0.289 \pm 0.034\ \mu\text{Hz}. \tag{4.3}$$

Thus, the inferred rotation period of the envelope is given by

$$P_{\rm rot,\ env} = \frac{1}{\Delta\nu_{\rm p\text{-}modes}} = 40.0 \pm 4.7\ \text{days}. \tag{4.4}$$

The observed rotation period thus agrees with estimates available in literature. From $P_{\rm rot,\ env}$, assuming that the star has no differential rotation, the frequency spacing would be given for $\ell = 1$ and $\ell = 2$ by (using Eq. (2.9)):

$$\Delta\nu_{k1} \simeq 0.145 \pm 0.017\ \mu\text{Hz and } \Delta\nu_{k2} \simeq 0.237 \pm 0.028\ \mu\text{Hz}. \tag{4.5}$$

Among all g-mode multiplets, only 9 are complete enough to have an identification: 7 multiplets of $\ell = 1$ and 2 multiplets of $\ell = 2$. The identification of rotationally-splitted g-modes is presented in Tab. 4.5.

Table 4.4: Rotationally-splitted p-mode multiplets used to determine the rotation period of KIC5807616. Associated errors are indicated next to the value. Central frequencies ($m = 0$) are highlighted in bold.

ID	Frequency (μHz)		$\Delta\nu$ (μHz)		Amplitude (%)		S/N	m	ℓ
	3431.53051	6.1E-04			0.0022	0.0003	7.72	-1	
			0.297	8.8E-04					
f2	**3431.82770**	**6.4E-04**			**0.0021**	**0.0003**	**7.30**	0	1
			0.302	7.7E-04					
	3432.12939	4.2E-04			0.0032	0.0003	11.28	+1	
	3446.66425	5.9E-04			0.0022	0.0003	7.92	-1	
			0.335	6.8E-04					
f1	**3446.99918**	**3.3E-04**			**0.0040**	**0.0003**	**14.13**	0	
			0.254	6.2E-04					2
	3447.25313	5.2E-04			0.0025	0.0003	9.05	+1	
			0.256	8.5E-04					
	3447.50927	6.8E-04			0.0020	0.0003	6.94	+2	

Table 4.5: Rotationally-splitted g-modes identification of KIC5807616. Associated errors are indicated next to the value. Central frequencies ($m = 0$) are highlighted in bold.

ID	Frequency (μHz)		$\Delta\nu$ (μHz)		Amplitude (%)		S/N	m	ℓ
f29	**301.65397**	**1.3E-05**			**0.1070**	**3.0E-04**	**358.50**	0	
			0.330	7.0E-04					
	301.98366	7.0E-04			0.0020	3.0E-04	6.73	+1	2
			0.290	9.0E-04					
	302.27376	5.7E-04			0.0024	3.0E-04	8.20	+2	
	212.61096	5.4E-04			0.0025	2.9E-04	8.67	-1	
			0.111	5.8E-04					
f44	**212.72219**	**2.1E-04**			**0.0066**	**2.9E-04**	**22.34**	0	1
			0.104	6.0E-04					
	212.82637	5.7E-04			0.0024	2.9E-04	8.28	+1	

Table 4.5 continued from previous page

ID	Frequency (μHz)		$\Delta\nu$ (μHz)		Amplitude (%)		S/N	m	ℓ
	201.62478	2.5E-04			0.0072	3.9E-04	18.43	-1	
			0.174	2.6E-04					
f46	**201.79927**	**2.2E-05**			**0.0821**	**3.8E-04**	**217.34**	0	2
			0.297	1.8E-04					
	202.09612	1.8E-04			0.0097	3.7E-04	26.04	+1	
	199.35091	2.6E-05			0.0712	3.9E-04	180.98	-1	
			0.085	2.6E-05					
f47	**199.43554**	**5.3E-06**			**0.3483**	**3.9E-04**	**888.4**	0	1
			0.119	4.6E-05					
	199.55408	4.6E-05			0.0402	3.9E-04	102.86	+1	
	167.81886	5.3E-06			0.3101	3.5E-04	889.92	-1	
			0.148	6.5E-06					
f51	**167.96648**	**3.7E-06**			**0.4359**	**3.5E-04**	**1262.72**	0	1
			0.119	5.2E-06					
	168.08571	3.6E-06			0.4514	3.4E-04	1313.55	+1	
	122.49085	7.9E-04			0.0021	3.6E-04	5.93	-1	
			0.135	9.8E-04					
f66	**122.62623**	**5.8E-04**			**0.0029**	**3.6E-04**	**8.03**	0	1
			0.173	9.7E-04					
	122.79942	7.8E-04			0.0022	3.6E-04	6.04	+1	
	113.36426	3.2E-04			0.0064	4.4E-04	14.63	-1	
			0.074	7.6E-04					
f69	**113.43798**	**6.9E-04**			**0.0030**	**4.4E-04**	**6.84**	0	1
			0.136	9.1E-04					
	113.57446	5.9E-04			0.0035	4.5E-04	7.94	+1	
	109.41878	5.1E-04			0.0033	3.6E-04	9.29	-1	
			0.115	9.4E-04					
f72	**109.53362**	**7.9E-04**			**0.0021**	**3.6E-04**	**5.96**	0	1
			0.105	9.8E-04					
	109.63852	5.9E-04			0.0029	3.6E-04	7.95	+1	

Table 4.5 continued from previous page

ID	Frequency (μHz)		$\Delta\nu$ (μHz)		Amplitude (%)		S/N	m	ℓ
	89.76150	6.1E-04			0.0024	3.2E-04	7.68	-1	
			0.087	1.0E-03					
f75	**89.84861**	**8.1E-04**			**0.0018**	**3.2E-04**	**5.78**	0	1
			0.112	1.0E-03					
	89.96083	6.4E-04			0.0024	3.2E-04	7.3	+1	

In this list, it is worth mentioning that some frequencies detected slightly under the S/N = 6.0 limit were included. For *f72* and *f75* (see Tab. 4.5), they are surrounded by frequencies with a much higher S/N, so they are very likely real modes. For the $m = -1$ component of *f66*, its S/N is very close to 6.0, it is thus also kept in the rotationally-splitted modes identification. Concerning the 15 remaining multiplets not complete enough to be identified, the frequency of highest S/N is retained for the main identification. Also, it is worth mentioning that for *f29* is identified as a $\ell = 2$ mode, even if observed spacings are larger than what would be expected for such a multiplet.

Regarding the available literature, the identification of rotationally-splitted modes proposed by Charpinet et al. (2011) [54] has similarities with the one realized in this work. Most of multiplets found by them were spotted in this analysis, but were not complete enough to have an identification. Inversely, multiplets presented in Tab. 4.5 were not spotted by their analysis. We remind that they only analyzed Q5-Q6 data, while we analyzed the whole *Kepler* data available for this star.

The mean spacing of $\ell = 1$ and $\ell = 2$ rotationally-splitted modes, respectively, can be estimated from Tab. 4.5 and are given by

$$\Delta\nu_{\ell=1} = 0.110 \pm 0.02 \ \mu\text{Hz and } \Delta\nu_{\ell=2} = 0.27 \pm 0.07 \ \mu\text{Hz}. \tag{4.6}$$

Thus, the rotation period of the core, suggested by observed $\Delta\nu_{\ell=1}$ and $\Delta\nu_{\ell=2}$ spacings would be $\sim$ 43.9 days, but with high errors on the estimation. It is however close to the rotation period of the envelope, and the star is therefore assumed to have a solid-body rotation.

4.2.2 Final identification

The frequency spectrum cleared from frequency modulations and from rotational splitting contains 79 modes in total, ranging from $\sim$300 s to $\sim$30000 s. The remaining 79 modes serve as the basis for the mode identification from period spacing. In theory, the cut-off frequency, which is the physical lower limit for which pulsation modes should not be visible, is known for KIC5807616 and is equal to 61.02 μHz for $\ell = 1$ modes. In term of period, this corresponds to an upper limit of $\sim$ 16400 s. This limit is computed from stellar models and can be different in the reality. In this work, the choice is made to keep modes above it in the identification with the goal to discuss their origin. The KS test has been performed on these 79 modes, and is shown on Fig. 4.13.

The minimum of $\log Q$ is at $\sim$ 239 s, which represents the period spacing between two consecutive $\ell = 1$ modes $\Delta P_{\ell=1}$. The second peak visible at $\sim$ 138 s highlights the period spacing between two consecutive $\ell = 2$ modes $\Delta P_{\ell=2}$. Indeed, from Eq. (2.13), $138 \times \sqrt{3} \simeq 239$ s.

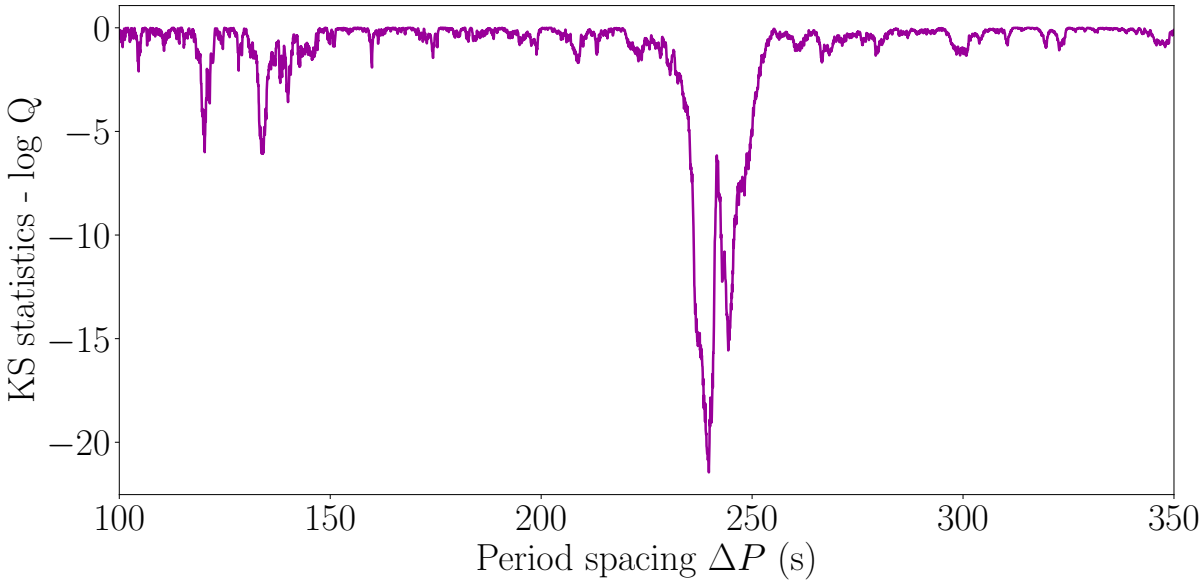

Figure 4.13: KS test of KIC5807616 extracted frequencies.

Based on the KS test, the identification from period spacing is performed by following the methodology described in Sec. 2.4. It is worth mentioning that additionally to $\ell = 1$ and $\ell = 2$ modes, two $\ell = 4$ modes have been identified. The main reasons leading to this $\ell = 4$ identification are discussed later in this section. At the end, instead of having one clear identification, there are three possible identification configurations. The first one has no mode trapping and the two others involve mode trapping. In this work, they will be denoted as followed: Config. without trapping, Config. 1 and Config. 2, respectively. The Configs. 1 and 2 are very similar, the difference being the possibility to have one trapped mode or another for the peak having the highest reduced period. They are thus most of the time discussed together. The final identification of ℓ and k numbers for KIC5807616 is presented in Tab. D.2 of Appendix D.

It appears that the identification led to a large number of modes with a consecutive k number for periods ranging from ∼2000 s to ∼10,000 s. For modes having a period longer than 10,000 s, the spacing between two consecutive modes becomes comparable to the width of multiplets, making the identification more challenging. For periods smaller than 2000 s, the limit between g-modes and p-modes begins to be reached and the identification from period spacing, only valid at the asymptotic regime ($k \gg \ell$), starts to be less accurate.

Among the 79 starting frequencies, a total of 58 modes for the Config. without trapping and 65 modes for the Configs. 1 and 2 have been identified. A summary of the number of identified modes for each category is shown on Tab. 4.6. For all configurations, the number of $\ell = 1$ modes is higher than the number of $\ell = 2$ modes. For the 20 modes of highest S/N, the amount of $\ell = 1$ and $\ell = 2$ of the Config. without trapping are nearly the same. For Configs. 1 and 2, two $\ell = 1$ trapped modes have a quite high S/N. There are also more identified $\ell = 1$ than $\ell = 2$ modes.

Table 4.6: Comparison of the number of identified $\ell = 1$, $\ell = 2$ and $\ell = 4$ modes for the different possible configurations, for all modes and among the 20 modes of highest S/N.

Parameter	**No trapping**	**Configs. 1 / 2**
All modes (79 modes)		
$\ell = 1$ (trapped)	37	42 (5)
$\ell = 2$ (trapped)	19	21 (2)
$\ell = 4$	2	2
Identified (trapped)	58	65 (7)
Unidentified	21	14
Highest S/N modes (20 modes)		
$\ell = 1$ (trapped)	9	11 (2)
$\ell = 2$	8	7
$\ell = 4$	1	1
Identified (trapped)	18	19 (2)
Unidentified	2	1

Long chains of consecutive $\ell = 1$ and $\ell = 2$ mode are located at reduced periods between 5000 and 14000 s. The associated period-spacing diagram for all configurations is presented in Fig. 4.14. For all configurations, the number of consecutive $\ell = 1$ modes is quite large compared to typical period-spacing diagrams of other sdB stars. The $\ell = 2$ modes chain length is also long, but with some gaps all along the chain. Concerning $\ell = 1$ and $\ell = 2$ overlaps, as defined in Sec. 2.4, all configurations seem to have a very good overlap, especially for reduced periods between 6000 and 9000 s. As overlap differences are difficult to be seen from the period-spacing diagram, they have been quantified by several overlap "quality" numbers. These "quality" numbers are presented in Tab. E.1 of Appendix E to have a better idea of which configuration could be more reliable than another. It appears that for the whole period range, the Config. without trapping has a slightly better overlap, but when it comes to the range of interest (5000 to 14000 s), the Configs. 1 and 2 present better vertical overlaps, while the horizontal ones are nearly the same for all configurations.

The S/N values for all the 79 periods is shown on Fig. 4.15, for each configuration. The first statement derived for this diagram is that all modes of high S/N have been identified, except for the Config. without trapping, where the frequency *f61* = 135.818 μHz (P = 7362.81 s, see Tab. D.2), having a S/N of 63.13, remains unidentified. Basic statistics about the S/N corresponding to each configuration are available in Tab. E.2. Again, the difference between configurations is very small. It is also worth mentioning that in general the mean S/N associated to the Config. without trapping is higher than the ones with trapping, even if much less modes are identified.

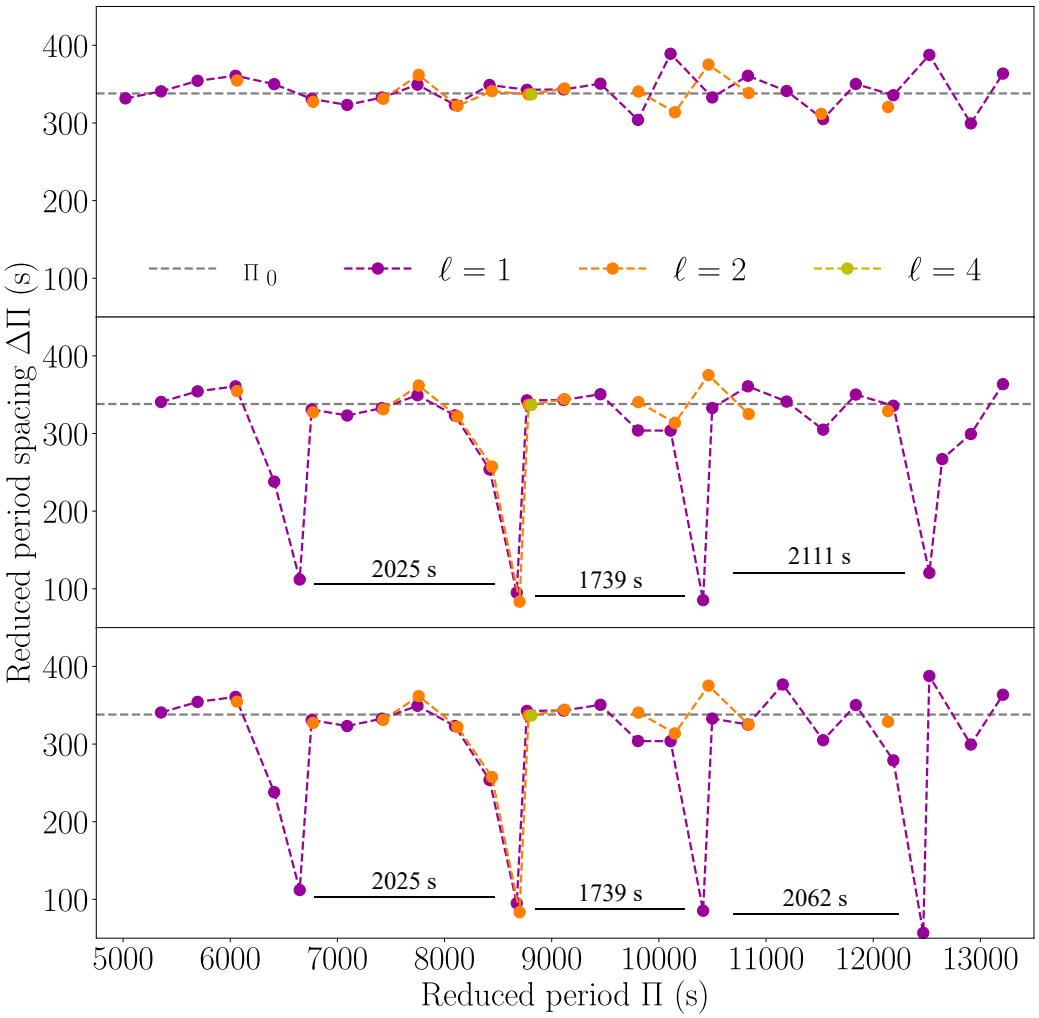

Figure 4.14: Period-spacing diagram for the 3 proposed configurations of KIC5807616 mode identification. Top panel: Config. without trapping. Middle panel: Config. 1. Bottom panel: Config. 2.

4.2.3 Relevant identified modes

In the very low-frequency region, the peaks suspected to be at the origin of potential planetary candidates have been detected (*f79* = 33.777 μHz and *f77* = 48.181 μHz) with a S/N of 7.66 and 8.95, respectively, which is higher than the 6.0 initial threshold. In addition to them, another weaker frequency is detected (*f78* = 45.200 μHz) at a S/N of 6.51. In this master thesis, *f77*, *f78* and *f79* could be identified as $\ell = 1$ modes, but as already mentioned, the analysis is challenging in this region. The fact that these frequencies are the signature of planets orbiting around KIC5807616 is therefore not rejected at all. Most unidentified modes are located either in this very low-frequency region or in the high-frequency regions, where the identification is also challenging. For the same reasons, they were not investigated further.

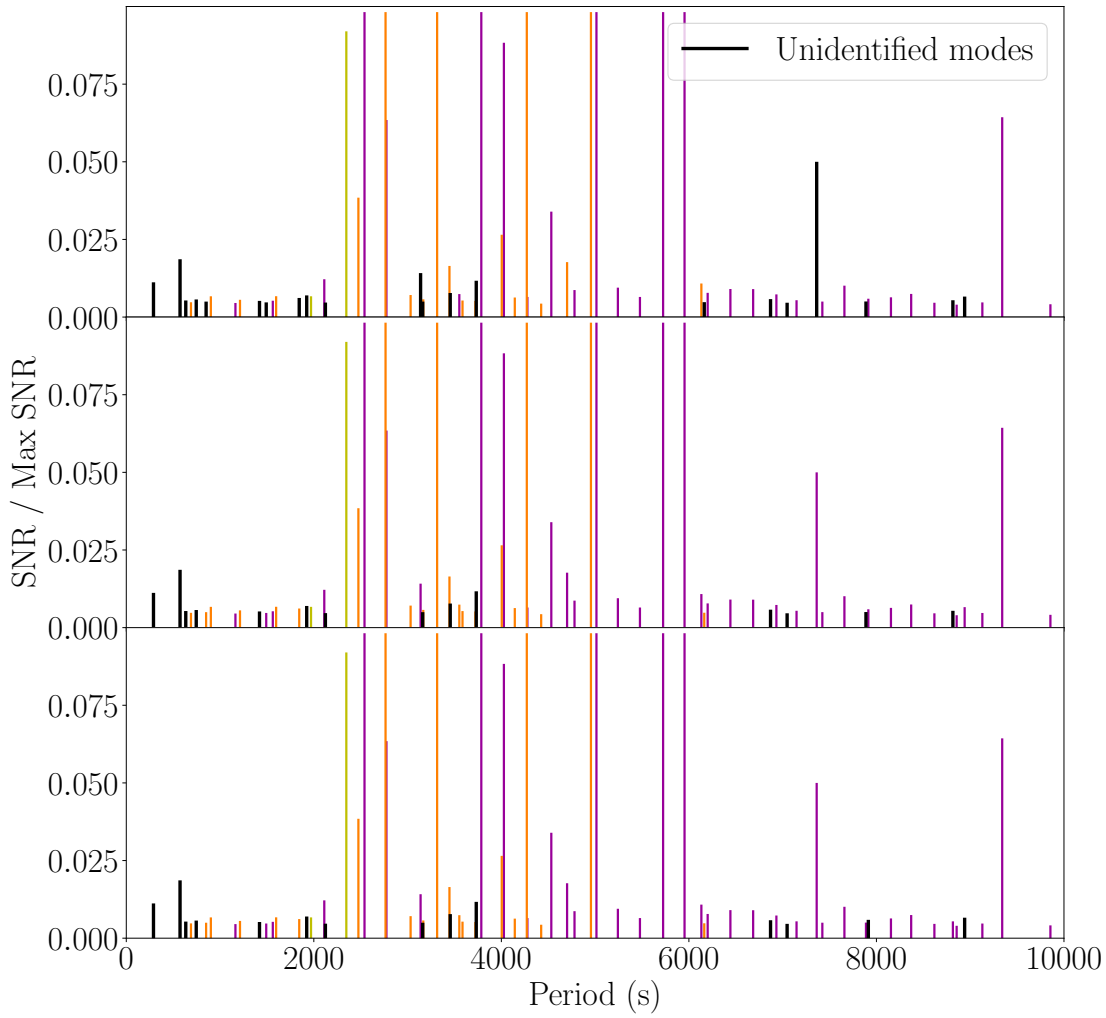

Figure 4.15: S/N diagram for the 3 proposed configurations of KIC5807616 mode identification. Unidentified modes are highlighted in black. Top panel: Config. without trapping. Middle panel: Config. 1. Bottom panel: Config. 2.

In the region of interest, i.e. for periods between ∼2000 s and ∼10000 s, three modes remain unidentified in all configurations: *f27* = 316.339 μHz, *f31* = 289.460 μHz and *f35* = 267.936 μHz (see Tab. D.2). For *f27*, its S/N is quite low (S/N = 6.29) and it is close to *f28* = 315.720 μHz. After the analysis of its time-frequency map, *f27* is likely to be part of the *f28* mode through frequency modulations or forming a potential multiplet. For *f31* and *f35*, the same conclusion can be done as they are close to *f30* = 290.150 μHz and *f34* = 268.587 μHz. The fact that all *f28*, *f30* and *f34* are identified as $\ell = 2$ multiplets, thus having potentially four components around the central frequency, also contribute to this statement. To summarize, these unidentified modes are possibly parts of $\ell = 2$ modes. Their values are nevertheless retained in case they are trapped modes or independent modes that could be identified in another way.

It is also worth mentioning that two modes are identified as $\ell = 4$ modes. Once all $\ell = 1$ and $\ell = 2$ modes were identified, an investigation among remaining modes has been done to spot potential $\ell = 4$ modes. First, *f17* = 507.577 μHz (S/N = 8.45) have a good reduced period overlap with both the $\ell = 1$ mode *f54* and the $\ell = 2$ mode *f33* (see Tab. D.2). Indeed, from Eq. (2.14),

$$\Pi_{\mathrm{f17}} = P_{\mathrm{f17}}\sqrt{4(4+1)} = P_{\mathrm{f54}}\sqrt{1(1+1)} = P_{\mathrm{f33}}\sqrt{2(2+1)}\ . \tag{4.7}$$

This frequency is actually the central component of an incomplete multiplet. The frequency spacing between components of $\ell = 4$ rotationally splitted modes can obtained from Eq. (2.9). It is given by

$$\Delta\nu_{k4} \simeq 0.275 \pm 0.032\ \mu\mathrm{Hz}, \tag{4.8}$$

by taking the rotation period estimated at Sec. 4.2.1. After analysis of the corresponding time-frequency maps, the multiplet is likely to be a $\ell = 4$ one, further confirming the present identification. The identification from observed splittings is presented in Tab. 4.7, where the frequency splitting between two consecutive m components is estimated to be $0.560/2 = 0.28$ μHz.

Table 4.7: Identification of the rotationally-splitted $\ell = 4$ mode *f17* of KIC5807616. Associated errors are indicated next to the value. Central frequencies ($m = 0$) are highlighted in bold.

ID	Frequency (μHz)		$\Delta\nu$ (μHz)		Amplitude (%)		S/N	m	ℓ
	506.98200	7.3E-04			0.0019	2.95E-04	6.40	+2	
			0.560	9.3E-04					4
f17	**507.54172**	**5.8E-04**			**0.0025**	**3.05E-04**	**8.14**	0	

The second mode also presenting an overlap with both $\ell = 1$ and $\ell = 2$ modes is *f20* (S/N = 116.18), with *f62* and *f40*, respectively. This mode has a very high S/N and when integrated in the period-spacing diagram (see Fig. 4.14), the vertical overlap is nearly perfect for the 3 possible configurations. The two mentioned $\ell = 4$ modes are thus identified as such in our final mode identification.

Concerning the trapped modes of Configs. 1 and 2, the period-spacing diagram of Fig. 4.14 shows clear overlaps between $\ell = 1$ and $\ell = 2$ modes. In addition to peaks visible in the diagram, other two trapped modes are identified for smaller periods (*f32* and *f44*), even if less modes were identified in this region. The reduced period distance between identified trapped modes minima is also relatively constant, around 2000 s for the three possible configurations.

These distances between trapped modes are indicated on Fig. 4.14 and agree well with the typical distances between trapped modes found in the literature [17, 18, 19, 20]. The depth of trapped modes in the period-spacing diagram is also interesting to measure. The mean depth is estimated to be 103 $\pm$ 16 s for the Config. 1 and 94 $\pm$ 21 s for the Config. 2. The relatively large S/N of trapped modes in general (see Tab. E.2) further justifies the likelihood of having such a configuration.

Finally, the identification presented in this master thesis fits well with the identification from rotationally splitted modes of Charpinet et al. (2011) [54]. In their analysis, only one mode (*f8*) was identified differently: $\ell = 2$ in this work and $\ell = 1$ according to their article. In contrast, the identification proposed by Krzesinski (2015) [55] has much more differences. Its analysis presents some similar $\ell = 1$ and $\ell = 2$ sequences but a non negligible amount of modes are identified differently. Even if the part of arbitrary in the identification is decreased from the methodology proposed in this work, it remains present. Differences between results available in the literature also highlight the arbitrary nature of the identification of pulsation modes from observational data. Thus, presented identifications should be taken as possibilities open to be discussed and tested when incorporating them in seismic modeling.

To conclude this section, after the extraction with FELIX and frequency modulations clearing, the main identification resulted in three possible configurations. The first one do not involve mode trapping, contrarily to the two others. The analysis of the three configurations revealed that all configurations presented in this work are nearly equally reliable, presenting different advantages and weaknesses. The biggest drawback of the configuration without trapping is nevertheless its lower amount of identified modes. When integrating this identification in seismic modeling, one should be careful to test all the possibilities.

General conclusion and perspectives

The motivation behind this work stems from the high amount of observational data provided by *Kepler* and *TESS* space telescopes, available to be identified and integrated in seismic modeling. The objective was to identify the pulsation gravity (g-) modes of a hot subdwarf B star, KIC5807616 (Kepler-70 or KPD 1943+4058), selected from a review conducted in this thesis for pulsating sdB stars observed in the original *Kepler* field. This work also aimed to present a methodology based on four quantitative quality criteria related to the period-spacing diagram: the length of consecutive $\ell = 1$ chains, the length of consecutive $\ell = 2$ chains, the vertical overlap between modes of different degree ℓ and the horizontal overlap between modes of different degree ℓ. These four criteria are believed to reduce the arbitrary part of classical identifications.

The analysis of the photometric data associated to the 18 sdB stars of the original *Kepler* field revealed that 14 sdB stars are dominated by g-modes (7 pure and 7 hybrid pulsators), 2 are dominated by p-modes (1 pure and 1 hybrid pulsator) and 2 could not be categorized, either due to a lack of observational data, for KIC2437937, or contamination by prominent binary harmonics, for KIC9472174.

In order to test and validate the proposed methodology for mode identification, the sdB star TIC441725813 (TYC 4427-1021-1), observed by *TESS*, was chosen, motivated by the available identification of its modes by Su et al. (2024). The analysis of *TESS* photometric data for 4 different datasets G1, G2, G3 and G4, covering more than 20 months of cumulated data, confirmed its hybrid, g-mode dominated nature. After the extraction with FELIX and the frequency modulation clearing, the identification of 5 complete triplets ($\ell = 1$) resulted in a mean frequency spacing of $\Delta\nu_{\ell\,=\,1} = 0.068 \pm 0.005$ μHz between triplets ($\ell = 1$) components, suggesting a differential rotation with the known envelope rotation period. The Kolmogorov-Smirnov test performed on the retained 47 modes originating from all datasets resulted in a mean period spacing of $\sim$266.7 s for $\ell = 1$ modes and $\sim$155.75 s for $\ell = 2$ modes. Based on the quality criteria, the identification of the degree ℓ and the radial order k was done on a set of 47 modes originating from all datasets, resulting in 28 modes of $\ell = 1$ and 16 modes of $\ell = 2$, showing no apparent trapping. The possible origin of 3 unidentified modes were discussed, involving a solution with possible trapping or $\ell = 4$ identifications, but the limited amount of detected modes left these solutions hypothetical. The identification of TIC441725813 pulsation modes lead to the same results than what was obtained by Su et al. (2024), making the methodology proposed in this work robust and valid.

KIC5807616 was selected among sdB pulsators of the original *Kepler* field mainly due to its rich g-mode spectrum and the absence of fully convincing identification in the literature. KIC5807616 was confirmed to be a hybrid, g-mode dominated pulsator from the *Kepler* photometry analysis over a cumulated period of nearly 3 years. After the extrac-

tion with FELIX, the analysis showed frequency modulations higher than the usual limit of 10-20 nHz, making the distinction between modulation of frequencies and rotational splitting more challenging. From two detected p-mode multiplets, the rotation period of the envelope was inferred and is equal to 40.0 $\pm$ 4.7 days. Despite the high amount of potential g-mode multiplets (34), only 9 of them were convincingly identified, including 7 triplets ($\ell = 1$), with a mean spacing of $\Delta\nu_{\ell=1} = 0.110 \pm 0.02$ μHz, and 2 quintuplets ($\ell = 2$), with a mean spacing of $\Delta\nu_{\ell=2} = 0.27 \pm 0.07$ μHz. The rotation period was inferred from g-mode multiplets: $\sim$ 43.9 days, but with high errors on the estimation. From this, the star is assumed to rotate like a solid body. The Kolmogorov-Smirnov test, done on the retained independent 79 modes cleared from modulations and splittings, gave a mean period spacing of $\sim$ 239 s and $\sim$ 138 s for consecutive $\ell = 1$ and $\ell = 2$ modes, respectively. The identification from period spacing, based on quality criteria, resulted in 3 possible different configurations for the identification: one configuration not showing any apparent trapping and two very close configurations showing strong evidences of trapping. Among the 79 retained modes, the configuration without trapping identified 37, 19 and 2 modes having $\ell = 1$, $\ell = 2$ and $\ell = 4$, respectively. For the two trapped configurations, 42, 21 and 2 modes were identified (in the same order). For unidentified modes in the region of interest, it was concluded that they were probably parts of $\ell = 2$ multiplets. The origin of peaks known to be potential planetary signatures in the very low-frequency region was also briefly discussed, not rejecting the existence of potential planets, but those modes could enter in the $\ell = 1$ sequence. Finally, the configurations with trapping are slightly favored given their higher number of identified modes.

To conclude, this work highlighted the importance of having an established methodology based on quantitative criteria to derive identification of the pulsation modes, where the part of arbitrary can be reduced, but not cancelled at all.

Perspectives concerning results displayed in this work are multiple. First, the identification provided here is aimed to be used in asteroseismic modeling, which will lead to a better understanding of the internal structures of studied stars. Second, the methodology proposed here is yet not fully automatized, but opens a possible way to further automatize such identifications.

Bibliography

[1] Dupret, Marc-Antoine, 2024. *Stellar Structure and Evolution.* https://www.astro.uliege.be/~dupret/coursevol-eng-7.pdf.

[2] Van Grootel, Valérie, Sept. 2008. "Etude des étoiles de la branche horizontale extrême par l'astérosismologie". fr. PhD thesis. Université Paul Sabatier - Toulouse III. URL: https://theses.hal.science/tel-00358838 (visited on 05/29/2025).

[3] Heber, U., Jan. 1986. "The atmosphere of subluminous B stars. II. Analysis of 10 helium poor subdwarfs and the birthrate of sdB stars." In: *Astronomy and Astrophysics* 155, pp. 33–45. URL: https://ui.adsabs.harvard.edu/abs/1986A&A...155...33H (visited on 05/30/2025).

[4] Marsh, Matthew C., 1995-01-01. *An EUV selected sample of DA white dwarfs from the ROSAT all sky survey.*

[5] Heber, U., Aug. 2016. "Hot Subluminous Stars". In: *Publications of the Astronomical Society of the Pacific* 128, p. 082001. DOI: 10.1088/1538-3873/128/966/082001. URL: https://ui.adsabs.harvard.edu/abs/2016PASP..128h2001H (visited on 05/29/2025).

[6] Fontaine, G., Brassard, P., Charpinet, S., et al., Mar. 2012. "A preliminary look at the empirical mass distribution of hot B subdwarf stars". en. In: *Astronomy & Astrophysics* 539, A12. DOI: 10.1051/0004-6361/201118220. URL: https://www.aanda.org/articles/aa/abs/2012/03/aa18220-11/aa18220-11.html (visited on 05/29/2025).

[7] Schaffenroth, V., Pelisoli, I., Barlow, B. N., et al., Oct. 2022. "Hot subdwarfs in close binaries observed from space - I. Orbital, atmospheric, and absolute parameters, and the nature of their companions". en. In: *Astronomy & Astrophysics* 666, A182. DOI: 10.1051/0004-6361/202244214. URL: https://www.aanda.org/articles/aa/abs/2022/10/aa44214-22/aa44214-22.html (visited on 06/04/2025).

[8] Guyot, N., Van Grootel, V., Charpinet, S., et al., Apr. 2025. "The theoretical pulsation spectra of hot B subdwarfs - Static and evolutionary STELUM models". en. In: *Astronomy & Astrophysics* 696, A13. DOI: 10.1051/0004-6361/202452423. URL: https://www.aanda.org/articles/aa/abs/2025/04/aa52423-24/aa52423-24.html (visited on 06/02/2025).

[9] Aerts, C., Christensen-Dalsgaard, J., and Kurtz, D. W., 2010. "Introducing Asteroseismology". en. In: *Asteroseismology.* Ed. by Aerts, C., Christensen-Dalsgaard, J., and Kurtz, D. W. Dordrecht: Springer Netherlands, pp. 1–30. DOI: 10.1007/978-1-4020-5803-5_1. URL: https://doi.org/10.1007/978-1-4020-5803-5_1 (visited on 06/02/2025).

[10] Dupret, Marc-Antoine, 2025. *Stellar stability and asteroseismology*. https://www.astro.uliege.be/~dupret/Stab-et-astero-ang.pdf.

[11] Unno, Wasaburo, Osaki, Yoji, Ando, Hiroyasu, et al., Jan. 1989. *Nonradial oscillations of stars*. URL: https://ui.adsabs.harvard.edu/abs/1989nos..book.....U (visited on 05/15/2025).

[12] Charpinet, Stephane, Giammichele, Noemi, Zong, Weikai, et al., July 2018. "Rotation in sdB stars as revealed by stellar oscillations". en. In: *Open Astronomy* 27.1, pp. 112–119. DOI: 10.1515/astro-2018-0012. URL: https://www.degruyterbrill.com/document/doi/10.1515/astro-2018-0012/html (visited on 05/11/2025).

[13] Guyot, N., 2024. "The pulsation spectra of hot subdwarf stars in the core-He burning stage". MA thesis. Liège, Belgique: Université de Liège. URL: https://matheo.uliege.be/handle/2268.2/19850.

[14] Cowling, T. G., Jan. 1941. "The non-radial oscillations of polytropic stars". In: *Monthly Notices of the Royal Astronomical Society* 101, p. 367. DOI: 10.1093/mnras/101.8.367. URL: https://ui.adsabs.harvard.edu/abs/1941MNRAS.101..367C (visited on 06/03/2025).

[15] Tassoul, M., Aug. 1980. "Asymptotic approximations for stellar nonradial pulsations." In: *The Astrophysical Journal Supplement Series* 43, pp. 469–490. DOI: 10.1086/190678. URL: https://ui.adsabs.harvard.edu/abs/1980ApJS...43..469T (visited on 05/17/2025).

[16] Brassard, P., Fontaine, G., Wesemael, F., et al., May 1992. "Adiabatic Properties of Pulsating DA White Dwarfs. II. Mode Trapping in Compositionally Stratified Models". In: *The Astrophysical Journal Supplement Series* 80, p. 369. DOI: 10.1086/191668. URL: https://ui.adsabs.harvard.edu/abs/1992ApJS...80..369B (visited on 06/02/2025).

[17] Østensen, R. H., Telting, J. H., Reed, M. D., et al., Sept. 2014. "Asteroseismology revealing trapped modes in KIC 10553698A". en. In: *Astronomy & Astrophysics* 569, A15. DOI: 10.1051/0004-6361/201423611. URL: https://www.aanda.org/articles/aa/abs/2014/09/aa23611-14/aa23611-14.html (visited on 04/21/2025).

[18] Uzundag, M., Baran, A. S., Østensen, R. H., et al., Nov. 2017. "KIC 10001893: a pulsating sdB star with multiple trapped modes". en. In: *Monthly Notices of the Royal Astronomical Society* 472.1, pp. 700–707. DOI: 10.1093/mnras/stx2011. URL: http://academic.oup.com/mnras/article/472/1/700/4067801/KIC10001893-a-pulsating-sdB-star-with-multiple (visited on 04/21/2025).

[19] Kern, J W, Reed, M D, Baran, A S, et al., Mar. 2018. "Asteroseismic analysis of the pulsating subdwarf B star KIC 11558725: an sdB+WD system with divergent frequency multiplets and mode trapping observed by Kepler". In: *Monthly Notices of the Royal Astronomical Society* 474.4, pp. 4709–4716. DOI: 10.1093/mnras/stx2893. URL: https://doi.org/10.1093/mnras/stx2893 (visited on 05/01/2025).

[20] Baran, A. S., Reed, M. D., Østensen, R. H., et al., Jan. 2017. "EPIC 211779126: a rare hybrid pulsating subdwarf B star richly pulsating in both pressure and gravity modes". en. In: *Astronomy & Astrophysics* 597, A95. DOI: 10.1051/0004-6361/201629651. URL: https://www.aanda.org/articles/aa/abs/2017/01/aa29651-16/aa29651-16.html (visited on 06/04/2025).

[21] Charpinet, S., Fontaine, G., Brassard, P., et al., July 1997. "A Driving Mechanism for the Newly Discovered Class of Pulsating Subdwarf B Stars". en. In: *The Astrophysical Journal* 483.2, p. L123. DOI: 10.1086/310741. URL: https://iopscience.iop.org/article/10.1086/310741/meta (visited on 06/04/2025).

[22] Jeffery, C. S. and Saio, H., Sept. 2006. "Fe-bump instability: the excitation of pulsations in subdwarf B and other low-mass stars". In: *Monthly Notices of the Royal Astronomical Society* 371, pp. 659–672. DOI: 10.1111/j.1365-2966.2006.10686.x. URL: https://ui.adsabs.harvard.edu/abs/2006MNRAS.371..659J (visited on 06/03/2025).

[23] Van Grootel, V., Charpinet, S., Brassard, P., et al., May 2013. "Third generation stellar models for asteroseismology of hot B subdwarf stars. A test of accuracy with the pulsating eclipsing binary PG 1336-018". In: *Astronomy and Astrophysics* 553, A97. DOI: 10.1051/0004-6361/201220896. URL: https://ui.adsabs.harvard.edu/abs/2013A&A...553A..97V (visited on 06/04/2025).

[24] Paxton, Bill, Schwab, Josiah, Bauer, Evan B., et al., Feb. 2018. "Modules for Experiments in Stellar Astrophysics (MESA): Convective Boundaries, Element Diffusion, and Massive Star Explosions". In: *The Astrophysical Journal Supplement Series* 234, p. 34. DOI: 10.3847/1538-4365/aaa5a8. URL: https://ui.adsabs.harvard.edu/abs/2018ApJS..234...34P (visited on 06/04/2025).

[25] Bédard, A., Brassard, P., Bergeron, P., et al., Mar. 2022. "On the Spectral Evolution of Hot White Dwarf Stars. II. Time-dependent Simulations of Element Transport in Evolving White Dwarfs with STELUM". en. In: *The Astrophysical Journal* 927.1, p. 128. DOI: 10.3847/1538-4357/ac4497. URL: https://dx.doi.org/10.3847/1538-4357/ac4497 (visited on 06/04/2025).

[26] *Mikulski Archive for Space Telescopes (MAST) Portal*. en-us. URL: https://mast.stsci.edu/portal/Mashup/Clients/Mast/Portal.html (visited on 05/09/2025).

[27] Charpinet, S., Green, E. M., Baglin, A., et al., June 2010. "CoRoT opens a new era in hot B subdwarf asteroseismology: Detection of multiple g -mode oscillations in KPD 0629–0016". en. In: *Astronomy and Astrophysics* 516, p. L6. DOI: 10.1051/0004-6361/201014789. URL: http://www.aanda.org/10.1051/0004-6361/201014789 (visited on 05/08/2025).

[28] Zong, W., Charpinet, S., Vauclair, G., et al., Jan. 2016. "Amplitude and frequency variations of oscillation modes in the pulsating DB white dwarf star KIC 08626021 - The likely signature of nonlinear resonant mode coupling". en. In: *Astronomy & Astrophysics* 585, A22. DOI: 10.1051/0004-6361/201526300. URL: https://www.aanda.org/articles/aa/abs/2016/01/aa26300-15/aa26300-15.html (visited on 05/08/2025).

[29] Van Grootel, V., Pozuelos, F. J., Thuillier, A., et al., June 2021. "A search for transiting planets around hot subdwarfs - I. Methods and performance tests on light curves from Kepler, K2, TESS, and CHEOPS". en. In: *Astronomy & Astrophysics* 650, A205. DOI: 10.1051/0004-6361/202140381. URL: https://www.aanda.org/articles/aa/abs/2021/06/aa40381-21/aa40381-21.html (visited on 10/20/2024).

[30] Lund, Mikkel, Handberg, Rasmus, Kjeldsen, Hans, et al., Oct. 2016. "Data preparation for asteroseismology with TESS". In: *EPJ Web of Conferences* 160. DOI: 10.1051/epjconf/201716001005.

[31] Ricker, George R., Winn, Joshua N., Vanderspek, Roland, et al., Oct. 2014. "The Transiting Exoplanet Survey Satellite". In: *Journal of Astronomical Telescopes, Instruments, and Systems* 1.1, p. 014003. DOI: 10.1117/1.JATIS.1.1.014003. URL: http://arxiv.org/abs/1406.0151 (visited on 05/14/2025).

[32] Su, Wenchao, Charpinet, Stéphane, Latour, Marilyn, et al., Oct. 2024. "TIC 441725813: A new bright hybrid hot B subdwarf pulsator with differential core versus envelope rotation". en. In: *Astronomy & Astrophysics* 690, A36. DOI: 10.1051/0004-6361/202450020. URL: https://www.aanda.org/articles/aa/abs/2024/10/aa50020-24/aa50020-24.html (visited on 05/10/2025).

[33] *TESS Observations*. en-US. URL: https://tess.mit.edu/observations/ (visited on 05/10/2025).

[34] Scargle, J. D., Dec. 1982. "Studies in astronomical time series analysis. II. Statistical aspects of spectral analysis of unevenly spaced data." In: *The Astrophysical Journal* 263, pp. 835–853. DOI: 10.1086/160554. URL: https://ui.adsabs.harvard.edu/abs/1982ApJ...263..835S (visited on 05/11/2025).

[35] Deeming, T. J., Aug. 1975. "Fourier Analysis with Unequally-Spaced Data". In: *Astrophysics and Space Science* 36, pp. 137–158. DOI: 10.1007/BF00681947. URL: https://ui.adsabs.harvard.edu/abs/1975Ap&SS..36..137D (visited on 05/11/2025).

[36] Salmon, S. J. a. J., Van Grootel, V., Sulis, S., et al., Oct. 2024. "HR 10 as seen by CHEOPS and TESS - Revealing δ Scuti pulsations, granulation-like signal and hint for transients". en. In: *Astronomy & Astrophysics* 690, A73. DOI: 10.1051/0004-6361/202346180. URL: https://www.aanda.org/articles/aa/abs/2024/10/aa46180-23/aa46180-23.html (visited on 05/13/2025).

[37] Zong, W., Charpinet, S., and Vauclair, G., Oct. 2016. "Signatures of nonlinear mode interactions in the pulsating hot B subdwarf star KIC 10139564". en. In: *Astronomy & Astrophysics* 594, A46. DOI: 10.1051/0004-6361/201629132. URL: https://www.aanda.org/articles/aa/abs/2016/10/aa29132-16/aa29132-16.html (visited on 04/21/2025).

[38] Montgomery, M. H. and O'Donoghue, D., July 1999. "A derivation of the errors for least squares fitting to time series data". In: *Delta Scuti Star Newsletter* 13, p. 28. URL: https://ui.adsabs.harvard.edu/abs/1999DSSN...13...28M (visited on 05/23/2025).

[39] Van Cleve, Jeffrey E. and Caldwell, Douglas A., 2016. *Kepler Data Characteristics Handbook (KSCI-19040-006)*. NASA Ames Research Center.

[40] Andrzej and Baran, S., June 2013. *Spurious frequencies in the {\it Kepler} short cadence data*. DOI: 10.48550/arXiv.1306.5472. URL: http://arxiv.org/abs/1306.5472 (visited on 05/11/2025).

[41] Zong, Weikai, Charpinet, Stéphane, Fu, Jian-Ning, et al., Jan. 2018. "Oscillation Mode Variability in Evolved Compact Pulsators from Kepler Photometry. I. The Hot B Subdwarf Star KIC 3527751". en. In: *The Astrophysical Journal* 853.2, p. 98. DOI: 10.3847/1538-4357/aaa548. URL: https://dx.doi.org/10.3847/1538-4357/aaa548 (visited on 05/01/2025).

[42] Zong, Weikai, Charpinet, Stéphane, and Vauclair, Gérard, Oct. 2021. "Oscillation Mode Variability in Evolved Compact Pulsators from Kepler Photometry. II. Comparison of Modulation Patterns between Raw and Corrected Flux". en. In: *The Astrophysical Journal* 921.1, p. 37. DOI: 10.3847/1538-4357/ac1b2c. URL: https://dx.doi.org/10.3847/1538-4357/ac1b2c (visited on 04/21/2025).

[43] Charpinet, S., Van Grootel, V., Fontaine, G., et al., June 2011. "Deep asteroseismic sounding of the compact hot B subdwarf pulsator KIC02697388 from Kepler time series photometry". en. In: *Astronomy & Astrophysics* 530, A3. DOI: 10.1051/0004-6361/201016412. URL: https://www.aanda.org/articles/aa/abs/2011/06/aa16412-10/aa16412-10.html (visited on 04/22/2025).

[44] Christensen-Dalsgaard, Jorgen and Frandsen, Soren, Jan. 1988. "Advances in helio- and asteroseismology: proceedings of the 123rd Symposium of the International Astronomical Union, held in Aarhus, Denmark, July 7-11, 1986." In: *Advances in Helio- and Asteroseismology* 123. URL: https://ui.adsabs.harvard.edu/abs/1988IAUS..123.....C (visited on 05/17/2025).

[45] Charpinet, S., Van Grootel, Valerie, Brassard, P., et al., Mar. 2013. "Asteroseismology of hot B subdwarf stars". In: *EPJ Web of Conferences* 43, pp. 04005–. DOI: 10.1051/epjconf/20134304005.

[46] Østensen, R. H., Green, E. M., Bloemen, S., et al., Oct. 2010. "2M1938+4603: a rich, multimode pulsating sdB star with an eclipsing dM companion observed with Kepler". In: *Monthly Notices of the Royal Astronomical Society* 408.1, pp. L51–L55. DOI: 10.1111/j.1745-3933.2010.00926.x. arXiv: 1006.4267 [astro-ph.SR].

[47] Zorotovic, M. and Schreiber, M. R., Jan. 2013. "Origin of apparent period variations in eclipsing post-common-envelope binaries". en. In: *Astronomy & Astrophysics* 549, A95. DOI: 10.1051/0004-6361/201220321. URL: https://www.aanda.org/articles/aa/abs/2013/01/aa20321-12/aa20321-12.html (visited on 04/30/2025).

[48] Baran, A. S., Zola, S., Blokesz, A., et al., May 2015. "Detection of a planet in the sdB + M dwarf binary system 2M 1938+4603". en. In: *Astronomy & Astrophysics* 577, A146. DOI: 10.1051/0004-6361/201425392. URL: https://www.aanda.org/articles/aa/abs/2015/05/aa25392-14/aa25392-14.html (visited on 04/30/2025).

[49] Sanjayan, S., Baran, A. S., Ostrowski, J., et al., 2022. "Pulsating subdwarf B stars in the oldest open cluster NGC 6791". In: *Monthly Notices of the Royal Astronomical Society* 509.1, pp. 763–774. DOI: 10.1093/mnras/stab2960. URL: https://academic.oup.com/mnras/article/509/1/763/6402925.

[50] Reed, M. D., Baran, A., Østensen, R. H., et al., 2012. "The discovery of two pulsating subdwarf B stars in NGC 6791 using Kepler data". In: *Monthly Notices of the Royal Astronomical Society* 427.2, pp. 1245–1251. DOI: 10.1111/j.1365-2966.2012.22054.x. URL: https://academic.oup.com/mnras/article/427/2/1245/975765.

[51] Foster, H. M., Reed, M. D., Telting, J. H., et al., May 2015. "The discovery of differential radial rotation in the pulsating subdwarf B star KIC 3527751". In: *The Astrophysical Journal* 805.2, p. 94. DOI: 10.1088/0004-637X/805/2/94. URL: http://arxiv.org/abs/1503.02225 (visited on 02/07/2025).

[52] Telting, J. H., Østensen, R. H., Baran, A. S., et al., Aug. 2012. "Three ways to solve the orbit of KIC 11 558 725: a 10-day beaming sdB+WD binary with a pulsating subdwarf". en. In: *Astronomy & Astrophysics* 544, A1. DOI: 10.1051/0004-6361/201219458. URL: https://www.aanda.org/articles/aa/abs/2012/08/aa19458-12/aa19458-12.html (visited on 05/01/2025).

[53] Van Grootel, V., Charpinet, S., Fontaine, G., et al., Aug. 2010. "Early Asteroseismic Results from Kepler: Structural and Core Parameters of the Hot B Subdwarf KPD 1943+4058 as Inferred from g-mode Oscillations". In: *The Astrophysical Journal* 718, pp. L97–L101. DOI: 10.1088/2041-8205/718/2/L97. URL: https://ui.adsabs.harvard.edu/abs/2010ApJ...718L..97V (visited on 05/04/2025).

[54] Charpinet, S., Fontaine, G., Brassard, P., et al., Dec. 2011. "A compact system of small planets around a former red-giant star". en. In: *Nature* 480.7378, pp. 496–499. DOI: 10.1038/nature10631. URL: https://www.nature.com/articles/nature10631 (visited on 05/03/2025).

[55] Krzesinski, J., Sept. 2015. "Planetary candidates around the pulsating sdB star KIC 5807616 considered doubtful". en. In: *Astronomy & Astrophysics* 581, A7. DOI: 10.1051/0004-6361/201526346. URL: https://www.aanda.org/articles/aa/abs/2015/09/aa26346-15/aa26346-15.html (visited on 02/07/2025).

[56] Baran, A. S., June 2012. "Mode Identification in the Pulsating Subdwarf B Star KIC 2697388". In: *Acta Astronomica* 62, pp. 179–200. URL: https://ui.adsabs.harvard.edu/abs/2012AcA....62..179B (visited on 02/07/2025).

[57] Kern, J. W., Reed, M. D., Baran, A. S., et al., Feb. 2017. "Kepler observations of the pulsating subdwarf B star KIC 2697388: the detection of converging frequency multiplets in the full data set". In: *Monthly Notices of the Royal Astronomical Society* 465.1, pp. 1057–1065. DOI: 10.1093/mnras/stw2794. URL: https://doi.org/10.1093/mnras/stw2794 (visited on 05/02/2025).

[58] Telting, J. H., Baran, A. S., Nemeth, P., et al., Oct. 2014. "KIC 7668647: a 14 day beaming sdB+WD binary with a pulsating subdwarf". en. In: *Astronomy & Astrophysics* 570, A129. DOI: 10.1051/0004-6361/201424169. URL: https://www.aanda.org/articles/aa/abs/2014/10/aa24169-14/aa24169-14.html (visited on 04/21/2025).

[59] Silvotti, R., Charpinet, S., Green, E., et al., Oct. 2014. "Kepler detection of a new extreme planetary system orbiting the subdwarf-B pulsator KIC 10001893". en. In: *Astronomy & Astrophysics* 570, A130. DOI: 10.1051/0004-6361/201424509. URL: https://www.aanda.org/articles/aa/abs/2014/10/aa24509-14/aa24509-14.html (visited on 05/04/2025).

[60] Baran, A. S., Reed, M. D., Stello, D., et al., Aug. 2012. "A pulsation zoo in the hot subdwarf B star KIC 10139564 observed by Kepler". In: *Monthly Notices of the Royal Astronomical Society* 424.4, pp. 2686–2700. DOI: 10.1111/j.1365-2966.2012.21355.x. URL: http://arxiv.org/abs/1206.3841 (visited on 05/02/2025).

[61] Baran, A. S., Telting, J. H., Németh, P., et al., Jan. 2015. "KIC 8302197: a non-rotating or low-inclination pulsating subdwarf B star observed with the Kepler spacecraft". en. In: *Astronomy & Astrophysics* 573, A52. DOI: 10.1051/0004-6361/201424877. URL: https://www.aanda.org/articles/aa/abs/2015/01/aa24877-14/aa24877-14.html (visited on 05/02/2025).

[62] Baran, A. S., Telting, J. H., Németh, P., et al., Jan. 2016. "A subsynchronously rotating pulsating subdwarf B star in a short-period binary with a white dwarf companion". en. In: *Astronomy & Astrophysics* 585, A66. DOI: 10.1051/0004-6361/201527182. URL: https://www.aanda.org/articles/aa/abs/2016/01/aa27182-15/aa27182-15.html (visited on 05/02/2025).

[63] Reed, M. D., Foster, H., Telting, J. H., et al., June 2014. "Analysis of the rich frequency spectrum of KIC 10670103 revealing the most slowly rotating subdwarf B star in the Kepler field". en. In: *Monthly Notices of the Royal Astronomical Society* 440.4, pp. 3809–3824. DOI: 10.1093/mnras/stu412. URL: http://academic.oup.com/mnras/article/440/4/3809/1098544/Analysis-of-the-rich-frequency-spectrum-of (visited on 04/21/2025).

[64] Baran, A. S. and Winans, A., Dec. 2012. "Mode Identification of Three Pulsating Subdwarf B Stars via Multiplets and Period Spacing". In: *Acta Astronomica* 62, pp. 343–355. URL: https://ui.adsabs.harvard.edu/abs/2012AcA....62..343B (visited on 05/03/2025).

[65] Pablo, Herbert, Kawaler, Steven D., Reed, M. D., et al., May 2012. "Seismic evidence for non-synchronization in two close sdB+dM binaries from Kepler photometry". In: *Monthly Notices of the Royal Astronomical Society* 422.2, pp. 1343–1351. DOI: 10.1111/j.1365-2966.2012.20707.x. URL: http://arxiv.org/abs/1202.3649 (visited on 05/03/2025).

[66] Østensen, R. H., Reed, M. D., Baran, A. S., et al., Apr. 2014. "Stochastic pulsations in the subdwarf-B star KIC 2991276". en. In: *Astronomy & Astrophysics* 564, p. L14. DOI: 10.1051/0004-6361/201423734. URL: https://www.aanda.org/articles/aa/abs/2014/04/aa23734-14/aa23734-14.html (visited on 05/03/2025).

[67] Pablo, Herbert, Kawaler, Steven D., and Green, Elizabeth M., Sept. 2011. "EXPLORING B4: A PULSATING sdB STAR, IN A BINARY, IN THE OPEN CLUSTER NGC 6791". en. In: *The Astrophysical Journal Letters* 740.2, p. L47. DOI: 10.1088/2041-8205/740/2/L47. URL: https://dx.doi.org/10.1088/2041-8205/740/2/L47 (visited on 05/03/2025).

[68] Høg, E., Fabricius, C., Makarov, V. V., et al., Mar. 2000. "The Tycho-2 catalogue of the 2.5 million brightest stars". In: *Astronomy and Astrophysics* 355, pp. L27–L30. URL: https://ui.adsabs.harvard.edu/abs/2000A&A...355L..27H (visited on 05/24/2025).

[69] Su, Wenchao, Charpinet, Stéphane, Latour, Marilyn, et al., 2024. *TIC 441725813 spectrum and prewhitened frequencies*. URL: https://cdsarc.cds.unistra.fr/ftp/J/A+A/690/A36/.

Appendix A

Python codes

Required modules

```
import numpy as np
import pandas as pd
```

Functions

```
def freq_modulations(df, lim_freq_mod):
    """
    Filters frequency-modulated signals, using the methodology described in the report.

    Parameters
    ----------
    df : pandas.DataFrame
        Input DataFrame with at least two columns: 'freq' (float) and 'SN' (float).
    lim_freq_mod : float
        Frequency modulation limit around the peak.

    Returns
    -------
    pandas.DataFrame
        A filtered DataFrame, sorted by frequency in ascending order.
    """
    N = len(df)
    br = True
    i = 0
    while i < len(df):
        df = df.sort_values('SN', ascending = False)
        ind0 = df.index[i]
        temp = np.where(np.abs(df.freq[ind0] - df.freq)  < lim_freq_mod)
        ind_temp = df.index[temp]
        index_rm = ind_temp[ind_temp != ind0]
        df = df.drop(index = index_rm)
        i = i+1

    return df.sort_values('freq')
```

```
def find_fitting_modes(periods, per_init, ref_spacing, lim):
    """
    Identify a sequence of modes close to a given reference period, and evaluate the
        value of n.

    Parameters
    ----------
    periods : array-like
        1D array of observed period values (not necessarily sorted).
    per_init : float
```

```
        Reference period to start the search.
    ref_spacing : float
        Period spacing.
    lim : float
        Limit to accept an identification.

    Returns
    -------
    n_arr : numpy.ndarray
        Array containing the n values of identified modes.
    per_arr : numpy.ndarray
        Array of period values in order of increasing 'n'.
    length : int
        Total number of identified modes.
    """
    periods = np.sort(np.asarray(periods))  # Ensure it's sorted

    per_arr = [per_init]
    n_arr = [0]

    # Upward search (per > per_init)
    val = per_init
    n = 1
    n_ref = 0
    crit_up = int(np.abs((np.max(periods) - per_init) / ref_spacing)) + 1

    for _ in range(crit_up):
        per_filtered = periods[periods > val]
        if per_filtered.size == 0:
            break

        expected = ref_spacing * abs(n - n_ref)
        per_diff = np.abs(np.abs(val - per_filtered) - expected)

        if np.min(per_diff) < lim:
            val = per_filtered[np.argmin(per_diff)]
            per_arr.append(val)
            n_arr.append(n)
            n_ref = n
        n += 1

    # Downward search (per < per_init)
    val = per_init
    n = 1
    n_ref = 0
    crit_down = int(np.abs((np.min(periods) - per_init) / ref_spacing)) + 1

    for _ in range(crit_down):
        per_filtered = periods[periods < val]
        if per_filtered.size == 0:
            break

        expected = ref_spacing * abs(n - n_ref)
        per_diff = np.abs(np.abs(val - per_filtered) - expected)

        if np.min(per_diff) < lim:
            val = per_filtered[np.argmin(per_diff)]
            per_arr.append(val)
            n_arr.append(-n)
            n_ref = n
        n += 1

    # Final sorting and re-indexing
    n_arr = np.array(n_arr)
    per_arr = np.array(per_arr)

    sort_idx = np.argsort(n_arr)
    n_arr = n_arr[sort_idx]
    per_arr = per_arr[sort_idx]
    n_arr -= np.min(n_arr)+1  # Shift so it starts from 1

    return n_arr, per_arr, len(n_arr)
```

```python
def mode_identification_per_spacing(periods, ref_spacing_l1, ref_spacing_l2, lim=30):
    """
    Identify potential l=1 and l=2 modes from a DataFrame of periods using
    reference spacing and a limit threshold.

    Parameters
    ----------
    periods : np.ndarray
        Array containing the periods corresponding the modes (cleared from frequency
            modulations or not).
    ref_spacing_l1 : float
        Reference spacing for l=1 modes.
    ref_spacing_l2 : float
        Reference spacing for l=2 modes.
    lim : float, optional
        Limit threshold for mode identification (in seconds).

    Returns
    -------
    df_l1 : pd.DataFrame
        DataFrame with identified l=1 modes and related parameters.
    df_l2 : pd.DataFrame
        DataFrame with identified l=2 modes and related parameters.
    """

    # Initialize for l=1 modes
    l1_N = 0
    l1_n = np.array(0)
    l1_per = np.array(0)

    # Initialize for l=2 modes
    l2_N = 0
    l2_n = np.array(0)
    l2_per = np.array(0)

    # Modes identification loop
    for i in range(len(periods)):
        per_init = periods[i]

        temp_l1_n, temp_l1_per, temp_l1_N = find_fitting_modes(periods, per_init,
            ref_spacing_l1, lim)
        if temp_l1_N > l1_N:
            l1_n = temp_l1_n
            l1_per = temp_l1_per
            l1_N = temp_l1_N

        temp_l2_n, temp_l2_per, temp_l2_N = find_fitting_modes(periods, per_init,
            ref_spacing_l2, lim)
        if temp_l2_N > l2_N:
            l2_n = temp_l2_n
            l2_per = temp_l2_per
            l2_N = temp_l2_N

    # Post transformations for l=1
    l = 1
    l1_per0 = l1_per * np.sqrt(l * (l + 1))
    l1_Delta_PI = np.diff(l1_per) / np.abs(np.diff(l1_n))
    l1_Delta_PI0 = l1_Delta_PI * np.sqrt(l * (l + 1))
    l1_split = np.zeros(len(l1_Delta_PI0))

    # Post transformations for l=2
    l = 2
    l2_per0 = l2_per * np.sqrt(l * (l + 1))
    l2_Delta_PI = np.diff(l2_per) / np.abs(np.diff(l2_n))
    l2_Delta_PI0 = l2_Delta_PI * np.sqrt(l * (l + 1))
    l2_split = np.zeros(len(l2_Delta_PI0))

    # DataFrames
    d_l1 = {
        'Periods': l1_per, # periods
        'Periods_0': l1_per0, # Reduced periods
        'n': l1_n, # n values
        'Delta_PI': np.append(l1_Delta_PI, 0), # Period spacing
```

```
71          'Delta_PI0': np.append(l1_Delta_PI0, 0), # Reduced period spacing
72      }
73      d_l2 = {
74          'Periods': l2_per,
75          'Periods_0': l2_per0,
76          'n': l2_n,
77          'Delta_PI': np.append(l2_Delta_PI, 0),
78          'Delta_PI0': np.append(l2_Delta_PI0, 0),
79      }
80
81      df_l1 = pd.DataFrame(data=d_l1)
82      df_l2 = pd.DataFrame(data=d_l2)
83
84      return df_l1, df_l2
```

Appendix B

SNR tresholds for the original *Kepler* field frequency extractions

Table B.1: SNR thresholds computed from the FAP calculation for frequency peaks detection in the LSP of pulsating sdBs of the original *Kepler* field with FELIX.

Sdb pulsator	**Quarter**	4σ	3σ	2σ	1σ
KIC9472174	Q9	4.97	3.77	4.12	3.77
KIC2437937	Q11	5.46	4.70	4.28	3.93
KIC3527751	Q12	4.95	4.69	4.28	3.95
KIC11558725	Q14	5.33	4.68	4.29	3.95
KIC5807616	Q10-11	5.14	4.81	4.38	4.05
KIC10553698	Q13	5.04	4.68	4.27	3.92
KIC2697388	Q11	5.02	4.71	4.26	3.93
KIC7668647	Q15	5.04	4.65	4.28	3.96
KIC10001893	Q9	5.20	4.68	4.28	3.96
KIC10139564	Q14	5.23	4.66	4.29	3.95
KIC8302197	Q10	5.27	4.87	4.44	4.12
KIC7664467	Q15	5.10	4.75	4.29	3.96
KIC10670103	Q14	5.32	4.65	4.27	3.93
KIC11179657	Q10	5.20	4.66	4.28	3.94
KIC2991403	Q17	5.03	4.67	4.23	3.89
KIC2991276	Q7	5.53	4.69	4.26	3.93
KIC2569576	Q16	5.23	4.67	4.28	3.95
KIC2438324	Q12	4.95	4.67	4.25	3.91

Appendix C

Extracted frequencies with the 4-sigma threshold

Table C.1: List of extracted frequencies of TIC441725813 from G1 (S14-25) with FELIX, by using the 4σ threshold (S/N > 5.34).

Id.	Frequency (μHz)	Freq. error (μHz)	Period (s)	Period error (s)	Amplitude (%)	Amplitude error (%)	S/N
f071:001	103.267997	0.002097	9683.542087	0.196644	0.010819	0.001159	9.34
f067:002	103.435477	0.001767	9667.862802	0.165179	0.012740	0.001150	11.08
f086:003	103.526688	0.002705	9659.345081	0.252394	0.008294	0.001146	7.24
f053:004	103.778335	0.001404	9635.922550	0.130346	0.015916	0.001141	13.95
f078:005	115.513642	0.002413	8656.986165	0.180837	0.009426	0.001162	8.11
f052:006	115.536870	0.001403	8655.245688	0.105069	0.016228	0.001163	13.96
f083:007	127.399689	0.002505	7849.312698	0.154333	0.008594	0.001100	7.82
f098:008	141.381532	0.002642	7073.059566	0.132197	0.007154	0.000966	7.41
f065:009	141.414339	0.001425	7071.418668	0.071280	0.013253	0.000965	13.73
f070:010	141.705406	0.001736	7056.893787	0.086459	0.010889	0.000966	11.28
f003:011	141.775220	0.000060	7053.418806	0.002962	0.317741	0.000966	328.77
f004:012	141.776463	0.000060	7053.356946	0.003002	0.313566	0.000966	324.45
f015:013	141.916621	0.000103	7046.391017	0.005121	0.183924	0.000969	189.83
f005:014	141.920654	0.000061	7046.190734	0.003042	0.309604	0.000969	319.54
f018:015	141.923997	0.000130	7046.024774	0.006442	0.146181	0.000969	150.87
f122:016	147.283589	0.003417	6789.622705	0.157536	0.005440	0.000950	5.73
f063:017	153.223822	0.001334	6526.400320	0.056832	0.013478	0.000919	14.67
f116:018	153.307496	0.003137	6522.838267	0.133464	0.005738	0.000919	6.24
f101:019	153.342275	0.002624	6521.358825	0.111605	0.006868	0.000921	7.46
f113:020	153.411401	0.003087	6518.420346	0.131160	0.005849	0.000922	6.34
f096:021	159.679773	0.002459	6262.533953	0.096443	0.007318	0.000919	7.96
f049:022	159.846474	0.001035	6256.002856	0.040513	0.017411	0.000921	18.91
f082:023	166.380843	0.002147	6010.307322	0.077569	0.008855	0.000971	9.12
f014:024	166.513429	0.000099	6005.521651	0.003556	0.192935	0.000972	198.57
f013:025	166.514291	0.000097	6005.490551	0.003494	0.196323	0.000972	202.05
f100:026	168.329984	0.002697	5940.712246	0.095199	0.006995	0.000964	7.26
f072:027	173.933070	0.001885	5749.337963	0.062300	0.010428	0.001004	10.39
f036:028	173.994198	0.000511	5747.318080	0.016890	0.038437	0.001004	38.29
f022:029	174.025089	0.000143	5746.297890	0.004710	0.137788	0.001004	137.25
f047:030	174.058445	0.001076	5745.196685	0.035521	0.018263	0.001004	18.19
f057:031	174.155100	0.001274	5742.008141	0.041993	0.015447	0.001005	15.37
f066:032	174.214028	0.001544	5740.065879	0.050877	0.012755	0.001006	12.68
f095:033	174.307841	0.002690	5736.976567	0.088547	0.007335	0.001008	7.28
f050:034	182.014899	0.001148	5494.055749	0.034657	0.016795	0.000985	17.05
f103:035	183.048501	0.002915	5463.032979	0.086997	0.006693	0.000997	6.72
f084:036	183.082165	0.002277	5462.028483	0.067943	0.008563	0.000996	8.60
f037:037	190.985191	0.000519	5236.008070	0.014232	0.035528	0.000942	37.71
f041:038	191.047815	0.000675	5234.291731	0.018494	0.027273	0.000940	29.00
f033:039	191.113755	0.000282	5232.485742	0.007720	0.065368	0.000942	69.43

Table C.1 continued from previous page

Id.	Frequency (μHz)	Freq. error (μHz)	Period (s)	Period error (s)	Amplitude (%)	Amplitude error (%)	S/N
f060:040	205.871994	0.001134	4857.387251	0.026763	0.014488	0.000839	17.26
f051:041	205.885437	0.000985	4857.070088	0.023234	0.016687	0.000839	19.88
f099:042	206.202868	0.002309	4849.593061	0.054309	0.007088	0.000836	8.48
f088:043	206.228640	0.002001	4848.987031	0.047043	0.008183	0.000836	9.78
f048:044	206.358995	0.000899	4845.923968	0.021122	0.018112	0.000832	21.77
f056:045	206.381958	0.001037	4845.384799	0.024341	0.015713	0.000832	18.88
f097:046	206.565785	0.002246	4841.072777	0.052638	0.007289	0.000836	8.72
f019:047	206.611632	0.000112	4839.998563	0.002622	0.146132	0.000835	174.91
f021:048	206.613188	0.000113	4839.962100	0.002651	0.144550	0.000835	173.02
f079:049	206.707593	0.001764	4837.751645	0.041278	0.009291	0.000837	11.10
f119:050	206.830105	0.002886	4834.886094	0.067475	0.005670	0.000836	6.78
f081:051	206.911832	0.001807	4832.976392	0.042199	0.009077	0.000838	10.84
f126:052	207.001133	0.003196	4830.891440	0.074577	0.005125	0.000837	6.13
f061:053	207.055124	0.001180	4829.631739	0.027530	0.013838	0.000834	16.59
f111:054	207.103731	0.002763	4828.498228	0.064419	0.005911	0.000834	7.09
f129:055	207.187432	0.003308	4826.547586	0.077071	0.004913	0.000830	5.92
f017:056	207.318209	0.000098	4823.502993	0.002289	0.165246	0.000831	198.96
f016:057	207.319384	0.000094	4823.475639	0.002191	0.172668	0.000831	207.89
f080:058	207.369983	0.001768	4822.298714	0.041110	0.009196	0.000830	11.07
f114:059	212.570739	0.002709	4704.316327	0.059943	0.005778	0.000799	7.23
f089:060	213.079657	0.001909	4693.080589	0.042049	0.008172	0.000797	10.25
f133:061	213.156015	0.003331	4691.399395	0.073319	0.004674	0.000795	5.88
f108:062	213.220257	0.002564	4689.985914	0.056406	0.006059	0.000794	7.63
f026:063	220.606830	0.000145	4532.951218	0.002977	0.105882	0.000784	135.10
f027:064	220.608102	0.000145	4532.925082	0.002983	0.105697	0.000784	134.87
f044:065	221.299197	0.000656	4518.769225	0.013388	0.023764	0.000796	29.86
f042:066	226.588861	0.000587	4413.279601	0.011438	0.026051	0.000781	33.34
f094:067	226.662826	0.002064	4411.839470	0.040166	0.007374	0.000777	9.49
f132:068	228.335281	0.003231	4379.524687	0.061967	0.004766	0.000787	6.06
f124:070	236.801648	0.002976	4222.943592	0.053063	0.005338	0.000811	6.58
f092:071	245.079351	0.002077	4080.311114	0.034576	0.007649	0.000811	9.43
f121:073	254.647819	0.002846	3926.992204	0.043882	0.005557	0.000808	6.88
f115:074	256.653073	0.002728	3896.310247	0.041422	0.005774	0.000805	7.17
f043:075	256.786499	0.000651	3894.285735	0.009875	0.024111	0.000802	30.06
f046:076	256.918379	0.000751	3892.286741	0.011377	0.020878	0.000801	26.07
f127:077	256.988083	0.003092	3891.231024	0.046825	0.005077	0.000802	6.33
f102:078	257.046743	0.002304	3890.343012	0.034873	0.006805	0.000801	8.50
f024:079	257.551249	0.000145	3882.722384	0.002189	0.108232	0.000803	134.84
f035:080	257.618502	0.000324	3881.708772	0.004878	0.048425	0.000801	60.47
f029:081	257.688462	0.000163	3880.654936	0.002457	0.095838	0.000799	120.02
f069:082	264.916421	0.001384	3774.775445	0.019718	0.011533	0.000815	14.15
f039:083	265.063298	0.000548	3772.683763	0.007802	0.029095	0.000815	35.71
f038:084	265.069109	0.000476	3772.601053	0.006770	0.033531	0.000815	41.16
f077:085	265.199806	0.001666	3770.741826	0.023682	0.009541	0.000812	11.75
f009:086	265.356063	0.000065	3768.521396	0.000918	0.246525	0.000814	302.94
f008:087	265.357302	0.000065	3768.503794	0.000916	0.246954	0.000814	303.47
f007:088	265.496808	0.000056	3766.523624	0.000796	0.284503	0.000815	348.99
f006:089	265.498355	0.000053	3766.501677	0.000750	0.301735	0.000815	370.26
f068:090	265.534851	0.001298	3765.984005	0.018404	0.012277	0.000814	15.09
f073:091	276.010290	0.001606	3623.053329	0.021075	0.009821	0.000805	12.19
f076:092	276.150748	0.001645	3621.210548	0.021566	0.009619	0.000808	11.90
f010:093	276.208474	0.000073	3620.453733	0.000955	0.217931	0.000811	268.56
f011:094	276.210183	0.000077	3620.431325	0.001012	0.205710	0.000811	253.50
f107:095	276.330259	0.002572	3618.858118	0.033687	0.006150	0.000808	7.61
f087:096	276.363589	0.001921	3618.421667	0.025147	0.008222	0.000807	10.19
f091:097	276.460391	0.001993	3617.154691	0.026082	0.007896	0.000804	9.82
f093:098	276.539601	0.002064	3616.118618	0.026984	0.007627	0.000804	9.49
f012:099	276.586220	0.000079	3615.509122	0.001038	0.198264	0.000804	246.49
f001:100	276.593585	0.000032	3615.412842	0.000418	0.492321	0.000804	612.52
f002:101	276.598178	0.000047	3615.352815	0.000611	0.336670	0.000804	418.87
f028:102	277.676460	0.000158	3601.313555	0.002051	0.100717	0.000814	123.78
f032:103	277.740223	0.000238	3600.486775	0.003080	0.066970	0.000813	82.40
f023:104	277.804799	0.000127	3599.649834	0.001646	0.125125	0.000812	154.16
f134:105	283.760839	0.003459	3524.094460	0.042957	0.004603	0.000813	5.66

Table C.1 continued from previous page

Id.	Frequency (μHz)	Freq. error (μHz)	Period (s)	Period error (s)	Amplitude (%)	Amplitude error (%)	S/N
f130:106	290.590894	0.003259	3441.264059	0.038597	0.004870	0.000811	6.01
f045:107	291.036964	0.000687	3435.989667	0.008111	0.023111	0.000811	28.49
f090:108	291.184214	0.001988	3434.252106	0.023444	0.007988	0.000811	9.85
f034:109	301.363697	0.000274	3318.249714	0.003013	0.056917	0.000796	71.55
f025:110	301.429814	0.000146	3317.521871	0.001605	0.106614	0.000794	134.21
f055:111	301.495454	0.000982	3316.799601	0.010798	0.015799	0.000792	19.94
f131:112	314.723776	0.003069	3177.389428	0.030984	0.004869	0.000763	6.38
f040:113	328.331228	0.000508	3045.704808	0.004716	0.027350	0.000710	38.50
f020:114	328.404972	0.000097	3045.020891	0.000897	0.144618	0.000714	202.46
f062:115	328.479115	0.001014	3044.333580	0.009402	0.013806	0.000715	19.30
f104:116	349.081363	0.002071	2864.661670	0.016999	0.006624	0.000701	9.45
f074:117	349.298875	0.001408	2862.877815	0.011544	0.009680	0.000696	13.90
f064:118	361.890732	0.001123	2763.265014	0.008576	0.013344	0.000766	17.43
f128:119	462.886710	0.002859	2160.355826	0.013342	0.004969	0.000726	6.85
f030:120	462.989613	0.000163	2159.875670	0.000759	0.087038	0.000724	120.29
f031:121	462.991142	0.000168	2159.868535	0.000784	0.084273	0.000724	116.47
f054:122	463.115032	0.000888	2159.290739	0.004142	0.015866	0.000720	22.04
f059:123	463.125479	0.000962	2159.242032	0.004486	0.014646	0.000720	20.35
f112:124	463.286031	0.002393	2158.493743	0.011149	0.005903	0.000722	8.18
f106:125	463.331655	0.002210	2158.281200	0.010292	0.006393	0.000722	8.86
f109:126	463.502288	0.002354	2157.486654	0.010956	0.006004	0.000722	8.32
f085:127	463.604113	0.001702	2157.012786	0.007921	0.008311	0.000723	11.50
f075:128	463.813181	0.001467	2156.040495	0.006821	0.009664	0.000724	13.34
f118:129	463.844894	0.002484	2155.893084	0.011547	0.005712	0.000725	7.88
f123:130	463.994983	0.002654	2155.195715	0.012327	0.005350	0.000725	7.38
f058:131	464.246353	0.000963	2154.028769	0.004468	0.014749	0.000726	20.33
f117:132	464.277486	0.002485	2153.884325	0.011528	0.005716	0.000726	7.88
f110:133	585.321232	0.002556	1708.463568	0.007461	0.005963	0.000779	7.66
f120:135	628.043033	0.002912	1592.247581	0.007384	0.005615	0.000835	6.72
f105:137	628.633803	0.002540	1590.751238	0.006426	0.006445	0.000836	7.71
f125:138	629.123460	0.003164	1589.513129	0.007994	0.005181	0.000837	6.19

Table C.2: List of extracted frequencies of TIC441725813 from G2 (S40-41) with FELIX, by using the 4σ threshold (S/N $>$ 5.25).

Id.	Frequency (μHz)	Freq. error (μHz)	Period (s)	Period error (s)	Amplitude (%)	Amplitude error (%)	S/N
f051:001	93.086367	0.020170	10742.711704	2.327746	0.010593	0.001873	5.66
f003:002	103.309667	0.001032	9679.636257	0.096666	0.211322	0.001911	110.59
f004:003	103.319201	0.001032	9678.743088	0.096676	0.211259	0.001911	110.56
f041:005	109.249424	0.016948	9153.366307	1.419976	0.012888	0.001914	6.73
f024:006	115.520309	0.008718	8656.486577	0.653244	0.025406	0.001941	13.09
f045:007	115.789137	0.018426	8636.388765	1.374374	0.012020	0.001941	6.19
f049:008	123.167260	0.019710	8119.040723	1.299240	0.011254	0.001944	5.79
f020:009	127.262808	0.008061	7857.755264	0.497726	0.027633	0.001952	14.15
f039:010	131.678963	0.015760	7594.227507	0.908934	0.014074	0.001944	7.24
f028:011	141.892775	0.011299	7047.575196	0.561205	0.019538	0.001935	10.10
f038:012	153.421335	0.015131	6517.998303	0.642836	0.014698	0.001949	7.54
f044:013	164.931427	0.017842	6063.125872	0.655913	0.012043	0.001883	6.39
f037:014	166.367676	0.014299	6010.783011	0.516631	0.015109	0.001894	7.98
f043:015	169.191973	0.017728	5910.445871	0.619286	0.012189	0.001894	6.44
f006:016	173.985069	0.001064	5747.619642	0.035134	0.203608	0.001898	107.28
f017:017	174.211600	0.005191	5740.145887	0.171038	0.041755	0.001900	21.98
f029:018	182.015546	0.011346	5494.036201	0.342478	0.018791	0.001869	10.06
f016:019	190.967496	0.004428	5236.493231	0.121414	0.046411	0.001801	25.77
f013:020	191.117030	0.003057	5232.396100	0.083693	0.067150	0.001799	37.32
f021:021	205.882422	0.007369	4857.141232	0.173856	0.027284	0.001762	15.48
f018:022	206.083049	0.006673	4852.412684	0.157113	0.030135	0.001762	17.10
f031:023	206.859658	0.011106	4834.195374	0.259552	0.018128	0.001765	10.27
f052:024	207.145199	0.019059	4827.531619	0.444166	0.010566	0.001765	5.99
f023:025	221.292313	0.007665	4518.909783	0.156518	0.026007	0.001747	14.89
f022:026	226.576753	0.007270	4413.515442	0.141616	0.026459	0.001686	15.69
f054:027	254.604018	0.017748	3927.667784	0.273797	0.010175	0.001583	6.43

Table C.2 continued from previous page

Id.	Frequency (μHz)	Freq. error (μHz)	Period (s)	Period error (s)	Amplitude (%)	Amplitude error (%)	S/N
f030:028	256.742169	0.009549	3894.958142	0.144864	0.018670	0.001563	11.95
f042:029	256.968259	0.014368	3891.531208	0.217589	0.012408	0.001563	7.94
f009:030	257.559925	0.001464	3882.591601	0.022074	0.121318	0.001557	77.92
f008:031	257.669142	0.001334	3880.945898	0.020088	0.133042	0.001555	85.55
f025:032	265.030052	0.007387	3773.157019	0.105171	0.023876	0.001546	15.44
f015:033	265.399957	0.002974	3767.898119	0.042228	0.059285	0.001546	38.36
f032:034	275.926121	0.009700	3624.158507	0.127403	0.017949	0.001526	11.76
f014:035	276.131992	0.002760	3621.456510	0.036192	0.063088	0.001526	41.34
f026:036	276.460650	0.008108	3617.151297	0.106080	0.021443	0.001524	14.07
f005:037	277.704904	0.000830	3600.944695	0.010763	0.209750	0.001526	137.46
f007:038	277.737691	0.001049	3600.519604	0.013595	0.166042	0.001526	108.80
f010:039	277.814426	0.001466	3599.525098	0.018989	0.118859	0.001527	77.85
f027:040	291.078619	0.008292	3435.497957	0.097862	0.021185	0.001540	13.76
f011:041	301.384686	0.001882	3318.018620	0.020720	0.091788	0.001514	60.62
f012:042	301.446337	0.002055	3317.340032	0.022612	0.084084	0.001514	55.53
f002:043	328.361381	0.000541	3045.425128	0.005016	0.320823	0.001521	210.98
f001:044	328.373706	0.000418	3045.310824	0.003879	0.414637	0.001520	272.77
f047:045	349.316998	0.014768	2862.729287	0.121031	0.011810	0.001529	7.73
f048:046	361.880786	0.014677	2763.340963	0.112077	0.011695	0.001504	7.77
f033:047	462.874419	0.010002	2160.413188	0.046684	0.016838	0.001476	11.41
f046:048	463.499363	0.014073	2157.500268	0.065507	0.012012	0.001482	8.11
f036:049	463.684797	0.010644	2156.637453	0.049507	0.015861	0.001480	10.72
f019:050	464.079060	0.005632	2154.805262	0.026149	0.030029	0.001482	20.26
f035:051	627.284077	0.010531	1594.174055	0.026764	0.016301	0.001505	10.83
f050:052	627.511919	0.016090	1593.595227	0.040862	0.010698	0.001509	7.09
f056:053	630.200568	0.020315	1586.796413	0.051152	0.008415	0.001498	5.62
f053:054	665.609105	0.016918	1502.383295	0.038186	0.010267	0.001522	6.74
f034:055	666.236339	0.010387	1500.968863	0.023401	0.016766	0.001526	10.98
f040:056	666.556073	0.013041	1500.248878	0.029352	0.013327	0.001523	8.75

Table C.3: List of extracted frequencies of TIC441725813 from G3 (S47-52) with FELIX, by using the 4σ threshold (S/N $>$ 5.39).

Id.	Frequency (μHz)	Freq. error (μHz)	Period (s)	Period error (s)	Amplitude (%)	Amplitude error (%)	S/N
f057:001	72.774156	0.005609	13741.141780	1.059095	0.009426	0.001343	7.02
f041:002	103.132769	0.004465	9696.239243	0.419786	0.013675	0.001551	8.82
f030:003	103.392432	0.002932	9671.887806	0.274236	0.020810	0.001549	13.43
f060:005	112.258224	0.006661	8908.033356	0.528610	0.009199	0.001556	5.91
f027:006	115.493713	0.002647	8658.479957	0.198453	0.023133	0.001555	14.88
f045:007	115.554013	0.005104	8653.961697	0.382218	0.011998	0.001555	7.72
f063:008	115.772696	0.006833	8637.615179	0.509828	0.008957	0.001554	5.76
f050:009	127.109820	0.005362	7867.212766	0.331857	0.011042	0.001504	7.34
f037:010	127.277707	0.003507	7856.835444	0.216467	0.016834	0.001499	11.23
f068:011	131.678320	0.006790	7594.264582	0.391607	0.008488	0.001464	5.80
f036:012	141.634716	0.003235	7060.415889	0.161275	0.016834	0.001383	12.17
f014:013	141.820254	0.001028	7051.179033	0.051106	0.052747	0.001377	38.31
f004:014	141.871226	0.000374	7048.645653	0.018599	0.144950	0.001378	105.19
f024:015	141.947751	0.002272	7044.845694	0.112749	0.023849	0.001376	17.33
f071:016	153.188739	0.006608	6527.894989	0.281586	0.008224	0.001380	5.96
f062:017	159.757542	0.005925	6259.485400	0.232138	0.009044	0.001361	6.65
f064:018	159.880050	0.006068	6254.689058	0.237389	0.008808	0.001357	6.49
f069:019	164.280057	0.006406	6087.166135	0.237367	0.008457	0.001376	6.15
f048:020	166.336852	0.004819	6011.896853	0.174166	0.011151	0.001365	8.17
f056:021	166.472888	0.005600	6006.984167	0.202082	0.009595	0.001365	7.03
f001:022	173.968838	0.000245	5748.155892	0.008103	0.214903	0.001338	160.57
f028:023	174.121666	0.002375	5743.110687	0.078328	0.022259	0.001342	16.58
f039:024	174.174577	0.003638	5741.366047	0.119907	0.014542	0.001343	10.83
f029:025	174.317371	0.002505	5736.662937	0.082444	0.021127	0.001344	15.72
f040:026	182.036500	0.003615	5493.403781	0.109085	0.014523	0.001333	10.89
f067:027	183.416655	0.006140	5452.067599	0.182506	0.008512	0.001327	6.41
f016:028	190.977907	0.001023	5236.207760	0.028054	0.050818	0.001320	38.49
f011:029	191.122347	0.000775	5232.250522	0.021210	0.067139	0.001321	50.83

Table C.3 continued from previous page

Id.	Frequency (μHz)	Freq. error (μHz)	Period (s)	Period error (s)	Amplitude (%)	Amplitude error (%)	S/N
f025:030	205.851621	0.002013	4857.867997	0.047498	0.023732	0.001213	19.57
f052:031	206.069150	0.004629	4852.739967	0.109006	0.010319	0.001213	8.51
f072:032	206.171646	0.005999	4850.327475	0.141125	0.007984	0.001216	6.56
f042:033	206.744260	0.003637	4836.893650	0.085091	0.013217	0.001221	10.83
f061:034	206.854003	0.005262	4834.327516	0.122986	0.009136	0.001221	7.48
f038:035	206.949720	0.003200	4832.091593	0.074717	0.015065	0.001224	12.31
f065:036	213.088321	0.005341	4692.889759	0.117624	0.008757	0.001188	7.37
f051:037	213.156299	0.004540	4691.393153	0.099914	0.010319	0.001190	8.67
f073:038	220.390053	0.006058	4537.409855	0.124729	0.007819	0.001203	6.50
f026:039	221.298601	0.002037	4518.781392	0.041588	0.023245	0.001202	19.33
f023:040	226.591054	0.001857	4413.236905	0.036173	0.025346	0.001195	21.20
f077:041	227.618786	0.006955	4393.310490	0.134245	0.006722	0.001187	5.66
f053:042	236.125264	0.004474	4235.040257	0.080244	0.010175	0.001156	8.80
f059:043	254.556399	0.005116	3928.402515	0.078947	0.009222	0.001198	7.70
f031:044	256.788685	0.002325	3894.252576	0.035259	0.020495	0.001210	16.94
f035:045	256.930038	0.002816	3892.110118	0.042654	0.016872	0.001206	13.99
f007:046	257.551284	0.000430	3882.721851	0.006475	0.109455	0.001194	91.68
f018:047	257.618392	0.001002	3881.710429	0.015102	0.046903	0.001194	39.29
f010:048	257.688060	0.000504	3880.660981	0.007587	0.093307	0.001194	78.16
f020:049	265.007677	0.001527	3773.475583	0.021746	0.030181	0.001170	25.79
f015:050	265.398139	0.000904	3767.923932	0.012841	0.051059	0.001173	43.54
f022:051	265.609266	0.001743	3764.928897	0.024704	0.026537	0.001174	22.60
f049:052	275.907140	0.004022	3624.407831	0.052829	0.011142	0.001138	9.79
f012:053	276.118366	0.000722	3621.635223	0.009467	0.062043	0.001137	54.56
f019:054	276.520084	0.001439	3616.373844	0.018820	0.031043	0.001134	27.36
f009:055	277.673510	0.000457	3601.351820	0.005927	0.096130	0.001116	86.17
f013:056	277.734248	0.000791	3600.564234	0.010248	0.055573	0.001116	49.81
f006:057	277.804387	0.000328	3599.655177	0.004244	0.134155	0.001116	120.23
f033:058	291.036731	0.002397	3435.992418	0.028302	0.017673	0.001076	16.43
f058:059	291.174179	0.004523	3434.370463	0.053354	0.009374	0.001077	8.71
f017:060	301.364232	0.000849	3318.243816	0.009353	0.050270	0.001084	46.36
f008:061	301.430889	0.000401	3317.510039	0.004418	0.106543	0.001086	98.09
f044:062	301.493214	0.003481	3316.824240	0.038298	0.012293	0.001087	11.31
f021:063	328.331631	0.001444	3045.701071	0.013399	0.028584	0.001048	27.26
f005:064	328.405131	0.000298	3045.019418	0.002763	0.138765	0.001050	132.14
f032:065	328.476556	0.002043	3044.357298	0.018932	0.020256	0.001051	19.28
f054:066	349.303665	0.003955	2862.838554	0.032416	0.010145	0.001019	9.96
f043:067	361.888293	0.003104	2763.283639	0.023705	0.012927	0.001019	12.68
f066:068	462.639213	0.004787	2161.511543	0.022364	0.008636	0.001050	8.23
f076:069	462.822781	0.006085	2160.654231	0.028409	0.006793	0.001050	6.47
f055:070	463.436815	0.004169	2157.791456	0.019411	0.009915	0.001050	9.45
f047:071	463.653436	0.003652	2156.783328	0.016987	0.011286	0.001047	10.78
f046:072	463.886716	0.003633	2155.698718	0.016881	0.011382	0.001050	10.84
f034:073	464.106404	0.002424	2154.678304	0.011253	0.017054	0.001050	16.25
f079:074	585.323919	0.006527	1708.455725	0.019050	0.006247	0.001035	6.03
f003:075	627.281241	0.000296	1594.181260	0.000751	0.147625	0.001108	133.22
f002:076	627.283407	0.000296	1594.175757	0.000751	0.147637	0.001108	133.23
f074:077	627.520693	0.005735	1593.572948	0.014563	0.007598	0.001106	6.87
f081:078	628.683113	0.007205	1590.626469	0.018230	0.006092	0.001115	5.47
f078:079	629.152637	0.006663	1589.439416	0.016832	0.006589	0.001115	5.91
f075:080	666.240038	0.005940	1500.960530	0.013383	0.007315	0.001104	6.63
f080:081	666.657865	0.007022	1500.019803	0.015800	0.006206	0.001107	5.61

Table C.4: List of extracted frequencies of TIC441725813 from G4 (S55-60) with FELIX, by using the 4σ threshold (S/N > 5.42).

Id.	Frequency (μHz)	Freq. error (μHz)	Period (s)	Period error (s)	Amplitude (%)	Amplitude error (%)	S/N
f063:001	72.774148	0.006869	13741.143401	1.297035	0.009432	0.001680	5.61
f006:002	103.128929	0.000520	9696.600300	0.048887	0.140475	0.001894	74.16
f005:003	103.132166	0.000519	9696.295957	0.048830	0.140631	0.001894	74.24
f032:004	103.375584	0.003682	9673.464115	0.344546	0.019854	0.001896	10.47
f034:005	103.600548	0.004268	9652.458632	0.397645	0.017120	0.001895	9.03

Table C.4 continued from previous page

Id.	Frequency (μHz)	Freq. error (μHz)	Period (s)	Period error (s)	Amplitude (%)	Amplitude error (%)	S/N
f049:006	109.343451	0.006031	9145.495101	0.504460	0.012255	0.001917	6.39
f054:007	136.675630	0.006305	7316.593283	0.337546	0.010966	0.001793	6.12
f047:008	141.640954	0.004887	7060.104927	0.243581	0.013633	0.001728	7.89
f024:009	141.806698	0.002364	7051.853082	0.117573	0.028130	0.001725	16.31
f008:010	141.883866	0.000499	7048.017711	0.024779	0.133189	0.001723	77.30
f013:011	141.895918	0.000770	7047.419081	0.038242	0.086287	0.001723	50.08
f052:012	153.205193	0.005787	6527.193912	0.246546	0.011276	0.001692	6.66
f057:013	159.747332	0.006524	6259.885468	0.255647	0.010016	0.001695	5.91
f060:014	164.161848	0.006906	6091.549365	0.256247	0.009448	0.001692	5.58
f043:015	166.570097	0.004430	6003.478510	0.159653	0.014682	0.001687	8.70
f003:016	173.964782	0.000307	5748.289895	0.010151	0.210192	0.001675	125.52
f022:017	174.115539	0.001663	5743.312789	0.054849	0.038964	0.001680	23.19
f021:018	174.174223	0.001614	5741.377685	0.053194	0.040271	0.001685	23.89
f001:019	174.344462	0.000195	5735.771533	0.006405	0.332813	0.001680	198.08
f002:020	174.347221	0.000197	5735.680745	0.006480	0.328917	0.001680	195.76
f062:021	182.059410	0.006967	5492.712509	0.210200	0.009432	0.001704	5.53
f018:022	190.972843	0.001294	5236.346611	0.035472	0.049918	0.001675	29.81
f014:023	191.125730	0.000951	5232.157923	0.026045	0.068113	0.001681	40.53
f036:024	205.870508	0.003946	4857.422318	0.093094	0.016323	0.001670	9.77
f044:025	205.989169	0.004416	4854.624167	0.104077	0.014584	0.001670	8.73
f035:026	206.559396	0.003879	4841.222515	0.090910	0.016605	0.001670	9.94
f046:027	206.660004	0.004670	4838.865666	0.109355	0.013838	0.001676	8.26
f061:028	206.898800	0.006850	4833.280807	0.160030	0.009436	0.001676	5.63
f059:029	213.119301	0.006753	4692.207583	0.148673	0.009538	0.001670	5.71
f050:030	220.662278	0.005387	4531.812181	0.110637	0.011873	0.001659	7.16
f030:031	221.296973	0.002975	4518.814630	0.060739	0.021399	0.001651	12.96
f026:032	226.585819	0.002339	4413.338866	0.045555	0.026683	0.001618	16.49
f058:033	236.113916	0.006199	4235.243808	0.111189	0.009662	0.001553	6.22
f031:034	256.793639	0.002831	3894.177452	0.042937	0.020801	0.001527	13.62
f045:035	256.910548	0.004231	3892.405387	0.064108	0.013877	0.001523	9.11
f009:036	257.551405	0.000516	3882.720031	0.007780	0.113300	0.001516	74.72
f020:037	257.624239	0.001369	3881.622338	0.020624	0.042719	0.001516	28.17
f011:038	257.689286	0.000657	3880.642520	0.009894	0.089005	0.001516	58.69
f053:039	264.780338	0.005377	3776.715476	0.076698	0.011037	0.001539	7.17
f029:040	264.983548	0.002516	3773.819203	0.035829	0.023591	0.001539	15.33
f016:041	265.417742	0.001005	3767.645647	0.014264	0.058898	0.001535	38.37
f027:042	265.649942	0.002335	3764.352415	0.033090	0.025346	0.001535	16.51
f038:043	275.867771	0.003782	3624.925074	0.049695	0.016103	0.001579	10.20
f015:044	276.097990	0.000914	3621.902495	0.011997	0.066596	0.001579	42.17
f033:045	276.547151	0.003347	3616.019897	0.043758	0.018202	0.001580	11.52
f042:046	276.765571	0.004035	3613.166173	0.052677	0.015096	0.001580	9.56
f023:047	277.674772	0.001563	3601.335444	0.020277	0.038716	0.001570	24.66
f012:048	277.675612	0.000695	3601.324554	0.009008	0.087156	0.001570	55.52
f019:049	277.736945	0.001258	3600.529270	0.016310	0.048113	0.001570	30.65
f007:050	277.803589	0.000444	3599.665523	0.005753	0.136404	0.001571	86.85
f039:052	291.043777	0.003663	3435.909230	0.043240	0.015913	0.001512	10.53
f064:053	291.175906	0.006457	3434.350096	0.076158	0.009025	0.001511	5.97
f017:054	301.367279	0.001107	3318.210265	0.012187	0.053680	0.001541	34.84
f010:055	301.428685	0.000582	3317.534291	0.006407	0.101778	0.001537	66.24
f025:056	328.326968	0.002108	3045.744325	0.019552	0.026715	0.001460	18.30
f004:057	328.406583	0.000400	3045.005954	0.003713	0.140737	0.001462	96.29
f028:058	328.473590	0.002272	3044.384790	0.021062	0.024802	0.001462	16.97
f051:059	349.306753	0.004871	2862.813247	0.039925	0.011456	0.001447	7.92
f056:060	361.893896	0.005152	2763.240858	0.039338	0.010583	0.001414	7.48
f048:061	462.790693	0.004304	2160.804043	0.020097	0.013508	0.001508	8.96
f065:062	463.009772	0.006495	2159.781628	0.030296	0.008958	0.001509	5.94
f041:063	463.458282	0.003727	2157.691510	0.017352	0.015637	0.001511	10.35
f037:064	463.895036	0.003624	2155.660060	0.016839	0.016119	0.001515	10.64
f055:065	463.941481	0.005449	2155.444256	0.025318	0.010730	0.001516	7.08
f040:066	464.147117	0.003735	2154.489304	0.017337	0.015695	0.001520	10.32

Table C.5: List of extracted frequencies of KIC5807616 from the whole dataset (Q2.3, Q5-Q17.2) with FELIX, by using the 4σ threshold (S/N > 5.14).

Id.	Frequency (μHz)	Freq. error (μHz)	Period (s)	Period error (s)	Amplitude (%)	Amplitude error (%)	S/N
f433:001	33.741996	0.000752	29636.658476	0.660126	0.001897	0.000304	6.24
f329:002	33.776507	0.000612	29606.377023	0.536746	0.002333	0.000304	7.66
f468:003	33.835705	0.000800	29554.578114	0.698696	0.001786	0.000304	5.87
f391:004	33.843883	0.000686	29547.436630	0.598532	0.002086	0.000305	6.85
f486:005	42.437274	0.000839	23564.190380	0.465596	0.001645	0.000294	5.60
f437:006	45.199545	0.000721	22124.116409	0.352685	0.001884	0.000289	6.51
f457:007	48.162730	0.000770	20762.942552	0.331856	0.001806	0.000296	6.10
f273:008	48.180881	0.000524	20755.120851	0.225807	0.002657	0.000297	8.95
f346:009	48.203205	0.000620	20745.508687	0.267003	0.002255	0.000298	7.56
f385:010	75.737838	0.000725	13203.440073	0.126389	0.002113	0.000326	6.47
f411:011	75.847385	0.000766	13184.370179	0.133096	0.001994	0.000325	6.13
f479:012	88.383542	0.000907	11314.323596	0.116061	0.001726	0.000333	5.18
f459:013	89.742327	0.000824	11143.013989	0.102285	0.001805	0.000317	5.70
f314:014	89.761501	0.000611	11140.633644	0.075836	0.002432	0.000317	7.68
f343:015	89.786143	0.000654	11137.576052	0.081176	0.002275	0.000317	7.17
f449:016	89.848608	0.000812	11129.832944	0.100603	0.001846	0.000319	5.78
f423:017	89.927621	0.000787	11120.054027	0.097366	0.001930	0.000324	5.96
f447:018	89.952921	0.000825	11116.926374	0.101939	0.001846	0.000324	5.69
f324:019	89.960831	0.000643	11115.948919	0.079492	0.002367	0.000324	7.30
f484:020	101.466691	0.000900	9855.450987	0.087427	0.001676	0.000321	5.21
f238:021	106.906697	0.000514	9353.950929	0.044954	0.003095	0.000339	9.13
f413:022	106.943810	0.000809	9350.704794	0.070777	0.001979	0.000341	5.80
f214:023	106.959272	0.000448	9349.353058	0.039183	0.003579	0.000342	10.47
f207:024	106.972908	0.000418	9348.161279	0.036550	0.003836	0.000342	11.22
f187:025	107.021785	0.000387	9343.891966	0.033790	0.004168	0.000344	12.13
f053:026	107.051419	0.000058	9341.305377	0.005040	0.027901	0.000343	81.25
f054:027	107.052289	0.000060	9341.229519	0.005205	0.027017	0.000343	78.68
f344:028	107.068493	0.000713	9339.815768	0.062169	0.002267	0.000344	6.59
f191:029	107.077673	0.000395	9339.015010	0.034450	0.004095	0.000345	11.88
f303:030	107.091869	0.000652	9337.777124	0.056846	0.002474	0.000344	7.20
f327:031	107.120413	0.000687	9335.288871	0.059849	0.002350	0.000344	6.83
f465:032	107.143532	0.000899	9333.274587	0.078342	0.001797	0.000344	5.22
f379:033	107.162468	0.000761	9331.625345	0.066244	0.002126	0.000345	6.17
f430:034	107.280978	0.000846	9321.316986	0.073530	0.001911	0.000345	5.55
f369:035	109.395975	0.000775	9141.104157	0.064798	0.002155	0.000356	6.05
f229:036	109.418776	0.000505	9139.199288	0.042189	0.003312	0.000356	9.29
f340:037	109.435902	0.000729	9137.769054	0.060858	0.002295	0.000356	6.44
f377:038	109.533615	0.000787	9129.617382	0.065630	0.002135	0.000358	5.96
f255:039	109.638517	0.000591	9120.882223	0.049124	0.002868	0.000361	7.95
f388:040	109.681949	0.000811	9117.270524	0.067393	0.002095	0.000362	5.79
f228:041	111.709087	0.000632	8951.823270	0.050616	0.003322	0.000447	7.43
f260:042	111.745592	0.000754	8948.898887	0.060418	0.002789	0.000448	6.22
f210:043	111.847349	0.000563	8940.757292	0.045029	0.003775	0.000453	8.33
f309:044	112.071976	0.000846	8922.837222	0.067370	0.002442	0.000440	5.55
f183:046	113.343244	0.000479	8822.757923	0.037292	0.004264	0.000435	9.80
f137:047	113.364261	0.000321	8821.122234	0.024963	0.006399	0.000437	14.63
f226:048	113.374159	0.000613	8820.352050	0.047696	0.003358	0.000439	7.66
f203:050	113.394433	0.000526	8818.775046	0.040930	0.003931	0.000441	8.92
f266:051	113.406613	0.000762	8817.827925	0.059258	0.002721	0.000442	6.16
f242:052	113.437976	0.000686	8815.390007	0.053293	0.003036	0.000444	6.84
f217:053	113.574460	0.000591	8804.796393	0.045824	0.003535	0.000445	7.94
f256:054	113.596482	0.000733	8803.089485	0.056826	0.002861	0.000447	6.40
f418:055	116.034566	0.000807	8618.121593	0.059903	0.001954	0.000336	5.82
f252:056	119.327864	0.000538	8380.272355	0.037798	0.002936	0.000337	8.72
f461:057	119.345650	0.000876	8379.023479	0.061501	0.001802	0.000336	5.36
f398:058	119.371441	0.000770	8377.213138	0.054041	0.002050	0.000336	6.09
f230:059	119.385778	0.000480	8376.207061	0.033670	0.003266	0.000334	9.78
f261:060	119.425790	0.000567	8373.400729	0.039738	0.002785	0.000336	8.28
f257:061	119.448675	0.000554	8371.796529	0.038841	0.002825	0.000334	8.47
f278:062	119.458086	0.000597	8371.136980	0.041859	0.002616	0.000333	7.86
f236:063	119.467037	0.000499	8370.509780	0.034936	0.003128	0.000332	9.41
f272:064	119.513142	0.000585	8367.280651	0.040957	0.002667	0.000332	8.02

Table C.5 continued from previous page

ID	Frequency (μHz)	Freq. error (μHz)	Period (s)	Period error (s)	Amplitude (%)	Amplitude error (%)	S/N
f182:065	119.529142	0.000366	8366.160621	0.025624	0.004269	0.000333	12.82
f158:066	119.540712	0.000313	8365.350905	0.021927	0.004993	0.000333	14.98
f364:067	119.613072	0.000719	8360.290237	0.050243	0.002176	0.000333	6.53
f382:069	122.490845	0.000792	8163.875415	0.052777	0.002123	0.000358	5.93
f250:070	122.597124	0.000570	8156.798213	0.037937	0.002957	0.000359	8.23
f254:071	122.626231	0.000584	8154.862045	0.038869	0.002883	0.000359	8.03
f300:072	122.682532	0.000680	8151.119697	0.045190	0.002487	0.000360	6.90
f367:073	122.799424	0.000776	8143.360670	0.051492	0.002171	0.000359	6.04
f262:074	126.364111	0.000629	7913.639369	0.039407	0.002768	0.000371	7.46
f335:075	126.681079	0.000754	7893.838665	0.046967	0.002303	0.000370	6.23
f330:076	126.767281	0.000740	7888.470866	0.046049	0.002330	0.000367	6.34
f407:077	126.975148	0.000857	7875.556897	0.053175	0.002013	0.000368	5.47
f189:078	130.573429	0.000368	7658.525979	0.021564	0.004151	0.000325	12.77
f426:079	130.605306	0.000798	7656.656776	0.046795	0.001918	0.000326	5.88
f443:080	130.807278	0.000824	7644.834570	0.048167	0.001860	0.000327	5.69
f429:081	134.654023	0.000827	7426.439856	0.045629	0.001912	0.000337	5.67
f375:082	134.713297	0.000745	7423.172206	0.041061	0.002138	0.000339	6.30
f201:083	135.682299	0.000398	7370.158122	0.021628	0.003956	0.000336	11.79
f200:084	135.700123	0.000399	7369.190068	0.021661	0.003957	0.000336	11.77
f129:085	135.718496	0.000234	7368.192492	0.012697	0.006735	0.000336	20.07
f112:086	135.732807	0.000192	7367.415621	0.010433	0.008187	0.000335	24.42
f081:087	135.742600	0.000117	7366.884114	0.006373	0.013399	0.000335	39.97
f098:088	135.755838	0.000160	7366.165696	0.008668	0.009787	0.000333	29.38
f142:089	135.765170	0.000258	7365.659405	0.013978	0.006057	0.000333	18.22
f076:090	135.776769	0.000103	7365.030174	0.005583	0.015190	0.000333	45.60
f094:091	135.791523	0.000143	7364.229948	0.007740	0.010936	0.000333	32.89
f175:092	135.801246	0.000345	7363.702707	0.018689	0.004528	0.000333	13.62
f062:093	135.815799	0.000074	7362.913633	0.003990	0.021244	0.000333	63.77
f065:094	135.817713	0.000074	7362.809906	0.004030	0.021031	0.000333	63.13
f169:095	135.840057	0.000339	7361.598813	0.018361	0.004644	0.000335	13.85
f408:096	135.865242	0.000787	7360.234221	0.042614	0.002002	0.000336	5.97
f205:097	135.878919	0.000403	7359.493368	0.021839	0.003914	0.000336	11.64
f282:098	139.898486	0.000685	7148.040194	0.034999	0.002602	0.000380	6.85
f259:099	141.698181	0.000694	7057.253602	0.034587	0.002790	0.000413	6.76
f315:100	141.893412	0.000805	7047.543529	0.039968	0.002421	0.000415	5.83
f359:101	141.978267	0.000894	7043.331500	0.044339	0.002192	0.000417	5.25
f220:102	144.020758	0.000588	6943.443541	0.028340	0.003487	0.000437	7.98
f271:103	144.049867	0.000762	6942.040411	0.036740	0.002684	0.000436	6.16
f287:104	144.149693	0.000799	6937.232936	0.038457	0.002547	0.000434	5.87
f322:105	144.164030	0.000852	6936.543030	0.041012	0.002384	0.000433	5.51
f337:106	144.184544	0.000884	6935.556168	0.042510	0.002299	0.000433	5.31
f199:107	144.234654	0.000509	6933.146611	0.024476	0.003960	0.000430	9.22
f307:108	144.244594	0.000822	6932.668805	0.039492	0.002445	0.000428	5.71
f318:109	144.265980	0.000832	6931.641103	0.039968	0.002400	0.000425	5.64
f341:110	144.293957	0.000864	6930.297173	0.041499	0.002287	0.000421	5.43
f213:111	144.306578	0.000547	6929.691041	0.026246	0.003598	0.000419	8.59
f223:112	144.316519	0.000578	6929.213708	0.027752	0.003397	0.000418	8.12
f336:113	144.341801	0.000852	6928.000005	0.040914	0.002300	0.000418	5.51
f224:114	144.366962	0.000576	6926.792585	0.027660	0.003389	0.000416	8.14
f338:115	145.486742	0.000770	6873.478551	0.036372	0.002299	0.000377	6.10
f311:116	145.504966	0.000724	6872.617658	0.034205	0.002438	0.000376	6.48
f264:117	145.544787	0.000643	6870.737325	0.030370	0.002751	0.000377	7.30
f384:118	145.563268	0.000836	6869.865020	0.039441	0.002118	0.000377	5.62
f241:119	145.592452	0.000577	6868.487935	0.027211	0.003060	0.000376	8.14
f450:120	149.540911	0.000899	6687.133266	0.040193	0.001841	0.000353	5.22
f295:121	149.553566	0.000658	6686.567426	0.029403	0.002520	0.000353	7.14
f195:122	149.583127	0.000413	6685.245999	0.018442	0.004008	0.000352	11.37
f352:123	149.596520	0.000738	6684.647463	0.032997	0.002241	0.000353	6.36
f355:124	149.617162	0.000753	6683.725239	0.033636	0.002208	0.000354	6.23
f244:125	149.631622	0.000553	6683.079313	0.024693	0.003011	0.000355	8.49
f370:126	155.206270	0.000683	6443.038658	0.028357	0.002150	0.000313	6.87
f215:127	155.216955	0.000411	6442.595121	0.017066	0.003572	0.000313	11.41
f441:128	155.261460	0.000787	6440.748391	0.032665	0.001868	0.000313	5.96
f392:129	155.285674	0.000706	6439.744087	0.029280	0.002080	0.000313	6.65

Table C.5 continued from previous page

ID	Frequency (μHz)	Freq. error (μHz)	Period (s)	Period error (s)	Amplitude (%)	Amplitude error (%)	S/N
f245:130	155.307479	0.000491	6438.839934	0.020373	0.003005	0.000315	9.55
f374:131	155.330319	0.000687	6437.893171	0.028483	0.002141	0.000313	6.83
f204:132	161.221351	0.000483	6202.652388	0.018568	0.003916	0.000403	9.72
f209:133	161.244216	0.000496	6201.772825	0.019090	0.003809	0.000403	9.46
f222:134	161.255544	0.000547	6201.337169	0.021021	0.003470	0.000404	8.59
f294:135	161.272001	0.000751	6200.704380	0.028884	0.002525	0.000404	6.25
f196:136	161.283580	0.000477	6200.259208	0.018324	0.003976	0.000404	9.85
f246:137	161.317714	0.000635	6198.947268	0.024387	0.002986	0.000404	7.40
f186:138	161.363178	0.000446	6197.200706	0.017144	0.004258	0.000405	10.51
f297:139	162.237083	0.000775	6163.818900	0.029445	0.002497	0.000412	6.06
f247:140	162.956975	0.000609	6136.589124	0.022938	0.002973	0.000386	7.70
f163:141	162.990610	0.000373	6135.322748	0.014026	0.004858	0.000386	12.60
f181:142	163.008645	0.000416	6134.643961	0.015673	0.004328	0.000384	11.27
f296:143	163.022972	0.000716	6134.104820	0.026944	0.002507	0.000383	6.55
f177:144	163.036037	0.000404	6133.613262	0.015192	0.004446	0.000383	11.62
f154:145	163.051673	0.000344	6133.025079	0.012936	0.005220	0.000383	13.65
f170:146	163.068621	0.000388	6132.387656	0.014596	0.004634	0.000383	12.09
f249:147	163.087693	0.000607	6131.670531	0.022829	0.002961	0.000383	7.73
f240:148	163.103603	0.000587	6131.072409	0.022076	0.003069	0.000384	7.99
f234:149	163.111772	0.000573	6130.765364	0.021551	0.003146	0.000384	8.19
f372:150	163.131365	0.000845	6130.029022	0.031771	0.002145	0.000386	5.55
f299:151	163.157464	0.000724	6129.048429	0.027214	0.002490	0.000384	6.48
f304:152	163.170402	0.000730	6128.562462	0.027432	0.002470	0.000384	6.43
f378:153	163.252526	0.000848	6125.479473	0.031821	0.002134	0.000386	5.53
f263:154	167.510183	0.000596	5969.786312	0.021223	0.002763	0.000351	7.88
f235:155	167.536356	0.000523	5968.853697	0.018635	0.003136	0.000349	8.97
f292:156	167.557323	0.000649	5968.106821	0.023111	0.002531	0.000350	7.23
f349:157	167.569733	0.000730	5967.664820	0.026003	0.002245	0.000349	6.43
f166:158	167.580855	0.000344	5967.268756	0.012252	0.004752	0.000348	13.64
f132:159	167.594428	0.000245	5966.785470	0.008736	0.006651	0.000348	19.13
f118:160	167.604020	0.000218	5966.444008	0.007750	0.007510	0.000348	21.56
f097:161	167.621385	0.000164	5965.825908	0.005830	0.009978	0.000348	28.65
f274:162	167.635890	0.000618	5965.309684	0.021974	0.002648	0.000348	7.60
f056:163	167.653982	0.000062	5964.665978	0.002190	0.026550	0.000348	76.24
f082:164	167.668717	0.000124	5964.141793	0.004394	0.013218	0.000348	37.99
f061:165	167.681443	0.000072	5963.689136	0.002552	0.022692	0.000347	65.40
f057:166	167.694266	0.000066	5963.233127	0.002341	0.024731	0.000347	71.28
f034:167	167.708894	0.000028	5962.712999	0.000986	0.058697	0.000347	169.19
f032:168	167.710349	0.000027	5962.661271	0.000968	0.059791	0.000347	172.34
f101:169	167.735013	0.000171	5961.784488	0.006061	0.009590	0.000348	27.52
f104:170	167.740618	0.000174	5961.585282	0.006178	0.009415	0.000349	27.00
f036:171	167.763735	0.000031	5960.763809	0.001087	0.053254	0.000347	153.40
f033:172	167.765191	0.000028	5960.712094	0.000985	0.058743	0.000347	169.31
f064:173	167.789235	0.000077	5959.857900	0.002723	0.021181	0.000346	61.22
f008:174	167.816670	0.000008	5958.883590	0.000298	0.194588	0.000348	558.39
f006:175	167.818864	0.000005	5958.805693	0.000187	0.310051	0.000348	889.92
f009:176	167.822550	0.000011	5958.674817	0.000394	0.147337	0.000348	423.07
f041:177	167.835703	0.000032	5958.207816	0.001136	0.050890	0.000347	146.68
f020:178	167.849891	0.000019	5957.704191	0.000681	0.084863	0.000347	244.59
f069:179	167.868510	0.000093	5957.043406	0.003294	0.017544	0.000347	50.56
f067:180	167.886372	0.000092	5956.409607	0.003252	0.017764	0.000347	51.20
f011:181	167.899523	0.000013	5955.943067	0.000446	0.129833	0.000348	373.22
f010:182	167.900415	0.000012	5955.911431	0.000434	0.133341	0.000348	383.30
f073:183	167.920022	0.000104	5955.215991	0.003687	0.015721	0.000348	45.14
f265:184	167.928664	0.000592	5954.909527	0.021007	0.002750	0.000347	7.92
f058:185	167.947572	0.000069	5954.239111	0.002436	0.023577	0.000345	68.29
f003:186	167.966483	0.000004	5953.568722	0.000132	0.435904	0.000345	1262.72
f004:187	167.967020	0.000004	5953.549683	0.000136	0.423259	0.000345	1226.09
f070:188	167.985263	0.000093	5952.903149	0.003306	0.017285	0.000344	50.30
f068:189	168.004780	0.000092	5952.211611	0.003244	0.017626	0.000344	51.26
f125:190	168.020899	0.000229	5951.640581	0.008094	0.007061	0.000344	20.54
f059:191	168.027935	0.000069	5951.391356	0.002455	0.023274	0.000344	67.72
f024:192	168.048236	0.000021	5950.672384	0.000745	0.076671	0.000344	222.99
f027:193	168.049110	0.000024	5950.641438	0.000844	0.067693	0.000344	196.85

Table C.5 continued from previous page

ID	Frequency (μHz)	Freq. error (μHz)	Period (s)	Period error (s)	Amplitude (%)	Amplitude error (%)	S/N
f105:194	168.069843	0.000176	5949.907378	0.006236	0.009155	0.000344	26.64
f002:195	168.085450	0.000004	5949.354934	0.000126	0.451339	0.000344	1313.52
f001:196	168.085706	0.000004	5949.345879	0.000126	0.451351	0.000344	1313.55
f039:197	168.106009	0.000031	5948.627344	0.001114	0.051239	0.000344	149.12
f037:198	168.106988	0.000030	5948.592685	0.001076	0.053016	0.000344	154.29
f133:199	168.124493	0.000244	5947.973336	0.008633	0.006609	0.000344	19.23
f018:200	168.145556	0.000019	5947.228246	0.000665	0.086007	0.000345	249.48
f021:201	168.146437	0.000019	5947.197079	0.000688	0.083216	0.000345	241.39
f055:202	168.169463	0.000061	5946.382773	0.002146	0.026847	0.000347	77.34
f050:203	168.171934	0.000052	5946.295408	0.001830	0.031458	0.000347	90.67
f071:204	168.187548	0.000099	5945.743397	0.003508	0.016410	0.000347	47.30
f106:205	168.207546	0.000182	5945.036503	0.006447	0.008894	0.000346	25.73
f313:206	168.236672	0.000662	5944.007277	0.023401	0.002435	0.000344	7.09
f159:207	168.257250	0.000323	5943.280320	0.011424	0.004986	0.000344	14.51
f277:208	168.278701	0.000616	5942.522684	0.021752	0.002618	0.000344	7.62
f439:209	168.308480	0.000860	5941.471267	0.030365	0.001875	0.000344	5.46
f474:210	174.580997	0.000879	5728.000276	0.028849	0.001749	0.000328	5.34
f176:211	174.602362	0.000340	5727.299385	0.011142	0.004522	0.000327	13.82
f088:212	174.611585	0.000124	5726.996874	0.004060	0.012404	0.000327	37.91
f048:213	174.620175	0.000040	5726.715143	0.001309	0.038485	0.000327	117.58
f325:214	174.638294	0.000651	5726.121000	0.021360	0.002359	0.000327	7.20
f040:215	174.671144	0.000030	5725.044095	0.000978	0.051136	0.000325	157.21
f031:216	174.673036	0.000025	5724.982087	0.000829	0.060347	0.000325	185.62
f066:217	174.677463	0.000080	5724.836975	0.002626	0.019030	0.000325	58.57
f269:218	174.695806	0.000566	5724.235878	0.018544	0.002691	0.000324	8.29
f446:219	174.721553	0.000823	5723.392340	0.026955	0.001848	0.000324	5.70
f124:220	174.730268	0.000214	5723.106886	0.007021	0.007080	0.000323	21.90
f438:221	174.752460	0.000806	5722.380088	0.026397	0.001882	0.000323	5.82
f317:222	182.487286	0.000668	5479.833817	0.020050	0.002409	0.000343	7.03
f258:223	182.549264	0.000574	5477.973331	0.017212	0.002817	0.000344	8.18
f185:224	190.741474	0.000393	5242.698300	0.010789	0.004259	0.000356	11.96
f298:225	190.770918	0.000670	5241.889136	0.018422	0.002494	0.000356	7.00
f419:226	190.797688	0.000861	5241.153651	0.023638	0.001952	0.000358	5.45
f218:227	190.843087	0.000477	5239.906866	0.013087	0.003525	0.000358	9.85
f312:228	199.194412	0.000770	5020.221149	0.019407	0.002438	0.000400	6.09
f227:229	199.235668	0.000564	5019.181597	0.014202	0.003328	0.000400	8.33
f357:230	199.245586	0.000849	5018.931762	0.021375	0.002203	0.000398	5.53
f305:231	199.293369	0.000749	5017.728424	0.018869	0.002469	0.000394	6.26
f211:232	199.307152	0.000494	5017.381413	0.012448	0.003765	0.000397	9.49
f148:233	199.319204	0.000338	5017.078024	0.008511	0.005461	0.000393	13.88
f085:234	199.343724	0.000148	5016.460926	0.003716	0.012502	0.000393	31.78
f026:235	199.350908	0.000026	5016.280124	0.000653	0.071189	0.000393	180.98
f028:236	199.352041	0.000028	5016.251622	0.000698	0.066502	0.000393	169.13
f087:237	199.394502	0.000149	5015.183418	0.003735	0.012438	0.000394	31.60
f074:238	199.404490	0.000120	5014.932217	0.003006	0.015442	0.000393	39.27
f035:239	199.421929	0.000035	5014.493660	0.000871	0.053283	0.000393	135.43
f029:240	199.425907	0.000028	5014.393644	0.000709	0.065441	0.000393	166.43
f005:241	199.435536	0.000005	5014.151549	0.000133	0.348335	0.000392	888.40
f007:242	199.435938	0.000006	5014.141441	0.000157	0.294267	0.000392	750.50
f091:243	199.452499	0.000155	5013.725096	0.003889	0.011849	0.000391	30.34
f130:244	199.470551	0.000273	5013.271355	0.006869	0.006732	0.000392	17.17
f072:245	199.490750	0.000113	5012.763743	0.002827	0.016376	0.000393	41.72
f044:246	199.499105	0.000042	5012.553806	0.001067	0.043402	0.000393	110.56
f014:247	199.511103	0.000019	5012.252381	0.000474	0.097559	0.000392	248.87
f025:248	199.513844	0.000025	5012.183521	0.000621	0.074391	0.000392	189.90
f093:249	199.529500	0.000158	5011.790228	0.003964	0.011615	0.000391	29.74
f047:250	199.552562	0.000046	5011.211038	0.001153	0.039929	0.000390	102.26
f046:251	199.554081	0.000046	5011.172896	0.001146	0.040164	0.000390	102.86
f281:252	199.568600	0.000703	5010.808313	0.017659	0.002610	0.000391	6.67
f342:253	200.799801	0.000836	4980.084621	0.020732	0.002277	0.000406	5.61
f267:254	200.974128	0.000706	4975.764835	0.017481	0.002720	0.000409	6.65
f386:255	201.581075	0.000872	4960.783149	0.021470	0.002112	0.000393	5.38
f139:256	201.599583	0.000294	4960.327709	0.007222	0.006264	0.000392	15.99
f202:257	201.609297	0.000464	4960.088716	0.011406	0.003955	0.000391	10.12

Table C.5 continued from previous page

ID	Frequency (μHz)	Freq. error (μHz)	Period (s)	Period error (s)	Amplitude (%)	Amplitude error (%)	S/N
f121:258	201.624780	0.000255	4959.707830	0.006265	0.007174	0.000389	18.43
f345:259	201.638203	0.000809	4959.377653	0.019887	0.002260	0.000389	5.80
f116:260	201.647177	0.000238	4959.156948	0.005861	0.007649	0.000388	19.69
f237:261	201.654491	0.000584	4958.977097	0.014370	0.003116	0.000388	8.03
f089:262	201.668785	0.000149	4958.625607	0.003667	0.012251	0.000389	31.47
f363:263	201.685522	0.000840	4958.214098	0.020640	0.002176	0.000389	5.59
f150:264	201.693891	0.000340	4958.008373	0.008362	0.005353	0.000388	13.80
f144:265	201.728263	0.000311	4957.163577	0.007653	0.005790	0.000384	15.07
f086:266	201.742062	0.000144	4956.824529	0.003546	0.012468	0.000383	32.52
f096:267	201.752521	0.000169	4956.567545	0.004141	0.010655	0.000383	27.84
f077:268	201.768153	0.000120	4956.183535	0.002942	0.014926	0.000381	39.19
f103:269	201.785178	0.000187	4955.765387	0.004585	0.009510	0.000378	25.14
f022:270	201.799267	0.000022	4955.419375	0.000530	0.082096	0.000378	217.34
f023:271	201.800215	0.000022	4955.396118	0.000546	0.079715	0.000378	211.04
f219:272	201.816210	0.000503	4955.003365	0.012347	0.003521	0.000377	9.33
f394:273	201.827081	0.000853	4954.736470	0.020953	0.002074	0.000377	5.50
f127:274	201.837750	0.000258	4954.474562	0.006335	0.006859	0.000377	18.19
f270:275	201.859039	0.000656	4953.952055	0.016106	0.002690	0.000376	7.15
f171:276	201.868751	0.000381	4953.713704	0.009349	0.004628	0.000376	12.32
f268:277	201.888973	0.000652	4953.217517	0.016000	0.002700	0.000375	7.20
f157:278	201.929610	0.000347	4952.220727	0.008522	0.005014	0.000371	13.51
f109:279	201.946183	0.000204	4951.814307	0.004992	0.008504	0.000369	23.05
f221:280	201.959218	0.000497	4951.494706	0.012183	0.003487	0.000369	9.44
f100:281	201.974547	0.000181	4951.118920	0.004426	0.009619	0.000370	26.00
f115:282	201.985231	0.000225	4950.857016	0.005525	0.007713	0.000370	20.82
f383:283	201.998786	0.000823	4950.524794	0.020158	0.002119	0.000371	5.71
f164:284	202.025544	0.000360	4949.869121	0.008821	0.004846	0.000372	13.04
f285:285	202.066086	0.000677	4948.875994	0.016569	0.002580	0.000372	6.94
f339:286	202.083443	0.000765	4948.450914	0.018728	0.002296	0.000374	6.14
f099:287	202.096122	0.000180	4948.140473	0.004413	0.009743	0.000374	26.04
f216:288	202.105447	0.000496	4947.912161	0.012146	0.003547	0.000375	9.46
f179:289	202.116236	0.000397	4947.648038	0.009717	0.004416	0.000373	11.82
f475:290	209.132430	0.000786	4781.659154	0.017978	0.001739	0.000291	5.97
f497:291	209.163066	0.000869	4780.958802	0.019861	0.001565	0.000290	5.40
f490:292	209.187715	0.000842	4780.395454	0.019249	0.001613	0.000289	5.57
f232:293	209.198708	0.000427	4780.144241	0.009763	0.003177	0.000289	10.98
f472:294	209.207097	0.000767	4779.952574	0.017522	0.001767	0.000289	6.12
f290:295	212.610959	0.000541	4703.426418	0.011969	0.002540	0.000293	8.67
f402:296	212.646984	0.000673	4702.629589	0.014881	0.002040	0.000293	6.97
f420:297	212.658713	0.000705	4702.370218	0.015594	0.001952	0.000293	6.66
f328:298	212.666471	0.000590	4702.198678	0.013055	0.002334	0.000294	7.95
f167:299	212.709495	0.000295	4701.247578	0.006515	0.004676	0.000294	15.92
f134:300	212.722193	0.000210	4700.966959	0.004642	0.006554	0.000293	22.34
f147:301	212.738052	0.000245	4700.616515	0.005422	0.005598	0.000293	19.13
f403:302	212.763781	0.000671	4700.048077	0.014812	0.002039	0.000291	7.00
f233:303	212.774815	0.000432	4699.804342	0.009552	0.003154	0.000291	10.85
f453:304	212.802277	0.000747	4699.197842	0.016489	0.001819	0.000289	6.29
f319:305	212.826368	0.000567	4698.665901	0.012519	0.002399	0.000290	8.28
f444:306	217.122313	0.000796	4605.698901	0.016882	0.001859	0.000315	5.90
f174:307	220.579955	0.000317	4533.503508	0.006516	0.004542	0.000307	14.80
f111:308	220.598734	0.000174	4533.117577	0.003576	0.008292	0.000307	26.97
f083:309	220.620863	0.000109	4532.662889	0.002249	0.013150	0.000307	42.87
f477:310	226.010629	0.000858	4424.570676	0.016798	0.001735	0.000317	5.47
f483:311	226.029490	0.000876	4424.201464	0.017154	0.001699	0.000317	5.36
f248:312	233.778284	0.000574	4277.557282	0.010499	0.002962	0.000362	8.18
f415:313	233.814319	0.000863	4276.898031	0.015787	0.001965	0.000361	5.44
f043:314	234.115276	0.000035	4271.400037	0.000639	0.048045	0.000359	133.93
f042:315	234.116103	0.000035	4271.384962	0.000631	0.048678	0.000359	135.70
f141:316	234.135777	0.000271	4271.026038	0.004948	0.006212	0.000359	17.30
f090:317	234.147610	0.000139	4270.810188	0.002543	0.012090	0.000359	33.66
f243:318	234.173317	0.000557	4270.341363	0.010151	0.003024	0.000359	8.43
f172:319	234.184821	0.000365	4270.131588	0.006647	0.004618	0.000359	12.87
f194:320	234.221848	0.000420	4269.456543	0.007657	0.004010	0.000359	11.17
f153:321	234.258245	0.000321	4268.793189	0.005850	0.005230	0.000358	14.62

Table C.5 continued from previous page

ID	Frequency (μHz)	Freq. error (μHz)	Period (s)	Period error (s)	Amplitude (%)	Amplitude error (%)	S/N
f192:322	234.277575	0.000417	4268.440980	0.007599	0.004026	0.000358	11.25
f320:323	234.303661	0.000698	4267.965743	0.012716	0.002396	0.000356	6.72
f306:324	234.341267	0.000677	4267.280846	0.012329	0.002467	0.000356	6.93
f253:325	234.353043	0.000581	4267.066425	0.010585	0.002888	0.000358	8.07
f208:326	234.377315	0.000439	4266.624518	0.007996	0.003820	0.000358	10.68
f280:327	234.392102	0.000645	4266.355363	0.011731	0.002613	0.000359	7.28
f366:328	241.240122	0.000696	4145.247444	0.011956	0.002174	0.000322	6.75
f347:329	241.277721	0.000672	4144.601478	0.011541	0.002255	0.000323	6.99
f432:330	241.330511	0.000803	4143.694863	0.013780	0.001898	0.000325	5.85
f286:331	241.353396	0.000591	4143.301964	0.010138	0.002571	0.000323	7.95
f399:332	241.386325	0.000741	4142.736756	0.012715	0.002044	0.000323	6.33
f360:333	241.397924	0.000693	4142.537700	0.011885	0.002188	0.000323	6.78
f405:334	241.458927	0.000747	4141.491120	0.012813	0.002026	0.000322	6.28
f310:335	241.574152	0.000618	4139.515717	0.010591	0.002441	0.000321	7.59
f332:336	248.314380	0.000625	4027.152999	0.010141	0.002319	0.000309	7.51
f049:337	248.321423	0.000042	4027.038781	0.000682	0.034458	0.000309	111.53
f180:338	248.338141	0.000333	4026.767684	0.005399	0.004354	0.000309	14.09
f435:339	248.358699	0.000770	4026.434370	0.012484	0.001888	0.000310	6.10
f404:340	249.426370	0.000746	4009.199195	0.011988	0.002030	0.000323	6.29
f212:341	249.470718	0.000406	4008.486473	0.006516	0.003726	0.000322	11.57
f458:342	249.483972	0.000838	4008.273521	0.013468	0.001806	0.000323	5.60
f152:343	249.496476	0.000288	4008.072649	0.004619	0.005258	0.000322	16.32
f123:344	249.513517	0.000214	4007.798907	0.003430	0.007090	0.000323	21.98
f145:345	249.532034	0.000264	4007.501498	0.004248	0.005715	0.000322	17.74
f122:346	249.536202	0.000212	4007.434553	0.003405	0.007130	0.000322	22.14
f373:347	249.555737	0.000706	4007.120870	0.011335	0.002145	0.000323	6.65
f197:348	249.568991	0.000381	4006.908052	0.006114	0.003968	0.000322	12.32
f128:349	249.585324	0.000224	4006.645845	0.003590	0.006756	0.000322	20.99
f063:350	249.610371	0.000071	4006.243795	0.001137	0.021215	0.000320	66.27
f107:351	249.625707	0.000175	4005.997671	0.002806	0.008584	0.000320	26.84
f136:352	249.635979	0.000234	4005.832827	0.003749	0.006439	0.000321	20.09
f113:353	249.650416	0.000183	4005.601182	0.002944	0.008171	0.000319	25.58
f120:354	249.658069	0.000207	4005.478382	0.003328	0.007224	0.000319	22.63
f138:355	249.674674	0.000235	4005.211995	0.003769	0.006385	0.000320	19.97
f114:356	249.690781	0.000185	4004.953634	0.002970	0.008101	0.000320	25.34
f428:357	249.709833	0.000784	4004.648066	0.012566	0.001916	0.000320	5.99
f455:358	249.721750	0.000828	4004.456960	0.013276	0.001817	0.000321	5.67
f095:359	249.731577	0.000140	4004.299392	0.002248	0.010730	0.000321	33.47
f119:360	249.737966	0.000205	4004.196937	0.003284	0.007359	0.000321	22.92
f165:361	249.753275	0.000317	4003.951492	0.005089	0.004760	0.000322	14.78
f397:362	249.762652	0.000733	4003.801179	0.011749	0.002062	0.000322	6.40
f291:363	249.777810	0.000597	4003.558207	0.009574	0.002532	0.000322	7.86
f162:364	249.794158	0.000309	4003.296189	0.004945	0.004875	0.000321	15.21
f184:365	249.812222	0.000353	4003.006699	0.005661	0.004262	0.000321	13.29
f102:366	249.824012	0.000158	4002.817797	0.002526	0.009585	0.000322	29.77
f467:367	249.840150	0.000846	4002.559235	0.013556	0.001787	0.000322	5.55
f156:368	249.862041	0.000296	4002.208569	0.004747	0.005128	0.000324	15.84
f251:369	249.870714	0.000515	4002.069646	0.008251	0.002955	0.000324	9.11
f190:370	249.884086	0.000368	4001.855491	0.005892	0.004136	0.000324	12.76
f321:371	249.917729	0.000639	4001.316774	0.010223	0.002386	0.000325	7.35
f348:372	249.927579	0.000678	4001.159073	0.010847	0.002248	0.000325	6.93
f288:373	249.942944	0.000599	4000.913111	0.009593	0.002544	0.000325	7.83
f155:374	264.077553	0.000240	3786.766385	0.003437	0.005143	0.000263	19.58
f038:375	264.083022	0.000024	3786.687954	0.000343	0.051518	0.000262	196.49
f110:376	264.103464	0.000146	3786.394870	0.002091	0.008424	0.000262	32.19
f045:377	264.120612	0.000029	3786.149038	0.000409	0.043200	0.000263	164.49
f015:378	264.121353	0.000013	3786.138415	0.000189	0.093663	0.000263	356.61
f173:379	267.935683	0.000318	3732.238980	0.004426	0.004597	0.000311	14.77
f400:380	268.587029	0.000713	3723.187986	0.009881	0.002042	0.000310	6.58
f469:381	268.775028	0.000813	3720.583740	0.011260	0.001783	0.000309	5.77
f481:382	268.814643	0.000848	3720.035451	0.011731	0.001713	0.000309	5.54
f193:383	268.855598	0.000363	3719.468764	0.005015	0.004024	0.000311	12.95
f406:384	268.875950	0.000721	3719.187226	0.009978	0.002014	0.000310	6.51
f436:385	278.886374	0.000697	3585.689698	0.008961	0.001888	0.000280	6.73

Table C.5 continued from previous page

ID	Frequency (μHz)	Freq. error (μHz)	Period (s)	Period error (s)	Amplitude (%)	Amplitude error (%)	S/N
f493:386	281.549355	0.000794	3551.775142	0.010014	0.001600	0.000271	5.91
f293:387	281.560663	0.000502	3551.632496	0.006332	0.002529	0.000271	9.35
f396:388	281.577492	0.000614	3551.420220	0.007745	0.002062	0.000270	7.64
f239:389	289.459746	0.000480	3454.711804	0.005724	0.003084	0.000315	9.79
f431:390	289.999972	0.000788	3448.276193	0.009366	0.001911	0.000321	5.96
f225:391	290.117843	0.000450	3446.875205	0.005347	0.003361	0.000322	10.43
f206:392	290.141503	0.000391	3446.594128	0.004650	0.003866	0.000323	11.99
f131:393	290.149621	0.000226	3446.497689	0.002682	0.006716	0.000323	20.79
f160:394	290.168871	0.000308	3446.269051	0.003656	0.004927	0.000323	15.25
f108:395	290.182098	0.000178	3446.111967	0.002115	0.008516	0.000323	26.35
f410:396	290.192370	0.000760	3445.989982	0.009024	0.001995	0.000323	6.18
f456:397	290.225285	0.000837	3445.599170	0.009938	0.001815	0.000324	5.61
f151:398	301.642114	0.000264	3315.186950	0.002903	0.005296	0.000298	17.77
f013:399	301.653106	0.000014	3315.066144	0.000152	0.101336	0.000298	339.55
f012:400	301.653969	0.000013	3315.056660	0.000144	0.106995	0.000298	358.50
f017:401	301.665752	0.000016	3314.927176	0.000173	0.088577	0.000298	297.61
f376:402	301.673921	0.000655	3314.837412	0.007195	0.002137	0.000298	7.17
f412:403	301.983658	0.000697	3311.437471	0.007642	0.001984	0.000295	6.73
f462:404	302.014667	0.000768	3311.097471	0.008419	0.001801	0.000295	6.11
f308:405	302.273761	0.000572	3308.259361	0.006264	0.002444	0.000298	8.20
f365:406	302.332877	0.000643	3307.612484	0.007038	0.002175	0.000298	7.30
f464:407	302.348531	0.000779	3307.441238	0.008521	0.001798	0.000298	6.03
f323:408	315.719912	0.000651	3167.364365	0.006531	0.002368	0.000328	7.21
f362:409	315.855640	0.000713	3166.003302	0.007147	0.002182	0.000332	6.58
f390:410	316.339044	0.000746	3161.165270	0.007454	0.002087	0.000332	6.29
f414:411	318.603153	0.000716	3138.700892	0.007053	0.001975	0.000301	6.56
f149:412	318.609704	0.000263	3138.636359	0.002586	0.005379	0.000301	17.88
f454:413	329.696781	0.000765	3033.089972	0.007034	0.001819	0.000296	6.14
f389:414	329.772097	0.000661	3032.397246	0.006074	0.002090	0.000294	7.11
f276:415	329.795547	0.000524	3032.181636	0.004816	0.002635	0.000294	8.96
f499:416	329.987848	0.000890	3030.414621	0.008169	0.001550	0.000294	5.28
f445:417	330.053502	0.000740	3029.811811	0.006797	0.001855	0.000293	6.34
f161:418	330.075784	0.000280	3029.607282	0.002568	0.004915	0.000293	16.78
f178:419	330.086904	0.000310	3029.505223	0.002847	0.004436	0.000293	15.13
f075:420	360.418073	0.000089	2774.555645	0.000685	0.015282	0.000290	52.72
f140:421	360.426597	0.000218	2774.490032	0.001677	0.006253	0.000290	21.54
f060:422	360.437798	0.000059	2774.403811	0.000451	0.023234	0.000290	80.12
f470:423	361.571838	0.000773	2765.702124	0.005914	0.001774	0.000292	6.07
f501:424	361.619176	0.000891	2765.340074	0.006813	0.001546	0.000293	5.27
f395:425	361.631229	0.000665	2765.247908	0.005086	0.002071	0.000294	7.06
f019:426	361.671934	0.000016	2764.936688	0.000123	0.085760	0.000294	292.12
f016:427	361.672691	0.000015	2764.930904	0.000118	0.089590	0.000294	305.17
f080:428	361.679919	0.000101	2764.875645	0.000772	0.013666	0.000294	46.46
f380:429	361.706932	0.000648	2764.669158	0.004954	0.002124	0.000293	7.24
f079:430	361.730610	0.000097	2764.488191	0.000741	0.014185	0.000293	48.38
f092:431	361.736834	0.000117	2764.440624	0.000897	0.011729	0.000293	40.00
f316:432	361.762158	0.000572	2764.247113	0.004374	0.002409	0.000294	8.20
f417:433	361.781741	0.000705	2764.097485	0.005388	0.001958	0.000294	6.66
f333:434	361.849294	0.000598	2763.581458	0.004569	0.002307	0.000294	7.84
f052:435	393.591233	0.000042	2540.706999	0.000273	0.030296	0.000273	110.91
f030:436	393.613652	0.000020	2540.562286	0.000129	0.064367	0.000273	235.54
f146:437	393.635144	0.000228	2540.423576	0.001470	0.005603	0.000272	20.61
f448:438	393.642391	0.000690	2540.376804	0.004451	0.001846	0.000271	6.80
f387:439	403.974162	0.000573	2475.405840	0.003510	0.002109	0.000257	8.19
f084:440	403.982057	0.000097	2475.357461	0.000592	0.012513	0.000258	48.55
f126:441	404.008520	0.000175	2475.195322	0.001074	0.006907	0.000258	26.77
f117:442	426.095672	0.000166	2346.890773	0.000915	0.007628	0.000270	28.24
f078:443	426.117804	0.000089	2346.768876	0.000489	0.014245	0.000269	52.91
f051:444	426.141814	0.000040	2346.636650	0.000222	0.031300	0.000269	116.18
f473:445	470.749407	0.000784	2124.272459	0.003538	0.001758	0.000294	5.99
f478:446	470.928987	0.000796	2123.462405	0.003588	0.001731	0.000294	5.90
f188:447	473.583754	0.000305	2111.558919	0.001360	0.004158	0.000270	15.38
f488:448	473.598140	0.000776	2111.494779	0.003458	0.001633	0.000270	6.05
f500:449	506.916794	0.000893	1972.710338	0.003474	0.001550	0.000295	5.26

Table C.5 continued from previous page

ID	Frequency (μHz)	Freq. error (μHz)	Period (s)	Period error (s)	Amplitude (%)	Amplitude error (%)	S/N
f434:450	506.981999	0.000734	1972.456621	0.002854	0.001889	0.000295	6.40
f460:451	506.995265	0.000769	1972.405008	0.002992	0.001802	0.000295	6.10
f494:452	507.089994	0.000870	1972.036547	0.003384	0.001589	0.000295	5.39
f492:453	507.234819	0.000866	1971.473492	0.003365	0.001608	0.000297	5.42
f471:454	507.381944	0.000805	1970.901825	0.003128	0.001769	0.000303	5.83
f302:455	507.519598	0.000577	1970.367259	0.002241	0.002475	0.000304	8.13
f301:456	507.541722	0.000576	1970.281372	0.002237	0.002484	0.000305	8.14
f326:457	507.568555	0.000610	1970.177212	0.002368	0.002351	0.000306	7.69
f284:458	507.577442	0.000556	1970.142714	0.002157	0.002583	0.000306	8.45
f498:459	519.678539	0.000764	1924.266494	0.002829	0.001552	0.000253	6.14
f424:460	519.691134	0.000617	1924.219857	0.002283	0.001927	0.000253	7.61
f354:461	519.712687	0.000533	1924.140060	0.001973	0.002223	0.000252	8.81
f368:462	542.175288	0.000604	1844.421945	0.002056	0.002161	0.000278	7.77
f334:463	625.732760	0.000554	1598.126331	0.001414	0.002307	0.000272	8.48
f480:464	639.971671	0.000705	1562.569166	0.001722	0.001715	0.000258	6.65
f463:465	670.048569	0.000786	1492.429125	0.001751	0.001799	0.000301	5.97
f425:466	703.619883	0.000785	1421.221918	0.001586	0.001926	0.000322	5.98
f381:467	703.881205	0.000713	1420.694278	0.001439	0.002123	0.000323	6.58
f466:468	703.912400	0.000843	1420.631317	0.001701	0.001795	0.000323	5.57
f331:469	824.611857	0.000669	1212.691755	0.000984	0.002323	0.000331	7.02
f350:470	824.759655	0.000692	1212.474439	0.001018	0.002245	0.000331	6.78
f485:471	859.076393	0.000819	1164.040832	0.001110	0.001645	0.000287	5.73
f491:472	1108.867295	0.000751	901.821169	0.000610	0.001613	0.000258	6.25
f361:473	1108.902415	0.000555	901.792607	0.000452	0.002184	0.000258	8.45
f442:474	1108.923289	0.000651	901.775632	0.000529	0.001861	0.000258	7.21
f496:475	1108.945130	0.000773	901.757871	0.000628	0.001567	0.000258	6.07
f506:476	1174.553754	0.000820	851.387173	0.000594	0.001440	0.000252	5.72
f508:477	1174.583951	0.000883	851.365285	0.000640	0.001337	0.000252	5.31
f495:478	1174.628573	0.000746	851.332943	0.000541	0.001579	0.000251	6.29
f451:479	1340.494640	0.000655	745.993285	0.000365	0.001840	0.000257	7.16
f502:480	1449.470330	0.000780	689.907188	0.000371	0.001537	0.000255	6.02
f421:481	1576.301591	0.000696	634.396365	0.000280	0.001948	0.000289	6.75
f504:482	1576.437461	0.000898	634.341688	0.000361	0.001504	0.000288	5.23
f505:483	1744.069951	0.000862	573.371498	0.000283	0.001499	0.000275	5.44
f275:484	1744.253629	0.000492	573.311119	0.000162	0.002635	0.000276	9.53
f487:485	1744.265966	0.000788	573.307064	0.000259	0.001640	0.000275	5.96
f143:486	1744.276363	0.000215	573.303647	0.000071	0.006029	0.000276	21.86
f135:487	1744.283141	0.000200	573.301419	0.000066	0.006487	0.000276	23.51
f168:488	1744.292761	0.000279	573.298257	0.000092	0.004648	0.000276	16.82
f507:489	1818.706598	0.000835	549.841300	0.000253	0.001396	0.000249	5.62
f356:490	3431.530505	0.000608	291.415157	0.000052	0.002207	0.000286	7.72
f489:491	3431.564839	0.000826	291.412241	0.000070	0.001626	0.000286	5.68
f393:492	3431.827699	0.000643	291.389920	0.000055	0.002075	0.000284	7.30
f503:493	3432.083891	0.000866	291.368169	0.000074	0.001534	0.000283	5.42
f279:494	3432.102469	0.000507	291.366592	0.000043	0.002616	0.000282	9.26
f283:495	3432.116996	0.000511	291.365359	0.000043	0.002587	0.000282	9.18
f231:496	3432.129387	0.000416	291.364307	0.000035	0.003184	0.000282	11.28
f440:497	3432.138792	0.000708	291.363508	0.000060	0.001868	0.000282	6.63
f358:498	3446.664253	0.000593	290.135600	0.000050	0.002201	0.000278	7.92
f371:499	3446.672604	0.000610	290.134897	0.000051	0.002146	0.000279	7.70
f476:500	3446.991254	0.000759	290.108076	0.000064	0.001737	0.000281	6.18
f198:501	3446.999181	0.000332	290.107409	0.000028	0.003964	0.000281	14.13
f353:502	3447.009031	0.000591	290.106580	0.000050	0.002229	0.000281	7.94
f409:503	3447.032530	0.000658	290.104602	0.000055	0.002002	0.000281	7.14
f422:504	3447.041699	0.000680	290.103830	0.000057	0.001936	0.000281	6.90
f427:505	3447.245665	0.000687	290.086665	0.000058	0.001918	0.000281	6.83
f289:506	3447.253130	0.000519	290.086037	0.000044	0.002544	0.000281	9.05
f452:507	3447.497163	0.000720	290.065503	0.000061	0.001839	0.000282	6.52
f416:508	3447.509272	0.000677	290.064485	0.000057	0.001962	0.000283	6.94

Appendix D

Final pulsation mode identification

Table D.1: Final identification of TIC441725813 pulsation modes observed by *TESS*, derived from G1 (S14-25), G2 (S40-41), G3 (S47-52) and G4 (S55-60) datasets.

ID	Frequency (μHz)	Period (s)	S/N	Datasets		Identification		
				Taken from	Present in	ℓ	k_1	k_2
f1	666.240	1500.96	6.63	G3	G2, 3	1	1	-
f2	627.283	1594.18	133.23	G3	G1, 2, 3	2	-	6
f3	585.321	1708.46	7.66	G1	G1, 3	1	2	-
f4	462.990	2159.88	120.29	G1	All	1	4	-
f5	361.891	2763.27	17.43	G1	All	1	6	-
f6	349.299	2862.88	13.90	G1	All	2	-	14
f7	328.405	3045.02	202.46	G1	All	1	7	-
f8	314.724	3177.39	6.38	G1	G1	2	-	16
f9	301.430	3317.52	134.21	G1	All	1	8	-
f10	291.037	3435.99	28.49	G1	All	-	-	-
f11	283.761	3524.09	5.66	G1	G1	-	-	-
f12	277.740	3600.49	82.40	G1	All	1	9	-
f13	276.594	3615.41	612.52	G1	All	2	-	19
f14	265.498	3766.50	370.26	G1	All	2	-	20
f15	257.619	3881.71	60.47	G1	All	1	10	-
f16	254.556	3928.40	7.70	G3	G1, 2, 3	2	-	21
f17	245.079	4080.31	9.43	G1	G1	2	-	22
f18	236.125	4235.04	8.80	G3	G1, 3, 4	2	-	23

Table D.1 continued from previous page

ID	Frequency (μHz)	Period (s)	S/N	Datasets		Identification		
				Taken from	Present in	ℓ	k_1	k_2
f19	228.335	4379.52	6.06	G1	G1	2	-	24
f20	226.589	4413.28	33.34	G1	All	1	12	-
f21	221.299	4518.77	29.86	G1	All	2	-	25
f22	213.156	4691.40	5.88	G1	G1, 3, 4	1	13	-
f23	207.319	4823.48	207.89	G1	All	2	-	27
f24	191.048	5234.29	29.00	G1	All	1	15	-
f25	183.082	5462.03	8.60	G1	G1, 3	2	-	31
f26	182.015	5494.06	17.05	G1	All	1	16	-
f27	174.308	5736.98	7.28	G1	All	2	-	33
f28	174.025	5746.30	137.25	G1	All	1	17	-
f29	169.192	5910.45	6.44	G2	G2	2	-	34
f30	168.330	5940.71	7.26	G1	G1	-	-	-
f31	166.514	6005.49	202.05	G1	All	1	18	-
f32	164.280	6087.17	6.15	G3	G2, 3, 4	2	-	35
f33	159.846	6256.00	18.91	G1	G1, 3, 4	1	19	-
f34	153.411	6518.42	6.34	G1	G1, 2	2	-	38
f35	153.224	6526.40	14.67	G1	All	1	20	-
f36	147.284	6789.62	5.73	G1	G1	1	21	-
f37	141.775	7053.42	328.77	G1	All	1	22	-
f38	136.676	7316.59	6.12	G4	G4	1	23	-
f39	131.679	7594.23	7.24	G3	G2, 3	1	24	-
f40	127.278	7856.84	11.23	G3	G1, 2, 3	1	25	-
f41	123.167	8119.04	5.79	G2	G2	1	26	-
f42	115.494	8658.48	14.88	G3	G1, 2, 3	1	28	-
f43	112.258	8908.03	5.91	G3	G3	1	29	-
f44	109.343	9145.50	6.39	G4	G2, 4	1	30	-
f45	103.132	9696.30	74.24	G4	All	1	32	-
f46	93.086	10742.71	5.66	G2	G2	1	36	-
f47	72.774	13741.14	7.02	G3	G3, 4	1	47	-

Table D.2: Final identification of KIC5807616 pulsation modes observed by *Kepler* (Q2.3, Q5-Q17.2). Trapped modes are highlighted by having a (*) in the ℓ identification and a t in the k identification.

ID	Frequency (μHz)	Period (s)	S/N	No trapping				Config. 1 / Config. 2			
				ℓ	k_1	k_2	k_4	ℓ	k_1	k_2	k_4
f1	3446.999	290.11	14.13	-	-	-	-	-	-	-	-
f2	3431.828	291.39	7.30	1	1	-	-	1	1	-	-
f3	1744.283	573.30	23.51	-	-	-	-	-	-	-	-
f4	1576.302	634.40	6.75	-	-	-	-	-	-	-	-
f5	1449.470	689.91	6.02	2	-	5	-	2	-	5	-
f6	1340.495	745.99	7.16	-	-	-	-	-	-	-	-
f7	1174.629	851.33	6.29	-	-	-	-	2*	-	t	-
f8	1108.902	901.79	8.45	2	-	7	-	2	-	7	-
f9	859.076	1164.04	5.73	1	5	-	-	1	5	-	-
f10	824.612	1212.69	7.02	2	-	9	-	2	-	9	-
f11	703.881	1420.69	6.58	-	-	-	-	-	-	-	-
f12	670.049	1492.43	5.97	-	-	-	-	1*	t	-	-
f13	639.972	1562.57	6.65	1	7	-	-	1	7	-	-
f14	625.733	1598.13	8.48	2	-	12	-	2	-	12	-
f15	542.175	1844.42	7.77	-	-	-	-	2	-	14	-
f16	519.713	1924.14	8.81	-	-	-	-	-	-	-	-
f17	507.577	1970.14	8.45	4	-	-	26	4	-	-	26
f18	473.584	2111.56	15.38	1	9	-	-	1	9	-	-
f19	470.929	2123.46	5.90	-	-	-	-	-	-	-	-
f20	426.142	2346.64	116.18	4	-	-	31	4	-	-	31
f21	403.982	2475.36	48.55	2	-	18	-	2	-	18	-
f22	393.614	2540.56	235.54	1	11	-	-	1	11	-	-
f23	361.673	2764.93	305.17	2	-	20	-	2	-	20	-
f24	360.438	2774.40	80.12	1	12	-	-	1	12	-	-
f25	329.796	3032.18	8.96	2	-	22	-	2	-	22	-
f26	318.610	3138.64	17.88	-	-	-	-	1	14	-	-
f27	316.339	3161.17	6.29	-	-	-	-	-	-	-	-

Table D.2 continued from previous page

ID	Frequency (μHz)	Period (s)	S/N	No trapping				Config. 1 / Config. 2			
				ℓ	k_1	k_2	k_4	ℓ	k_1	k_2	k_4
f28	315.720	3167.36	7.21	2	-	23	-	2	-	23	-
f29	301.653	3315.07	339.55	2	-	24	-	2	-	24	-
f30	290.150	3446.50	20.79	2	-	25	-	2	-	25	-
f31	289.460	3454.71	9.79	-	-	-	-	-	-	-	-
f32	281.561	3551.63	9.35	1	15	-	-	2*	-	t	-
f33	278.886	3585.69	6.73	2	-	26	-	2	-	26	-
f34	268.587	3723.19	6.58	2	-	27	-	2	-	27	-
f35	267.936	3732.24	14.77	-	-	-	-	-	-	-	-
f36	264.121	3786.14	356.61	1	16	-	-	1	16	-	-
f37	249.732	4004.30	33.47	2	-	29	-	2	-	29	-
f38	248.321	4027.04	111.53	1	17	-	-	1	17	-	-
f39	241.353	4143.30	7.95	2	-	30	-	2	-	30	-
f40	234.116	4271.38	135.70	2	-	31	-	2	-	31	-
f41	233.778	4277.56	8.18	1	18	-	-	1	18	-	-
f42	226.011	4424.57	5.47	2	-	32	-	2	-	32	-
f43	220.621	4532.66	42.87	1	19	-	-	1	19	-	-
f44	212.722	4700.97	22.34	2	-	34	-	1*	t	-	-
f45	209.199	4780.14	10.98	1	20	-	-	1	20	-	-
f46	201.799	4955.42	217.34	2	-	36	-	2	-	36	-
f47	199.436	5014.15	888.40	1	21	-	-	1	21	-	-
f48	190.741	5242.70	11.96	1	22	-	-	1	22	-	-
f49	182.549	5477.97	8.18	1	23	-	-	1	23	-	-
f50	174.673	5724.98	185.62	1	24	-	-	1	24	-	-
f51	167.966	5953.57	1262.72	1	25	-	-	1	25	-	-
f52	163.052	6133.03	13.65	2	-	45	-	1*	t	-	-
f53	162.237	6163.82	6.06	-	-	-	-	2	-	45	-
f54	161.284	6200.26	9.85	1	26	-	-	1	26	-	-
f55	155.217	6442.60	11.41	1	27	-	-	1	27	-	-
f56	149.583	6685.25	11.37	1	28	-	-	1	28	-	-

Table D.2 continued from previous page

ID	Frequency (μHz)	Period (s)	S/N	No trapping				Config. 1 / Config. 2			
				ℓ	k_1	k_2	k_4	ℓ	k_1	k_2	k_4
f57	145.545	6870.74	7.30	-	-	-	-	-	-	-	-
f58	144.235	6933.15	9.22	1	29	-	-	1	29	-	-
f59	141.893	7047.54	5.83	-	-	-	-	-	-	-	-
f60	139.898	7148.04	6.85	1	30	-	-	1	30	-	-
f61	135.818	7362.81	63.13	-	-	-	-	1*	t	-	-
f62	134.713	7423.17	6.30	1	31	-	-	1	31	-	-
f63	130.573	7658.53	12.77	1	32	-	-	1	32	-	-
f64	126.767	7888.47	6.34	-	-	-	-	- / 1	- / 33	-	-
f65	126.364	7913.64	7.46	1	33	-	-	1 / -	33 / -	-	-
f66	122.626	8154.86	8.03	1	34	-	-	1	34	-	-
f67	119.467	8370.51	9.41	1	35	-	-	1	35	-	-
f68	116.035	8618.12	5.82	1	36	-	-	1	36	-	-
f69	113.438	8815.39	6.84	-	-	-	-	- / 1*	- / t	-	-
f70	112.920	8855.53	5.04	1	37	-	-	1	37	-	-
f71	111.847	8940.76	8.33	-	-	-	-	1* / -	t / -	-	-
f72	109.534	9129.62	5.96	1	38	-	-	1	38	-	-
f73	107.051	9341.31	81.25	1	39	-	-	1	39	-	-
f74	101.467	9855.45	5.21	1	41	-	-	1	41	-	-
f75	89.849	11129.83	5.78	1	46	-	-	1	46	-	-
f76	75.738	13203.44	6.47	1	55	-	-	1	55	-	-
f77	48.181	20755.12	8.95	1	87	-	-	1	87	-	-
f78	45.200	22124.12	6.51	1	93	-	-	1	93	-	-
f79	33.777	29606.38	7.66	1	124	-	-	1	124	-	-

Appendix E

Statistics of KIC5807616 configurations

Table E.1: Comparison of the overlaps "quality" as defined in Sec. 2.4 for the whole period range and for reduced periods between 5000 s and 14,000 s.

Parameter	**No trapping**	**Configs. 1 / 2**
Overlaps "quality" - whole period range		
Total l=1 & l=2 overlaps	18	20
Mean H distance (s)	19.08	22.82
Mean V distance (s)	16	21.67 / 22.05
Mean distance (s)	27.24	36.67 / 36.22
Overlaps "quality" - $\Pi_{k,l}$ between 5000 s and 14000 s		
Total l=1 & l=2 overlaps	14	14
Mean H distance (s)	19.58	20.19
Mean V distance (s)	17.04	12.79 / 13.33
Mean distance (s)	28.72	27.01 / 26.36

Table E.2: Comparison of the mean S/N of identified $\ell = 1$, $\ell = 2$ and $\ell = 4$ modes for the different possible configurations, for all modes and among the 20 modes of highest S/N.

Parameter	**No trapping**	**Configs. 1 / 2**
All modes (79 modes) - Mean S/N: 64.02		
$\ell = 1$ (trapped)	94.01	85.72 (22.03) / 85.66 (22.39)
$\ell = 2$ (trapped)	63.65	57.28 (7.82)
$\ell = 4$	62.32	62.32
Unidentified	11.69	9.29 / 9.47
Highest S/N modes (20 modes)		
$\ell = 1$	360.52	302.74
$\ell = 2$	140.36	157.22
$\ell = 4$	116.18	116.18
Unidentified	43.32	23.51